Sixth-order time-convolutionless master equation and beyond: Late-time resummations, two types of divergences, and the limits of validity

Lance Lampert,[*] Srikar Gadamsetty,[†] Shantanu Chaudhary,[‡] Yiting Pei,[§] Jiahao Chen [ ],
Elyana Crowder [ ], and Dragomir Davidović [ ][‖]

Georgia Institute of Technology, Atlanta, Georgia 30332, USA

Perturbative master equations are essential for modeling open quantum systems but often exhibit late-time divergences when environmental correlations decay algebraically. In this work, we analyze the time-convolutionless (TCL) master equation expanded to order TCL_{2n} and demonstrate that, while van Kampen's cumulants suppress early-time secular growth, they ultimately diverge at long times. To overcome this, we introduce a resummation technique based on the Hadamard trick, which incorporates time integrals directly into the bath's spectral density via elementwise multiplication. This approach establishes a maximum expansion order, $n_{\max} = \lceil s + 1 \rceil$, and defines a precision limit of the asymptotic states of $O(\lambda^{2\lceil s \rceil})$, where s is the power-law exponent and λ is the weak-coupling constant. The resummed master equation features renormalized Bohr frequencies that capture decoherence and spectral overlap effects. In the unbiased spin-boson model, this results in an inflation of the generator at a temperature-independent rate equal to the decoherence rate ν_2 and a finite validity time $t_L \approx (s + 1)/\nu_2$. For exponentially decaying correlations, the method recovers a proper Markovian limit below a critical coupling threshold.

I. INTRODUCTION

Over the last decade, significant progress has been made in developing methods to describe non-Markovian dynamics in open quantum systems [1–7]. Unlike Markovian dynamics, where the system's evolution depends only on its present state, non-Markovian systems retain memory effects due to their interactions with the environment. These memory effects play a vital role in condensed matter physics, atomic and molecular physics, quantum chemistry, and quantum information processing, making their study both fundamental and practically significant. Understanding and controlling such effects is essential for accurately describing non-Markovian dynamics, optimizing quantum coherence, and improving the performance of quantum technologies.

Among the many approaches for treating non-Markovian dynamics, perturbative master equations (MEs) provide a valuable framework with distinct advantages and limitations. The development of these equations traces back to the Bloch-Redfield formalism [8,9], which describes the reduced system dynamics via a first-order differential equation derived from the full system's unitary evolution. An alternative derivation was later introduced by van Kampen using *time-ordered cumulants* [10,11], which helps eliminate secular growth in the Dyson expansion and, remarkably, can yield a Markovian master equation at late times. Following we present some of the fundamental challenges facing perturbative master equations.

Understanding secular growth. Secular growth is a fundamental issue in perturbative expansions of quantum dynamics. It arises when an exponential function, such as the unitary propagator $U(t) = e^{-iHt}$, is approximated using a truncated polynomial expansion, e.g.,

$$e^{-iHt} \approx \sum_{n=0}^{N} \frac{(-iHt)^n}{n!}. \tag{1}$$

This approximation leads to divergence at large times, regardless of how small H is. Examples of secular growth in open quantum systems include the Schaller-Brandes exponent in open quantum systems [12], the Dyson series in quantum chemistry [13], and the behavior of hot accelerated qubits in Unruh-DeWitt detectors [14]. Avoiding secular growth requires a precise determination of the perturbative expansion's validity and appropriate late-time resummations. However, this task is complicated by the fact that the time-convolutionless (TCL) master equation at order $2n$ (TCL_{2n}) does not follow a standard perturbative expansion and exhibits inherently non-Markovian features.

Challenges with numerical approaches. Existing numerical methods for non-Markovian dynamics, such as tensor network approaches, have provided valuable insights but come with challenges. These include time discretization errors, reliance on auxiliary density operators, and slow state evolution that does not necessarily scale polynomially with time. Many of

---

[*]Also at Physics Department, Duke University, Durham, North Carolina.

[†]Also at University of California, Berkeley, Berkeley, California.

[‡]Also at University of Central Florida, Orlando, Florida.

[§]Also at Physics Department, Northwestern University, Evanston, Illinois.

[‖]Contact author: dragomir.davidovic@physics.gatech.edu

these methods also rely on truncating the system's memory depth, which becomes problematic when dealing with algebraically decaying bath correlation functions (BCFs). Recent advances in tensor network models have sought to mitigate these issues by capturing long-time correlations and approaching the infinite-time limit [15–19]. A key advantage of TCL_{2n} over these approaches is its computational efficiency: by explicitly eliminating early secular growth, utilizing the van Kampen cumulant expansion [10,11], TCL_{2n} optimizes computational resources. In contrast, tensor network methods mitigate such effects indirectly through singular value compression, which makes it difficult to resolve late-dynamical effects.

Challenges with algebraically decaying correlation functions. The van Kampen cumulant expansion becomes less effective when bath correlations decay algebraically rather than exponentially. Under these conditions, the perturbative generators exhibit late-time growth, a phenomenon we analyzed previously using the TCL_4 master equation [20]. This growth is intrinsically linked to the power-law decay of the BCF, characterized by

$$C(t) \propto t^{-s-1} \tag{2}$$

for large t. In contrast, second-order master equations, such as the TCL_2-Bloch-Redfield or Davies MEs [21], do not display such divergence, even in sub-Ohmic environments where the decay is relatively weak ($0 < s < 1$). Our earlier findings [20] thus raise concerns about the applicability of second-order master equations in regimes dominated by algebraically decaying correlations.

Potential resolutions and unitarity issues. A key question is whether this divergence represents a fundamental limitation or merely an artifact of truncation. One potential resolution is to incorporate all higher-order perturbative generators, thereby stabilizing the TCL series through late-time resummations. Although partial resummation of the Dyson series can sometimes restore unitarity, it remains uncertain whether summing all van Kampen cumulants in open quantum systems guarantees unitarity of the overall evolution (even if the reduced dynamics remain nonunitary). If unitarity is not restored, it may indicate an intrinsic limitation of the TCL framework in such open quantum systems. To explore this further, let us now examine the deficiencies in the derivations of the TCL master equation.

(i) Tokuyama-Mori derivation: The Tokuyama-Mori approach to deriving the TCL ME is based on eliminating convolutions from the exact Nakajima-Zwanzig master equation [22–24]. This method relies on the assumption that certain dynamical superoperators remain invertible, an assumption that is generally valid under short-time evolution or weak-coupling conditions (λ^2) [25].

However, at later times or under strong coupling, this invertibility assumption may break down, leading to potential failures in the formalism. Such breakdowns raise concerns about the universal applicability of master equations derived through this approach, particularly in regimes where system-bath interactions are strong or persist over long timescales.

(ii) van Kampen's derivation: van Kampen's derivation models the reduced density matrix as an exponential function, with the exponent expressed as a series of successive cumulants [10]. This approach provides a compact representation of the master equation and assumes the invertibility of the quantum dynamical map.

However, our analysis indicates that the loss of this invertibility does not necessarily lead to the failure of master equations [26]. This conclusion is supported by comparisons of second-order (TCL_2) and fourth-order (TCL_4) time-convolutionless solutions with results from nonperturbative methods, such as the hierarchical equations of motion (HEOM) [27] and time-evolved matrix product operators (TEMPO) [1]. Master equations do not abruptly break down when the dynamical map becomes noninvertible; instead, solutions from both perturbative and nonperturbative approaches remain closely aligned and continuous over time [26].

Impact of environmental correlations. A central assumption in van Kampen's approach is that environmental correlation times are short (a prerequisite for reaching the Markovian regime, as in the quantum dynamical semigroup limit). When this assumption fails, leading to secular or late-time growth in cumulants, the validity of the TCL must be reconsidered.

A. Our contributions: TCL and resummation techniques

Our study employs cumulant techniques to eliminate early secular growth, which arises from cumulants containing statistically uncorrelated segments. By canceling those cumulants, we isolate the key contributions that persist at long times and investigate how the slower decay of the bath correlation function (BCF) influences the late-time evolution of the remaining cumulants. Our primary objective is to resolve ambiguities regarding the range of validity and practical applicability of time-convolutionless (TCL) master equations.

We demonstrate that the bath memory encoded in the time-convolutionless master equation (TCL_{2n}) grows with the perturbative order n, scaling as the moment $\langle t^{n-1} e^{i\omega t} \rangle$ of the bath correlation function, where ω represents a Bohr frequency. When the BCF exhibits algebraic decay, this moment diverges beyond a specific perturbative order. The presence of the exponent $e^{i\omega t}$ in the moments is crucial. It reveals two distinct types of divergences. One occurs at $\omega = 0$ and corresponds to an *infrared divergence*. The other occurs at nonzero Bohr frequencies ω, for which we introduce a new term: *secular inflation*, a concept that will be elucidated throughout this paper.

Understanding these divergences is particularly challenging because, while the open quantum system behaves as weakly coupled at and below the critical perturbative order, it effectively transitions into a strongly coupled regime beyond it. Consequently, neither conventional weak-coupling perturbation theory nor strong-coupling polaron approaches remain valid in this regime, leading to a breakdown of standard analytical techniques.

To address this issue, we introduce the *resummed master equation* (rTCL), which approximates the time-convolutionless (TCL) master equation by summing the leading cumulants across all perturbative orders. This resummation aims to capture dominant contributions beyond the perturbative regime while maintaining the TCL-like structure. Additionally, we define the truncated equations $rTCL_{2n}$,

which approximate rTCL at order $O(\lambda^{2n})$. However, despite this refinement, we find that divergences at finite n persist and do not cancel within the rTCL framework.

In the infinite-time limit, we identify two distinct types of divergences. The first is the *infrared divergence*, which arises in the generator matrix elements at zero frequency and exhibits power-law secular growth. This divergence was previously analyzed in Ref. [20]. The second divergence occurs at nonzero Bohr frequencies, leading to exponential growth in the generator. This results in a superexponential increase in the density matrix, such as an exponentiated exponential function, suggesting the presence of instabilities that may necessitate further refinements or alternative resummation techniques. As introduced before, we refer to this second divergence as *secular inflation*.

Relationship with Bogoliubov–van Hove limit and practicality. Further insight into late-time growth behaviors comes from the Bogoliubov–van Hove limit [28,29]. Davies' seminal work [21] applied this limit to master equations, showing that under the *secular approximation*, open quantum system dynamics converge to exact dynamics as $\lambda^2 \to 0$, provided that t remains within a finite bound proportional to λ^{-2}. This result implies that although TCL_{2n} or TCL master equations may produce divergences at arbitrarily weak coupling; these divergences only manifest on timescales much longer than the system's relaxation time. Consequently, any late-time growth in higher-order TCL_{2n} or TCL master equations is largely irrelevant in practical scenarios, as it occurs only after the system has reached quasistability, though this does not necessarily imply the existence of a true asymptotic state.

Key result: Precision and time limits. We demonstrate that the late-time growth in higher-order perturbative master equations imposes a fundamental precision limit on the asymptotic generator, determined by the properties of the bath correlation function. Specifically, if TCL_{2n} generator converges at $t \to \infty$ and TCL_{2n+2} does not converge, then the precision limit of the asymptotic generator is $O(\lambda^{2n})$. This precision limit constrains the achievable accuracy of asymptotic states to $O(\lambda^{2n-2})$.

In contrast, *resummation-based master equations* remain valid only within a finite-time window, during which the generator's precision is effectively capped at the previously defined limit $O(\lambda^{2n})$. Beyond this window, their accuracy deteriorates. Nevertheless, despite the fundamental limitations of perturbative expansions, resummation techniques offer a controlled approximation that remains well behaved within practical timescales, offering accuracy comparable to or even surpassing that of the Bogoliubov–van Hove limit.

Additionally, the rTCL framework preserves *continuous-time evolution*, avoiding discretization-induced noise that can arise in other numerical approaches. The method also benefits from a *straightforward implementation*, leveraging principles from the *Fermi golden rule (FGR)* and *Förster resonant energy transfer (FRET)* [30,31], both of which offer well-established techniques for handling transition rates in open quantum systems.

At this stage, we interpret the secular inflation as a sign of instability that cannot be fully captured within the master-equation framework. However, we do not yet explore the deeper question of why such precision limits emerge or their fundamental physical significance. Addressing these open questions remains a compelling direction for future research.

B. Brief review of quantum master equations

Numerous master equations (MEs) have been developed beyond the TCL_{2n} framework. Among these, the Davies secular master equation [21] is notable for its adherence to the Gorini-Kossakowski-Sudarshan-Lindblad (GKSL) form. This structure guarantees complete positivity for the full convex set of initial density matrices [32,33] and achieves return to equilibrium in the zeroth order of the interaction. Although its derivation is based on linear algebra rather than microscopic physics, the GKSL master equation remains widely popular in quantum computing, quantum gravity, cosmology, and quantum chemistry. Moreover, in baths characterized by an exponentially decaying BCF, Davies' ME can remain valid beyond the Bogoliubov–van Hove limit and at all timescales [34,35].

Nevertheless, late-time Markovian dynamics need not satisfy the GKSL criteria. In previous work [36] we demonstrated that the TCL master equation does not, in general, conform to the GKSL form. Benchmark comparisons with exact solutions further indicate that basic GKSL MEs fail to authentically capture non-Markovian dynamics [37]. In contrast, the TCL_2-Bloch-Redfield master equation, despite not adhering to the GKSL form, computes asymptotic coherences with quadratic accuracy in the interaction [38,39], a performance unattainable by any GKSL ME [40]. Additionally, enforcing complete positivity on the Bloch-Redfield equation in environments with memory can lead to violations of energy conservation, which poses significant challenges [40].

To further contextualize these developments, we introduce a "bestiary" of quantum master equations, a term coined by Colas, Grain, and Vennin [41]. Initially, several MEs implement the GKSL format; among these are the coarse-graining GKSL equations discussed in Refs. [12,42,43]. Subsequent advancements have focused on GKSL equations generated through frequency averaging, methods that include frequency binning [44,45] and the geometric-arithmetic approximation, which relates closely to both the universal Lindblad equation [46] and the geometric-arithmetic master equation [47].

A second entry within this bestiary comprises MEs that enforce thermodynamic consistency [48–50]. For example, the canonically consistent master equation [49] ensures return to equilibrium for the TCL_2 ME through generator manipulation. Although this approach mitigates population inaccuracies inherent in the Bloch-Redfield formulation, it suffers from a lack of uniqueness and is not derived from microscopic principles. Other strategies in this vein involve reconciling thermodynamic consistency with complete positivity [51–53] and enforcing positivity on the Kossakowski matrix [42,54]. Recent advancements in the TCL_{2n} approach, such as recursive formulations [55,56], HEOM-compatible versions [57], the Bogoliubov method [58], a fully algebraic TCL_{2n} [59], and extensive benchmarking against exactly solvable models and exact methods [26,60], have further enriched this landscape. Notably, the Hadamard-ordered

cumulant method introduced in this work builds on the TCL_4 generator as outlined in Ref. [20].

Perhaps the most intriguing MEs are those tailored to the physical conditions of open quantum systems. Examples include the Caldeira-Leggett master equation [61], which describes quantum diffusion; the Förster equation [30,31], applicable in systems subject to strong dephasing; as well as the modified Redfield equation [62] and the strong decoherence limit master equation [63]. We will show that these strongly dephasing MEs are closely connected to the TCL formalism developed here.

Finally, the ability of master equations to resum secular growth and perform nonperturbative resummations has been applied in modeling the early inflationary universe in cosmology [14,41,64–72]. However, it is crucial to distinguish the secular inflation discussed here, arising from the failure of cumulants to suppress the generator's growth, leading to superexponential behavior in the density matrix, from cosmic inflation in the early universe, which describes the rapid expansion of space-time driven by a scalar field. Instead, it bears closer resemblance to the problem of asymptotic completeness [73–75], often linked to infrared divergence issues in quantum field theories.

In our study, generator inflation emerges at nonzero discrete Bohr frequencies. While the model allows for ground states [76,77], it does not admit a true asymptotic state in the sense of a Kubo-Martin-Schwinger or cyclic or invariant state. From a broader perspective, if the universe itself is considered a subsystem of a larger system, then any late-time growth observed in the model should be carefully distinguished from genuine cosmic inflation.

C. Overview of the paper

This overview outlines the structure of the paper and provides guidance on how to navigate its key sections. Below is a breakdown of the main components:

(1) Setup (Sec. II)

This section consists of two parts:

(i) Standard setup: A quantum system with a finite Hilbert space dimension is coupled to a bath of linear harmonic oscillators. This follows the conventional framework used in open quantum systems [25].

(ii) Nonstandard setup: Introduces a toy model that illustrates a more complex and general phenomenon occurring in the time-convolutionless (TCL) master equation. This suggests an extension beyond conventional treatments, possibly to include stronger coupling to the bath and nontrivial non-Markovian effects.

(2) Main result (Sec. III)

(i) The paper introduces the *resummed time-convolutionless (rTCL) master equation* and its truncated versions $rTCL_{2n}$.

(ii) These resummed versions address secular growth issues by systematically incorporating higher-order corrections.

(iii) A key takeaway is that rTCL provides a natural extension of standard perturbative approaches (e.g., the TCL2-Bloch-Redfield master equation), much like how

Hartree-Fock theory extends free-electron theory in many-body physics.

(3) Derivation of resummation (Secs. IV–VI)

These sections present a detailed technical analysis of resummation methods, including partial resummations and renormalization techniques in time-ordered cumulants. Together with the Appendixes, they form a self-contained discussion that can be studied independently. Readers primarily interested in the main results may skip ahead to Sec. VII.

The content is organized as follows:

(i) Reduced state propagator and cumulant expansion: Introduction of the reduced state propagator and transition to the standard time-ordered cumulant expansion in open quantum systems.

(ii) Cumulative correlation terms: Examination of cumulative correlation terms, focusing on van Kampen's approach to cancel early secular growth.

(iii) The Hadamard trick: Extension of previous work on the TCL_4 master equation to the TCL_6 case using the Hadamard trick.

(iv) Late-time growth analysis: Identification and isolation of the fastest-growing (or slowest-decaying) cumulants at late times.

(v) Partial resummation of leading cumulants: Methods for partially resumming leading cumulants to mitigate secular growth.

(vi) Two forms of divergences: In open quantum systems interacting with spectral baths, *infrared divergence* and *secular inflation* both lead to unbounded growth in quantities such as the density matrix or correlation functions. However, they differ in their origins and long-term effects. Infrared divergence occurs at low frequencies due to a power-law behavior in the bath's spectral density, while secular inflation takes place at nonzero frequencies, resulting in superexponential growth in system observables.

(4) Properties of resummation and application to the spin-boson model (Sec. VII)

The subsections of Sec. VII can be read independently, allowing readers to focus on areas of interest without the need to go through the entire section.

(i) The discussion begins with the *general properties of the resummed time-convolutionless (rTCL) ME* in arbitrary open quantum systems.

(ii) It then examines how rTCL evolves over time in the *spin-$\frac{1}{2}$ boson model*, emphasizing the impact of complex frequency renormalization on late-time inflation in the generator.

(iii) The *critical* TCL_{2n} is introduced, marking the boundary between secular growth and the proper Markovian limit. This is followed by an analysis of rTCL behavior in an *Ohmic environment* and an investigation into the *time limit of resummation's validity*.

(iv) The section further explores the system's *approach to the ground state* and its *return to equilibrium*. It then addresses the proper Markovian limit in cases where the bath correlation function decays exponentially.

(v) Finally, the *strong dephasing limit* is discussed, along with its connection to Förster's resonant energy transfer model.

II. SETUP AND MODEL

In the standard framework of open quantum systems that we adopt, the total Hamiltonian is given by

$$H_T = H_0 + H_I, \quad (3)$$

where H_0 represents the Hamiltonian of the decoupled system and environment (bath), and H_I describes the interaction between them. We further decompose H_0 as as

$$H_0 = H_S + H_B, \quad (4)$$

where H_S represents the Hamiltonian of the isolated system, acting on the Hilbert space $\mathcal{H}_S$:

$$H_S = \sum_{n=1}^{N} E_n |n\rangle\langle n|. \quad (5)$$

The eigenenergies E_n are nondegenerate and arranged in ascending order. The Bohr frequencies are defined as $\omega_{nm} = E_n - E_m$.

The bath Hamiltonian H_B operates within the bath Fock space $\mathcal{H}_F$ and is given as

$$H_B = \sum_k \omega_k b_k^\dagger b_k, \quad (6)$$

where k denotes normal modes with frequencies $\omega_k \geqslant 0$. We adopt a system of units where $\hbar = 1$. The creation and annihilation operators $b_k^\dagger$ and b_k satisfy the canonical commutation relation

$$[b_k, b_q^\dagger] = \delta_{k,q}, \quad (7)$$

where $\delta_{k,q}$ is the Kronecker delta.

The interaction Hamiltonian H_I describes the system-bath coupling and is a Hermitian operator proportional to a dimensionless coupling constant λ. In the weak-coupling limit, $\lambda \ll 1$. The interaction Hamiltonian is bilinear and takes the form

$$H_I = A \otimes F, \quad (8)$$

where A and F are the system and bath coupling operators, respectively. A is dimensionless. The bath coupling operator can be expressed as

$$F = \sum_k g_k(b_k + b_k^\dagger), \quad (9)$$

where g_k is a real form factor with the physical units of frequency.

Liouville master equation and initial state. The Liouville master equation for the total system in the interaction picture is given by

$$\frac{d\varrho_T(t)}{dt} = -i[H_I(t), \varrho_T(t)] \equiv \mathcal{L}_I(t)\varrho(t), \quad (10)$$

where

(a) $H_I(t) = e^{iH_0t} H_I e^{-iH_0t}$ is the interaction Hamiltonian in the interaction picture,

(b) $\varrho_T(t) = e^{iH_0t}\rho_T(t)e^{-iH_0t}$ is the total system-bath density matrix in the interaction picture, and

(c) $\mathcal{L}_I(t)$ is the interaction picture Liouvillian, a superoperator acting on the density matrix.

At the initial time $t = t_i$, the system and bath are assumed to be in a *factorized state*

$$\varrho_T(t_i) = \varrho(t_i) \otimes \rho_B. \quad (11)$$

This assumption ensures that the evolution of the system's reduced state,

$$\varrho(t) = \text{Tr}_B[\varrho_T(t)], \quad (12)$$

defines a completely positive quantum-dynamical map.

The reference state of the bath ρ_B is taken to be the *Kubo-Martin-Schwinger (KMS) state*, which corresponds to the thermal equilibrium state of the isolated bath

$$\rho_B = \frac{e^{-\beta H_B}}{\text{Tr}[e^{-\beta H_B}]}. \quad (13)$$

This ensures that the bath satisfies detailed balance conditions and remains in thermal equilibrium in the absence of interaction with the system.

Spectral density and bath correlation function. The harmonic bath is fully characterized by its spectral density at absolute zero temperature:

$$J_\omega = \pi \sum_k g_k^2 \delta(\omega - \omega_k) \mapsto 2\pi\lambda^2 \frac{\omega^s}{\omega_c^{s-1}} e^{-\frac{\omega}{\omega_c}} \Theta(\omega), \quad (14)$$

where ω_c is the cutoff frequency, λ^2 (the Kondo parameter) represents the weak-coupling constant, and $\Theta(\omega)$ is the Heaviside step, respectively. The dispersion parameter s determines the bath type: (i) Ohmic ($s = 1$), (ii) sub-Ohmic ($0 < s < 1$), and (iii) super-Ohmic ($s > 1$). The bath correlation function (BCF) is defined as

$$C(t) = \langle F(t)F(0)\rangle = \text{Tr}[\rho_B F(t)F(0)]. \quad (15)$$

At zero temperature, the BCF takes the form

$$C(t) = \frac{1}{\pi}\int_{-\infty}^{\infty} d\omega\, J_\omega e^{-i\omega t} = \frac{2\lambda^2\omega_c^2\Gamma(s+1)}{(1 + i\omega_c t)^{s+1}}. \quad (16)$$

At finite temperature T, the BCF is given by

$$C_\beta(t) = \frac{1}{\pi}\int_0^\infty d\omega\, J_\omega\left[\cos(\omega t)\coth\frac{\beta\omega}{2} - i\sin(\omega t)\right] \quad (17)$$

$$= \frac{1}{\pi}\int_{-\infty}^\infty d\omega\, J_{\beta,\omega} e^{-i\omega t}, \quad (18)$$

where $\beta = 1/k_B T$. The finite-temperature spectral density satisfies the KMS conditions

$$J_{\beta,\omega} = \frac{J_\omega}{1 - e^{-\beta\omega}}, \quad \omega > 0 \quad (19)$$

$$J_{\beta,-\omega} = e^{-\beta\omega}J_{\beta,\omega}. \quad (20)$$

We introduce the time-dependent spectral density as

$$\Gamma_{\beta,\omega}(t) = \int_0^t dt_1\, C_\beta(t_1)e^{i\omega t_1} \equiv J_{\beta,\omega}(t) + iS_{\beta,\omega}(t). \quad (21)$$

At $T = 0$, the subscript β is omitted. The spectral density satisfies

$$\Gamma_{\beta,\omega}(t) = -\Gamma_{\beta,\omega}^\star(-t). \quad (22)$$

For the BCF in Eq. (16), $\Gamma_\omega(t)$ is expressed in terms of incomplete gamma functions [20, Eq. (25)]. In the asymptotic

limit $t \to \infty$, we define

$$\Gamma_\omega \equiv \lim_{t \to \infty} \Gamma_\omega(t) = J_\omega + iS_\omega \tag{23}$$

(real and imaginary parts), where

$$\Gamma_\omega = \begin{cases} -2i\lambda^2 \Gamma(s+1)\omega_c(-\omega/\omega_c)^s e^{-\omega/\omega_c} \Gamma\left(-s, -\frac{\omega}{\omega_c}\right) & \text{if } \omega \neq 0, \\ -2i\lambda^2 \omega_c \Gamma(s) & \text{otherwise.} \end{cases} \tag{24}$$

At $t \gg 1/\omega_c$, the asymptotic behavior is

$$\Gamma_\omega(t) = \Gamma_\omega + \begin{cases} \frac{-2i\lambda^2 \Gamma(s+1)\omega_c^2}{\omega} \frac{e^{i\omega t}}{(1+i\omega_c t)^{1+s}}, & \omega \neq 0 \\ \frac{-2i\lambda^2 \omega_c \Gamma(s)}{(1+i\omega_c t)^s}, & \omega = 0. \end{cases} \tag{25}$$

The spectral density satisfies the *Kramers-Kronig* relation

$$S_{\beta,\omega} = \int_{-\infty}^{\infty} d\omega' \frac{J_{\beta,\omega'}}{\pi(\omega - \omega')}. \tag{26}$$

At zero frequency, the *reorganization energy* (temperature independent) is given by

$$E_r \equiv -S_0 = \int_0^\infty \frac{d\omega \, J_\omega}{\pi \omega}. \tag{27}$$

Nonstandard setup. When using resummation techniques to capture the late-time dynamics of master equations, we may encounter complex frequencies. These frequencies always appear in antisymmetric pairs, which has significant consequences for the evolution of the density matrix. Specifically, while some matrix elements exhibit exponential decay (associated with relaxation), others exhibit superexponential growth due to the exponential growth of the generator,–a phenomenon we refer to as *secular inflation*. This unphysical growth presents a fundamental problem of the resummation, as it contradicts the unitarity of the combined system and environment.

To illustrate this phenomenon, we consider a simplified toy model that captures key aspects of a more complex behavior in the TCL master equation. In this example, the system exhibits four complex frequencies: $\omega = \pm 1 \pm 0.15i$. Our goal is to compute the time-dependent spectral density using Eq. (21).

Figures 1(a) and 1(b) show $\text{Re} \, \Gamma_\omega(t)$ for $\omega = -1 \pm 0.15i$, represented by the solid red lines. The dashed black lines indicate the asymptotic spectral density ($t \to \infty$), $\text{Re} \, \Gamma_\omega$, obtained by analytical continuation of Eq. (24) from the real axis. For frequencies with $\text{Im} \, \omega = 0.15i$, the spectral density smoothly approaches the analytic continuation. In contrast, for frequencies with $\text{Im} \, \omega = -0.15i$, the spectral density fails to reach the analytic continuation due to increasing oscillation amplitudes over time. The average value of these oscillations corresponds to the analytic continuation represented by the dashed line.

Specifically, when $\text{Im} \, \omega < 0$, Eq. (25) explicitly demonstrates this growth. However, the asymptotic limit described by Eq. (24) is an analytic function of ω on the real axis (except at isolated points or along a branch cut) and can be analytically continued into both the upper and lower complex planes. This suggests that a Markovian regime can still be defined even for $\text{Im} \, \omega < 0$, but such regime cannot be seen as the limit of non-Markovian dynamics.

To enforce the Markovian regime in such cases, we simply remove the oscillatory inflationary term. In this context, a master equation at complex frequencies can be interpreted in two ways: as a non-Markovian equation with a finite-time window of validity, or as a Markovian equation valid in the infinite-time limit. Similarly, Figs. 1(c) and 1(d) show $\text{Re} \, \Gamma_\omega(t)$ at $\omega = 1 \pm 0.15i$, revealing slight downward shifts relative to 2π (e.g., the spectral density at $\omega = 1$). For frequencies with a negative imaginary part, the time-dependent spectral density exhibits oscillations around the analytic continuation, with these oscillations growing exponentially over time. In the Markovian description, the increasing oscillations are replaced by the analytic continuation (dashed line). In this toy example, the inflation rate is 0.15. Later, we will see that this rate remains independent of temperature. However, the onset of inflation in the time-dependent spectral density,– corresponding to the time limit of validity for the master equations, shows a significant temperature dependence.

Figure 2 illustrates $\text{Re} \, \Gamma_{\beta,\omega}(t)$ at $\omega = 1 - 0.15i$ for different temperatures $k_B T = 0$, 0.01, 0.05, 0.2, and 0.5. As
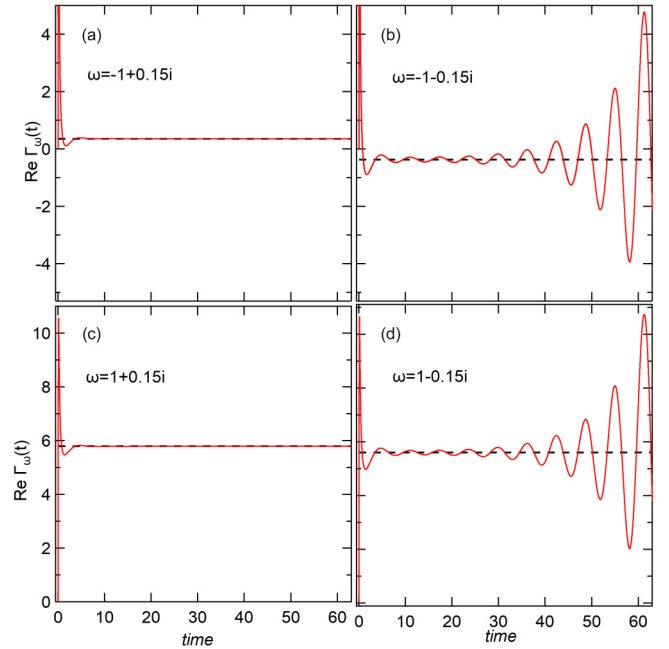

FIG. 1. Real-part time-dependent spectral density at complex frequencies and zero temperature (full red curves) and analytic continuation of the asymptotic spectral density from real frequency axis (dashed black lines). (a) $\omega = -1 + 0.15i$; (b) $\omega = -1 - 0.15i$; (c) $\omega = 1 + 0.15i$; and (d) $\omega = 1 - 0.15i$. $\omega_c = 10$, $\lambda^2 = 1$, and $s = 1$. The inflation at discrete Bohr frequencies manifests in (c) and (d) as increasing oscillation amplitude around the dashed line.
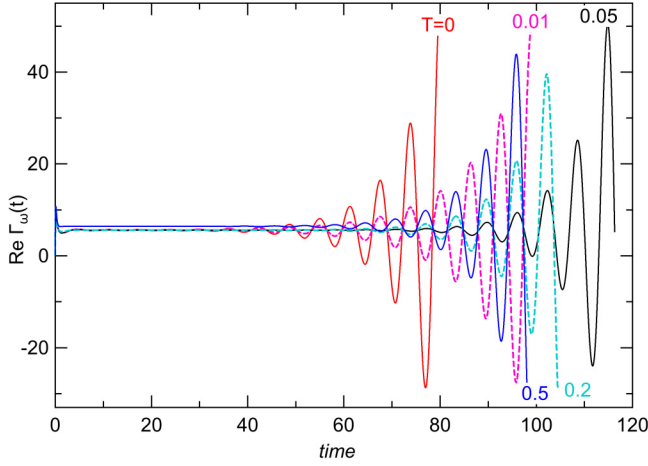
FIG. 2. Real-part time-dependent spectral density at $\omega = 1 - 0.15i$ and five temperatures. The onset of inflation in time has strong temperature dependence at very small temperatures relative to ω, and includes a maximum onset time near $T = 0.05$ associated with a phase change.

temperature increases from 0 to approximately 0.05, the onset of growth shifts to later times. However, at higher temperatures, this trend reverses, and the time limit decreases with increasing temperature. Despite these changes, the average spectral density remains nearly constant over this temperature range.

III. MAIN RESULT

An infinite variety of master equations can be constructed by performing partial resummations of time-ordered cumulants. In this work, we highlight two key formulations: the resummed time-convolutionless (rTCL) master equation and the renormalized TCL_{2n} master equation (rTCL_{2n}). These two approaches are related as follows:

$$\text{rTCL} = \lim_{n \to \infty} \text{rTCL}_{2n}. \tag{28}$$

These MEs preserve trace and Hermiticity; however, they are not guaranteed to be completely positive. rTCL_{2n} are much more user friendly than the TCL_{2n} master equations. The reason is that rTCL_{2n} and rTCL represent a modification of TCL_2. Specifically, they can be explicitly formulated in terms of the spectral density and its derivatives at a single frequency, requiring little overhead relative to the TCL_2.

A. Resummed TCL (rTCL and mrTCL)

The resummed master equation (rTCL) extends the conventional TCL_2-Bloch-Redfield master equation by incorporating renormalized Bohr frequencies. In the Schrödinger picture, it takes the form

$$\frac{\partial \rho_{nm}}{\partial t} = -i\omega_{nm}\rho_{nm} + \sum_{ij} A_{ni}A_{jm}\left[\Gamma_{\omega'_{in}(j,t)}(t) + \Gamma^\star_{\omega'_{jm}(i,t)}(t)\right]\rho_{ij}$$

$$- \sum_{ik} A_{nk}A_{ki}\Gamma_{\omega'_{ik}(j,t)}(t)\rho_{im}$$

$$- \sum_{jk} A_{jk}A_{km}\Gamma^\star_{\omega'_{jk}(i,t)}(t)\rho_{nj}. \tag{29}$$

The corresponding dissipator has matrix elements

$$L^r_{nm,ij}(t) = A_{ni}A_{jm}\left[\Gamma_{\omega'_{in}(j,t)}(t) + \Gamma^\star_{\omega'_{jm}(i,t)}(t)\right]$$

$$- \sum_k \left[\delta_{jm}A_{nk}A_{ki}\Gamma_{\omega'_{ik}(j,t)}(t)\right.$$

$$\left. + \delta_{ni}A_{jk}A_{km}\Gamma^\star_{\omega'_{jk}(i,t)}(t)\right]. \tag{30}$$

Although this structure resembles the conventional TCL_2-Bloch-Redfield dissipator

$$L^2_{nm,ij}(t) = A_{ni}A_{jm}\left[\Gamma_{\omega_{in}}(t) + \Gamma^\star_{\omega_{jm}}(t)\right]$$

$$- \sum_k \left[\delta_{jm}A_{nk}A_{ki}\Gamma_{\omega_{ik}}(t) + \delta_{ni}A_{jk}A_{km}\Gamma^\star_{\omega_{jk}}(t)\right], \tag{31}$$

the key distinction in rTCL lies in the *frequency renormalization*:

$$\omega_{in} \mapsto \omega'_{in}(j,t) = \omega_{in} - i\left[\sum_c (|A_{ic}|^2 \Gamma_{\omega_{ic}}(t) - |A_{nc}|^2 \Gamma_{\omega_{nc}}(t))\right.$$

$$\left. + 2J_0(t)A_{jj}(A_{nn} - A_{ii})\right]. \tag{32}$$

A crucial observation is that this equation may not have a well-defined limit as $t \to \infty$. To address this, we introduce a Markovian approximation (mrTCL) by taking the following steps:

(1) *Asymptotic limit of frequencies*: We evaluate the frequency renormalization in the long-time limit:

$$\omega'_{in}(j) = \omega_{in} - i\left[\sum_c \left(|A_{ic}|^2 \Gamma_{\omega_{ic}} - |A_{nc}|^2 \Gamma_{\omega_{nc}}\right)\right.$$

$$\left. + 2J_0 A_{jj}(A_{nn} - A_{ii})\right]. \tag{33}$$

Here, the terms $-i\sum_c(|A_{ic}|^2\Gamma_{\omega_{ic}} - |A_{nc}|^2\Gamma_{\omega_{nc}})$ and $-2iJ_0A_{jj}(A_{nn} - A_{ii})$ represent the *quasiparticle shift* and the *spectral overlap*, respectively, as explained in Secs. VII A and VII H.

(2) *Analytical continuation of the spectral density*: Provided that Γ_ω is analytic at real ω, we replace ω_{in} with $\omega'_{in}(j)$ in $\Gamma_{\omega_{in}}$, leading to the *Markovian rTCL (mrTCL)* master equation with the generator

$$L^{mr}_{nm,ij} = A_{ni}A_{jm}\left[\Gamma_{\omega'_{in}(j)} + \Gamma^\star_{\omega'_{jm}(i)}\right]$$

$$- \sum_k \left[\delta_{jm}A_{nk}A_{ki}\Gamma_{\omega'_{ik}(j)} + \delta_{ni}A_{jk}A_{km}\Gamma^\star_{\omega'_{jk}(i)}\right]. \tag{34}$$

Interpretation and limitations. It is important to note that *mrTCL is not a direct continuation of rTCL* when the limit $t \to \infty$ does not exist in Eq. (30). Since the spectral overlap involves the nonlocal term A_{jj}, the renormalization is meaningful *only* when incorporated into the master equations (29) or the generators (30) and (34). The renormalized Bohr frequencies satisfy an *antisymmetry* property

$$\omega'_{in}(j,t) = -\omega'_{ni}(j,t), \tag{35}$$

which ensures that the diagonal elements vanish:

$$\omega'_{nn}(j,t) = 0. \tag{36}$$

For *nonzero temperatures*, a subscript β is appended to all spectral densities.

Finally, in special cases (i) if A_{nn} is *uniform* (pure relaxation), the renormalized frequency becomes *localized*, meaning that $\omega'_{in}(j, t)$ looses the dependence on j; (ii) if A is *diagonal* (pure dephasing), the resummation equation includes only *diagonal frequencies*, ensuring that $\omega'_{nn}(j, t) = 0$. In this case, the TCL$_2$ and rTCL equations become identical.

B. Renormalized TCL$_{2n}$ (rTCL$_{2n}$ and mrTCL$_{2n}$)

The renormalized master equations are derived using a multivariable Taylor expansion of the generator in Eq. (29), achieving a precision of $O(\lambda^{2n})$. This procedure introduces a renormalization of the spectral density, which is now expressed as a function of the bare Bohr frequencies:

$$\Gamma^n_{\omega_{il}}(j, t) = \sum_{k=0}^{n-1} \frac{(-i)^k}{k!} \frac{\partial^k \Gamma_{\omega_{il}}(t)}{\partial \omega_{il}^k} \left[\sum_c \left(|A_{ic}|^2 \Gamma_{\omega_{ic}}(t) \right. \right.$$
$$\left. \left. - |A_{lc}|^2 \Gamma_{\omega_{lc}}(t) \right) + 2J_0(t) A_{jj}(A_{ll} - A_{ii}) \right]^k. \quad (37)$$

The rTCL$_{2n}$ dissipator remains nonlocal in frequency and takes the form

$$L^{r2n}_{lm,ij}(t) = A_{li} A_{jm} \Gamma^n_{\omega_{il}}(j, t)$$
$$- \sum_k \delta_{jm} A_{lk} A_{ki} \Gamma^n_{\omega_{ik}}(j, t) + \text{r.H.c.} + \tilde{L}^{r2n}_{lm,ij}, \quad (38)$$

where r.H.c. represents the realigned Hermitian conjugate (e.g., $L_{lm,ij} \mapsto L^\star_{ml,ji}$). The additional Liouvillian term $\tilde{L}^{r2n}$ is optional and accounts for nonembeddable terms in the TCL$_{2n}$ generator that contribute to the same late-time growth category as the embeddable terms. For $n = 1$, these terms are absent, so $\tilde{L}^{r2} = 0$.

For example, when $n = 2$ and $T > 0$, we include the $\tilde{L}^{r4}$ term given by Eqs. (G22)–(G24). As we will see, rTCL$_4$ provides a significantly improved approximation of the system's approach to the ground state in the spin-boson model (SBM) for a qubit, achieving quadratic precision in the interaction Hamiltonian. This is a notable improvement over TCL$_2$ and the Davies master equation. However, at zero temperature, $\tilde{L}^{r4}$ does not contribute to ground-state corrections and can be omitted.

Nevertheless, we include $\tilde{L}^{r4}$ because, while the first two terms in Eq. (38) correctly indicate ground-state approach at zero temperature, they fail to restore equilibrium at finite temperatures with quadratic precision. The inclusion of $\tilde{L}^{r4}$ ensures equilibrium restoration with quadratic precision for population dynamics, provided there is no dephasing. However, in the presence of dephasing, characterized by nonuniform A_{nn} and $T > 0$, achieving quadratic precision for equilibrium restoration using only the slowest-decaying cumulants is not feasible. In such cases, only the full TCL$_4$ generator guarantees quadratic precision in an arbitrary open quantum system.

For practical applications, the full TCL$_4$ master equation, as derived in [20], should be used whenever possible, as it is more robust despite being computationally more demanding. However, for quick assessments of the dynamics, rTCL$_4$

may serve as a sufficient approximation. Depending on the dispersion parameter s, rTCL$_{2n}$ may or may not reach the Markovian limit as $t \to \infty$. Regardless of this, we define the Markovian version of these generators, mrTCL$_{2n}$, by applying a multivariable Taylor expansion to the generator in Eq. (34) and taking the limit $t \to \infty$ in Eqs. (37) and (31).

IV. DERIVATION

Although rTCL and rTCL$_{2n}$ are expressed in relatively simple forms, their derivation involves intricate methodologies, including systematic resummation techniques, multivariable Taylor expansions, and frequency renormalization to mitigate secular divergences. These techniques extend beyond conventional perturbative methods, ensuring a more refined description of open quantum system dynamics.

A common approach in open quantum systems employs the projection superoperator:

$$\mathcal{P}\varrho_T = (\text{Tr}_B \varrho_T) \otimes \rho_B \equiv \varrho \otimes \rho_B. \quad (39)$$

The reduced state propagator is then obtained by applying $\mathcal{P}$ to the formal solution of the Liouville equation (10):

$$\varrho_T(t) = T_\leftarrow e^{\int_{t_i}^t d\tau \, \mathcal{L}_I(\tau)} \varrho_T(t_i), \quad (40)$$

where $T_\leftarrow$ denotes chronological time ordering. Using the factorized initial condition $\varrho_T(t_i) = \mathcal{P}\varrho_T(t_i)$ and the property $\mathcal{P}\mathcal{L} I^k \mathcal{P} = 0$ for odd k [25], we obtain

$$\mathcal{P}\varrho_T(t) = \left[1 + \iint_\leftarrow^t dt_{12} \mathcal{P}\mathcal{L}_I(t_1)\mathcal{L}_I(t_2)\mathcal{P} \right.$$
$$+ \iiiint_\leftarrow^t dt_{1234} \mathcal{P}\mathcal{L}_I(t_1)\mathcal{L}_I(t_2)\mathcal{L}_I(t_3)\mathcal{L}_I(t_4)\mathcal{P}$$
$$\left. + \cdots \right] \mathcal{P}\varrho_T(t_i). \quad (41)$$

Here, the integral notation is shorthand for

$$\int \cdots \int_\leftarrow^t dt_{1...n} = \int_{t_i}^t dt_1 \int_{t_i}^{t_1} dt_2 \cdots \int_{t_i}^{t_{n-1}} dt_n. \quad (42)$$

By tracing over the bath, we express the reduced state propagator as

$$\varrho(t) = Y(t)\varrho(t_i) = \sum_{n=0}^\infty Y^{2n}(t)\varrho(t_i), \quad (43)$$

where $Y^0 = \mathbb{1}$ and

$$Y^{2n}(t) = \text{Tr}_B \int \cdots \int_\leftarrow^t dt_{1...2n} \mathcal{P}\mathcal{L}_I(t_1)\ldots\mathcal{L}_I(t_{2n})\mathcal{P}. \quad (44)$$

Expanding $\mathcal{L}_I(t_a) = -i[H_I(t_a), \ldots]$ leads to a nested commutator structure, which is challenging to handle. To simplify this, Wick's theorem is applied after unnesting the commutators, as detailed in Appendix B of Ref. [72].

However, the propagators $Y^{2n}(t)$ exhibit secular growth, which makes them impractical for direct applications. A partial resummation method can be used to eliminate this growth by summing the dominant terms while neglecting subleading contributions. Master equations offer an alternative approach, effectively implementing partial resummations.

A. Time-convolutionless (TCL) master equation

Following the approach in [11], we begin by differentiating Eq. (43):

$$\frac{d\varrho(t)}{dt} = \sum_{n=0}^{\infty} \frac{dY_{2n}(t)}{dt} \varrho(t_i). \qquad (45)$$

Since $Y_0 = 1$, its derivative vanishes, leaving

$$\frac{d\varrho(t)}{dt} = \sum_{n=1}^{\infty} \frac{dY^{2n}(t)}{dt} \varrho(t_i). \qquad (46)$$

Using Eq. (44), we differentiate each term:

$$\frac{dY_{2n}(t)}{dt} = \text{Tr}_B \int \cdots \int_{\leftarrow}^{t} dt_{1\dots 2n-1} \mathcal{P}\mathcal{L}_I(t)\mathcal{L}_I(t_1)$$
$$\times \dots \mathcal{L}_I(t_{2n-1})\mathcal{P}. \qquad (47)$$

Next, we express $\varrho(t_i)$ in terms of $\varrho(t)$. This requires inverting $\varrho(t_i)$ in Eq. (43). Inserting $\varrho(t_i)$ into the right-hand

side of Eq. (46), the result is the *time-convolutionless (TCL) master equation*

$$\frac{d\varrho(t)}{dt} = L(t)\varrho(t). \qquad (48)$$

The formal solution to this equation is given by

$$\varrho(t) = T_{\leftarrow} e^{\int_{t_i}^{t} L(t_1)dt_1} \varrho(t_i), \qquad (49)$$

where the generator $L(t)$ is expanded as

$$L(t) = \sum_{n=1}^{\infty} L^{2n}(t), \qquad (50)$$

with each term $L^{2n}(t)$ representing an $O(\lambda^{2n})$ contribution. This formulation helps mitigate secular divergences under specific conditions and enables systematic truncation at finite orders, providing approximate solutions for the system's dynamics.

The generators for the TCL$_2$, TCL$_4$, and TCL$_6$ master equations are given in terms of the moments of the interaction-picture Liouvillians:

$$L^2(t) = \text{Tr}_B \int_{t_i}^{t} dt_1 \, \mathcal{P}\mathcal{L}_I(t)\mathcal{L}_I(t_1)\mathcal{P}, \qquad (51)$$

$$L^4(t) = \text{Tr}_B \iiint_{\leftarrow}^{t} dt_{123}[\mathcal{P}\mathcal{L}_I(t)\mathcal{L}_I(t_1)\mathcal{L}_I(t_2)\mathcal{L}_I(t_3)\mathcal{P} - \mathcal{P}\mathcal{L}_I(t)\mathcal{L}_I(t_1)\mathcal{P}\mathcal{L}_I(t_2)\mathcal{L}_I(t_3)\mathcal{P}] \qquad (52)$$

$$- [\mathcal{P}\mathcal{L}_I(t)\mathcal{L}_I(t_2)\mathcal{P}\mathcal{L}_I(t_1)\mathcal{L}_I(t_3)\mathcal{P} - \mathcal{P}\mathcal{L}_I(t)\mathcal{L}_I(t_3)\mathcal{P}\mathcal{L}_I(t_1)\mathcal{L}_I(t_2)\mathcal{P}]. \qquad (53)$$

$$L^6(t) = \text{Tr}_B \int \cdots \int_{\leftarrow}^{t} dt_{1\dots 5} \Bigg[\mathcal{P}\mathcal{L}_I(t)\mathcal{L}_I(t_1)\mathcal{L}_I(t_2)\mathcal{L}_I(t_3)\mathcal{L}_I(t_4\mathcal{L}_I(t_5)\mathcal{P} \qquad (54)$$

$$- \sum_p \mathcal{P}\mathcal{L}_I(t)\mathcal{L}_I(t_{p_1})\mathcal{P}\mathcal{L}_I(t_{p_2})\mathcal{L}_I(t_{p_3})\mathcal{L}_I(t_{p_4})\mathcal{L}_I(t_{p_5})\mathcal{P} \qquad (55)$$

$$- \sum_p \mathcal{P}\mathcal{L}_I(t)\mathcal{L}_I(t_{p_1})\mathcal{L}_I(t_{p_2})\mathcal{L}_I(t_{p_3})\mathcal{P}\mathcal{L}_I(t_{p_4})\mathcal{L}_I(t_{p_5})\mathcal{P} \qquad (56)$$

$$+ \sum_q \mathcal{P}\mathcal{L}_I(t)\mathcal{L}_I(t_{q_1})\mathcal{P}\mathcal{L}_I(t_{q_2})\mathcal{L}_I(t_{q_3})\mathcal{P}\mathcal{L}_I(t_{q_4})\mathcal{L}_I(t_{q_5})\mathcal{P} \Bigg]. \qquad (57)$$

In Eqs. (55) and (56), the product of six interaction-picture Liouvillians $\mathcal{L}_I$ is split into two subproducts by inserting a projection operator $\mathcal{P}$. The variable p represents represents all possible permutations of the time arguments $t_1, \dots, t_5$, with the only constraint that the time arguments within each subproduct must be arranged chronologically. The ordered cumulant in each term is obtained by summing over five and ten permissible distributions of the time variables t_{p_i}, for equation lines (55) and (56), respectively. Similarly, in Eq. (57), the summation over q is taken over the 30 valid distributions of time indices among the nested terms, ensuring proper chronological ordering.

V. GENERATOR LATE-TIME GROWTHS

In our previous work [20], we derived the irreducible form of the TCL$_4$ generator, meaning that it cannot be further simplified. Here, we take a different approach by expressing the TCL$_4$ generator in a more fundamental form and extending

this methodology to derive the TCL$_6$ generator in the same representation. By directly comparing these formulations, we aim to identify the dominant polynomial growth terms that emerge in environments where the BCF exhibits algebraic decay. This comparison provides insight into the late-time behavior of the generator and its dependence on bath properties.

A. Cumulative correlation terms

The subsequent step involves transforming Eqs. (51)–(57) into cumulative correlation terms. We first demonstrate this explicitly for the TCL$_2$ generator. From Eq. (51), we find

$$L^2(t)\varrho(t) = \text{Tr}_B \int_{t_i}^{t} dt_1 \mathcal{P}\mathcal{L}_{\mathcal{I}}(t)\mathcal{L}_{\mathcal{I}}(t_1)\mathcal{P}\varrho_T(t) \qquad (58)$$

$$= -\text{Tr}_B \mathcal{P} \int_{t_i}^{t} dt_1 [A(t) \otimes F(t),$$
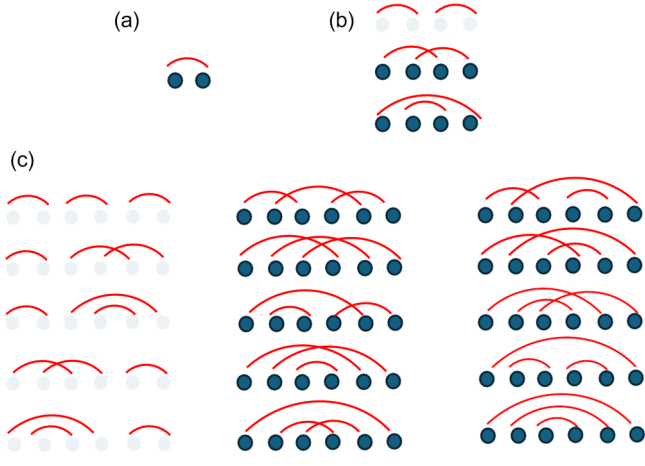$$[A(t_1) \otimes F(t_1), \mathcal{P}\varrho_T(t)]]. \qquad (59)$$

FIG. 3. Time connections in the expansion of ordered cumulants. (a) TCL$_2$ pair and (b) TCL$_4$ quartets consist of three pairings, of which two are nonzero (bold blue). TCL$_6$ comprises 15 distinct sixtuplets with varying time pairings. In the cumulants, the nonoverlapping pairings sum up zero (left column, light blue). Ten remaining pairings contribute to the cumulants (middle and right columns, dark blue).

Introducing the shorthand $t_0 = t$, as well as $A(t) = \hat{0}$, $A(t_1) = \hat{1}$, and $C(t - t_1) = \langle 01 \rangle$, and tracing over the bath we obtain the single cumulative correlation term

$$L^2(t)\varrho(t) = -\left[\hat{0}, \int_{t_i}^{t} dt_1 \langle 01 \rangle \hat{1} \varrho(t)\right] + \text{H.c.} \quad (60)$$

This term is represented diagrammatically in Fig. 3(a) as a pair of dots connected by the BCF $\langle 01 \rangle$.

Analogous cumulative correlation terms in this shorthand notation were derived for TCL$_4$ in Ref. [78, Eq. (29)] for TCL$_4$. In Fig. 3(b), these correspond to four points at times t, t_1, t_2, and t_3, with three possible pairings. The first consists of two disconnected pairs, each contributing to a TCL$_2$ cumulative term. However, time-ordered cumulants systematically exclude such cumulants containing statistically uncorrelated segments. The remaining two pairings, which remain nonzero in the cumulant expansion, exhibit late-time growth that is constrained solely by the decay properties of the BCF. This results in a competition between the polynomial growth dictated by the triple time-ordered integral and the relaxation in the BCF. In van Kampen's original approach [10,11], bath correlations decay rapidly enough to suppress this growth. However, in the present case, the decay is not always sufficiently fast to prevent secular growths from emerging.

Next, we examine how competition between different terms manifests in the TCL$_6$ generator. The analysis begins by unnesting the commutators in the relevant equations and applying Wick's theorem to express products of bath operators in terms of BCFs with valid time arguments.

The term $\mathcal{PLLLLLLP}$ expands into 960 products of three BCFs and system operators, plus the Hermitian conjugates. To simplify the expression, the system operators and the density matrix are reorganized into nested commutators, significantly reducing the number of terms. This leads to 60 nested commutators, each paired with one of 60 BCF triplets at permissible

time arguments. These triplets are further categorized into 15 unique time pairings, as depicted in Fig. 3(c).

A similar approach is applied to the additional term $\mathcal{PLLPLLLLP}$, $\mathcal{PLLLLPLLP}$, and $\mathcal{PLLPLLPLLP}$. Each of these also results in 60 nested commutators distributed across 60 BCF triplets and 15 time pairings. When summing over the nested commutators for all these terms, it is found that five pairings from the leftmost column of Fig. 3(c) cancel out. These cancellations correspond to statistically unconnected segments of the cumulative correlation terms from TCL$_2$ and TCL$_4$. As a result, 10 statistically connected time pairings remain.

If the BCF exhibits algebraic decay, the remaining cumulants may experience growth depending on the decay parameter ss. A detailed investigation of this behavior follows in the next subsections.

The complete set of TCL$_6$ cumulative correlation terms and the link to a repository with further details is given in Appendix F. Three representative terms include

$$\frac{d\varrho}{dt} = -\left[\hat{0}, \int \cdots \int_{\leftarrow}^{t} dt_{1...5} \left(\cdots \right.\right. \quad (61)$$

$$+ \langle 02 \rangle \langle 14 \rangle \langle 35 \rangle ([\hat{1}, \hat{2}][\hat{3}, \hat{4}]\hat{5}\varrho) + \cdots \quad (62)$$

$$+ \langle 03 \rangle \langle 14 \rangle \langle 52 \rangle (\hat{3}[\hat{1}, [\hat{2}, \hat{4}]\varrho\hat{5}] \right.$$

$$- [\hat{1}, [\hat{2}, \hat{3}\hat{4}]\varrho\hat{5}] + [\hat{2}, \hat{3}][\hat{1}, \hat{4}\varrho]\hat{5}) + \cdots \quad (63)$$

$$+ \langle 04 \rangle \langle 12 \rangle \langle 35 \rangle (-[\hat{3}, \hat{4}]\hat{5}[\hat{1}, \hat{2}\varrho]$$

$$\left.\left. + [\hat{1}, \hat{2}[\hat{3}, \hat{4}]\hat{5}\varrho]) + \cdots \right) \right] \quad (64)$$

$$+ \text{H.c.} \quad (65)$$

B. Hadamard trick

In the next step, we simplify the number of time-ordered integrals by applying the Hadamard trick. This technique allows us to obtain exact time-ordered cumulants without assuming that bath correlations decay very rapidly. This assumption was a key factor in van Kampen's approach to avoiding secular growth. However, in our case, we will see that late-time growth of the generator matrix elements begins at $n > n_{\max}$, depending on the parameter s and whether the frequency is zero or not.

To proceed, we first examine the expression for a cumulative correlation term of order $2n$. Before restructuring the system operators into commutators to reduce the number of terms, we had the following integral to evaluate:

$$\int \cdots \int_{\leftarrow}^{t} dt_{1...2n-1} C(t_{p_0} - t_{p_1}) C(t_{p_2} - t_{p_3}) \ldots$$

$$C(t_{p_{2n-1}} - t_{p_{2n-2}}) \hat{0}\hat{1} \ldots \varrho \ldots \hat{K}. \quad (66)$$

Here, $K = 2n - 1$ and p denotes a permutation of the set $0, 1, 2, \ldots, 2n - 1$, and t_0 is defined as t. As in the previous section, we will use the shorthand $\langle ab \rangle = C(t_a - t_b)$ for the bath correlation terms.

The Hadamard trick involves integrating the products of system operators $\hat{0}\hat{1} \ldots \varrho \ldots \hat{K}$, which oscillate at Bohr frequencies, together with the correlation functions. This method

embeds the time integral into the spectral density function of the bath, thereby reducing the computational complexity of the cumulants. Specifically, it incorporates the time integration into the preexisting time-dependent spectral density function, as given in Eq. (21).

The direct implementation of the Hadamard trick on nested commutators is essential for maintaining the compactness of the cumulative correlation terms established in the preceding section. To formalize this, let $\mathcal{B} : L(\mathcal{H}_S) \to L(\mathcal{H}_S)$ be a linear superoperator mapping system operators to system operators, where $\mathcal{H}_S$ is the Hilbert space of the system, and $L(\mathcal{H}_S)$ is the Hilbert space of linear operators on the Hilbert space of the system. For example, we may define $\mathcal{B}(\hat{Q}) = [\hat{Q}, \hat{1}]\hat{2}$, or a similar transformation. We assume that $\mathcal{B}$ does not explicitly depend on t_a, meaning that $\hat{a}$ or t_a does not appear in the expression for $\mathcal{B}(\hat{Q})$. In general, we consider $\mathcal{B}$ satisfying

$$\int dt_a \langle ab \rangle \mathcal{B}[\hat{Q}(t_a)] = \mathcal{B}\left[\int dt_a \langle ab \rangle \hat{Q}(t_a)\right] \quad (67)$$

for any time-dependent operator $\hat{Q} : \mathbb{R} \to L(\mathcal{H}_S)$.

The Hadamard trick is then summarized in the following identities:

$$\int_{t_i}^{t_f} dt_a\, \mathcal{B}(\hat{a})\langle ab \rangle = \mathcal{B}(\hat{b} \circ [\Gamma(t_f - t_b) - \Gamma(t_i - t_b)]),$$

$$\int_{t_i}^{t_f} dt_a\, \mathcal{B}(\hat{a})\langle ba \rangle = \mathcal{B}(\hat{b} \circ [\Gamma^T(t_b - t_i) - \Gamma^T(t_b - t_f)]),$$
$$(68)$$

where $\circ$ denotes the Hadamard (elementwise) product in the system energy basis. For rank 2 tensors, this is simply defined as $\hat{A} \circ \hat{B} = A_{nm} B_{nm}$. The function $\Gamma(t)$ has matrix elements given by $[\Gamma(t)]_{nm} = \Gamma_{\omega_{nm}}(t)$. A full proof of identity (68) is given in Appendix A.

The full Hadamard trick involves an algorithm that systematically applies Eq. (68) to cumulative correlation terms. This process requires executing all permutations within the iterated time-ordered integral and appropriately transforming the integration domains in the $(2n - 1)$-dimensional space.

Further details of this algorithm, including the handling of integration bounds and iterated integrals, are provided in Appendixes B and C. We have numerically implemented the Hadamard trick using computational scripts. However, for the purposes of this paper, all calculations have also been verified independently through manual derivations. The reduction in computational complexity achieved through this method is exponential for all n and is highly significant. A thorough explanation of this complexity reduction is given in Appendixes C and D.

Let us apply the Hadamard trick to the TCL$_2$ generator, specifically to the cumulative correlation term given by Eq. (60). In this instance, we utilize the second equation in identity (68) to find

$$L^2(t)\varrho(t) = -[\hat{0}, \hat{0} \circ \Gamma^T(t)\varrho(t)] + \text{H.c.} \quad (69)$$

This result corresponds to the well-known Bloch-Redfield master equation. The role of the Hadamard product in this context is to disrupt the unitarity of the system's dynamics

by modifying the interaction with the bath. Since $\Gamma^T(t)$ saturates over time, the TCL$_2$ generator does not exhibit late-time growth.[1]

In terms of the matrix elements of the generator, after rotating to the Schrödinger picture, and setting $t_i = 0$ from now on, we have

$$L^0_{nm,ij} = -iE_n \delta_{ni}\delta_{mj} + \text{r.H.c.} \quad \text{(unitary dynamics)}, \quad (70)$$

$$L^2_{nm,ij}(t) = A_{ni}A_{jm}\Gamma_{in}(t) - \sum_{k=1}^{N} A_{nk}A_{ki}\delta_{jm}\Gamma_{ik}(t) + \text{r.H.c.} \quad (71)$$

The TCL$_4$ generator involves a sequence of two alternating Hadamard and standard matrix products, and one remaining integral. Applying the Hadamard trick onto [78, Eq. (29)] we obtain

$$L^4(t)\varrho(t)$$

$$= -\Bigg[\hat{0}, \int_0^t dt_a \quad (72)$$

$$- [\hat{a}, (\hat{0} \circ \Delta\Gamma^T(t, t - t_a))](\hat{a} \circ \Gamma^T(t_a))\hat{\varrho} \quad (73)$$

$$+ [(\hat{a} \circ (-\Gamma(-t_a))), (\hat{0} \circ \Delta\Gamma^T(t, t - t_a))]\hat{\varrho}\hat{a} \quad (74)$$

$$- [(\hat{a} \circ \Delta\Gamma^T(t_a, t_a - t)), (\hat{0} \circ \Delta\Gamma^T(t, t - t_a))]\hat{\varrho}\hat{a}$$
$$(75)$$

$$+ [\hat{a}, (\hat{0} \circ \Delta\Gamma^T(t, t - t_a))]\hat{\varrho}(\hat{a} \circ (-\Gamma(-t_a))) \quad (76)$$

$$- [(\hat{a} \circ \Gamma^T(t_a)), (\hat{0} \circ \Delta\Gamma^T(t, t - t_a))]\hat{a}\hat{\varrho} \quad (77)$$

$$+ [(\hat{a} \circ \Delta\Gamma(t - t_a, -t_a)), (\hat{0} \circ \Delta\Gamma^T(t, t - t_a))]\hat{a}\hat{\varrho}$$
$$(78)$$

$$+ [(\hat{a} \circ (-\Gamma^T(t_a - t))), (\hat{0} \circ \Delta\Gamma^T(t, t - t_a))]\hat{\varrho}\hat{a} \quad (79)$$

$$- [(\hat{0} \circ \Delta\Gamma^T(t, t - t_a)), \hat{a}]\hat{\varrho}(\hat{a} \circ \Delta\Gamma(t - t_a, -t_a))$$
$$(80)$$

$$- [(\hat{a} \circ \Delta\Gamma(t - t_a, -t_a))\hat{a}, (\hat{0} \circ \Delta\Gamma^T(t, t - t_a))]\hat{\varrho}$$
$$(81)$$

$$+ [(\hat{0} \circ \Delta\Gamma^T(t, t - t_a)), \hat{a}]\hat{\varrho}(\hat{a} \circ (-\Gamma(-t_a))) \quad (82)$$

$$+ [(\hat{a} \circ (-\Gamma(-t_a)))\hat{a}, (\hat{0} \circ \Delta\Gamma^T(t, t - t_a))]\hat{\varrho}\Bigg] + \text{H.c.}$$
$$(83)$$

Here $\Delta\Gamma(t_1, t_2) \equiv \Gamma(t_1) - \Gamma(t_2)$.

For the BCF given by Eq. (16), the asymptotics of $\Delta\Gamma(t_1, t_2)$ at $t_1, t_2 \gg 1/\omega_c$ is given as follows:

$$\Delta\Gamma_\omega(t_1, t_2)$$

$$= \begin{cases} \dfrac{2i\lambda^2\Gamma(s+1)\omega_c^2}{\omega}\left[\dfrac{e^{i\omega t_2}}{(1+i\omega_c t_2)^{1+s}} - \dfrac{e^{i\omega t_1}}{(1+i\omega_c t_1)^{1+s}}\right], & \text{if } \omega \neq 0 \\ 2i\lambda^2\omega_c\Gamma(s)\left[\dfrac{1}{(1+i\omega_c t_2)^s} - \dfrac{1}{(1+i\omega_c t_1)^s}\right], & \text{otherwise.} \end{cases}$$
$$(84)$$

If t_1 and t_2 vary over long timescale (of order t), then $\Delta\Gamma_\omega(t_1, t_2)$ will be significantly suppressed over most of the integration range. For the integrand to remain appreciable, at least one of the time arguments must be small.

---

[1] An exception would be $1/f$ noise, which exhibits a diverging dephasing rate [79]; however, this does not lead to divergent dynamics.

Thus, the primary effect of $\Delta\Gamma_\omega(t_1, t_2)$ in Eqs. (73)–(83) is to mitigate secular growth, trying to ensure that the higher-order terms in the TCL expansion do not lead to unbounded divergence over long timescales. We observe that each integrand in lines (73)–(83) contains the term $\Delta\Gamma_\omega(t_1, t_2)$, which serves to suppress the growth of the integral over t_a, provided that $\Delta\Gamma_\omega(t_1, t_2)$ decays sufficiently rapidly. Specifically, at zero frequency we have $\Delta\Gamma_0(t, t') \sim$ $t^{-s} - t'^{-s}$. In this case, growth will occur if $s < 1$, as noted in Ref. [20].

The TCL$_6$ generator exhibits a greater diversity of terms, reflecting the increased complexity of higher-order cumulants. For a complete description of the generator, please refer to Appendix F.

Representative terms that correspond to the cumulative correlation terms in Eqs. (62) and (63) include

$$L^6(t)\varrho(t) = -\left[\hat{0}, \int_0^t dt_a \int_0^{t_a} dt_b \right. \tag{85}$$

$$+ [\hat{a}, (\hat{0} \circ \Delta\Gamma^T(t - t_b, t - t_a))][\hat{b}, (\hat{a} \circ \Delta\Gamma^T(t_a, t_a - t_b))](\hat{b} \circ \Gamma^T(t_b))\hat{\varrho} \tag{86}$$

$$- [\hat{a}, (\hat{0} \circ \Delta\Gamma^T(t, t - t_a))][(\hat{b} \circ \Gamma(t_a - t_b)), (\hat{a} \circ \Delta\Gamma^T(t_a, t_a - t_b))]\hat{b}\hat{\varrho} \tag{87}$$

$$+ [(\hat{b} \circ \Delta\Gamma(t - t_b, -t_b)), (\hat{0} \circ \Delta\Gamma^T(t, t - t_a))][\hat{a}, \hat{b}](\hat{a} \circ \Gamma^T(t_a - t_b))\hat{\varrho} \tag{88}$$

$$\cdots$$

$$- [(\hat{b} \circ \Delta\Gamma(t - t_b, t_a - t_b)), [(\hat{0} \circ \Delta\Gamma^T(t - t_b, t - t_a))\hat{b}, \hat{a}](\hat{a} \circ \Delta\Gamma^T(t_a, t_a - t_b))\hat{\varrho}] \tag{89}$$

$$- [\hat{a}, (\hat{0} \circ \Delta\Gamma^T(t - t_b, t - t_a))](\hat{a} \circ \Delta\Gamma^T(t_a, t_a - t_b))[(\hat{b} \circ \Delta\Gamma(t - t_b, t_a - t_b)), \hat{b}\hat{\varrho}] \tag{90}$$

$$+ (\hat{0} \circ \Delta\Gamma^T(t - t_b, t - t_a))[(\hat{b} \circ \Delta\Gamma(t - t_b, t_a - t_b)), [\hat{a}, \hat{b}]\hat{\varrho}(\hat{a} \circ \Delta\Gamma(t_b - t_a, -t_a))] \tag{91}$$

$$\cdots$$

$$- [\hat{b}, (\hat{0} \circ \Delta\Gamma^T(t, t - t_b))](\hat{b} \circ \Gamma^T(t_b))[(\hat{a} \circ \Gamma(t - t_a)), \hat{a}\hat{\varrho}] \tag{92}$$

$$+ [(\hat{a} \circ \Gamma(t - t_a)), \hat{a}[\hat{b}, (\hat{0} \circ \Delta\Gamma^T(t, t - t_b))](\hat{b} \circ \Gamma^T(t_b))\hat{\varrho}] \tag{93}$$

$$+ [(\hat{b} \circ \Gamma(t_a - t_b)), (\hat{0} \circ \Delta\Gamma^T(t, t - t_b))]\hat{b}[(\hat{a} \circ \Gamma(t - t_a)), \hat{a}\hat{\varrho}] \tag{94}$$

$$\cdots$$

$$\left. \vphantom{\int} \right] + \text{H.c.} \tag{95}$$

These terms are part of the extended generator that accounts for more complex interactions and higher-order corrections in the time evolution of the system, where each term involves intricate nested commutators and bath correlation functions with varying time arguments. The cancellation and growth behaviors observed in the TCL expansion are influenced by these additional terms, and their analysis is crucial for understanding the system dynamics at long timescale.

In this formulation, we have three Hadamard products interspersed among standard matrix products and iterated time-ordered integrals. The critical insight arises from the observation that the time-dependent spectral density appears in two distinct forms. Consider Eq. (73) as an example. In the first Hadamard product, the spectral function is represented by the correlation $\Delta\Gamma^T(t, t - t_a)$. According to Eq. (84), if t is sufficiently large, $\Delta\Gamma^T(t, t - t_a)$ will be near zero for most of the integration domain, except within the correlation interval $t_a \gtrsim t - \tau_c$. This means that $\Delta\Gamma^T(t, t - t_a)$ suppresses the late-time growth of the integral over t_a. On the other hand, in the second Hadamard product on Eq. (73), the spectral function is $\Gamma^T(t_a)$, which does not suppress the growth. This term can be factored out of the integral as a constant, i.e., $\Gamma^T(t)$. More precisely, we can replace $\Gamma^T(t_a) = \Gamma^T(t) - \Delta\Gamma^T(t, t_a)$ and split the integral into two parts. One part will involve the product $\Delta\Gamma^T(t, t - t_a)\Delta\Gamma^T(t, t_a)$, which is subleading and can be neglected in the resummation of the leading cumulants.

This is equivalent to replacing $\Gamma^T(t_a)$ with $\Gamma^T(t)$ in the initial integral.

In the next example, consider Eq. (86), which contains two correlation terms $\Delta\Gamma$:

$$\Delta\Gamma^T(t - t_b, t - t_a), \tag{96}$$

which is significant if $t_a \gtrsim t - \tau_c$, and

$$\Delta\Gamma^T(t_a, t_a - t_b), \tag{97}$$

which is significant if $t_b \gtrsim t_a - \tau_c$. Substituting $t_a \gtrsim t - \tau_c$ into the second condition gives $t_b \gtrsim t - \tau_c$. Thus, the correlations governed by $\Delta\Gamma$ constrain both t_a and t_b to be within the correlation time interval τ_c, thereby suppressing the late-time growth of the double integral, provided the correlations decay sufficiently rapidly. The remaining term $\Gamma^T(t_b)$ does not contribute to growth suppression and can be factored out as $\Gamma^T(t)$, when we estimate the asymptotics of the double integral.

Similarly, consider Eq. (87). The two $\Delta\Gamma$ terms again restrict t_a and t_b to values satisfying $t_a, t_b \gtrsim t - \tau_c$. The remaining term $\Gamma(t_a - t_b)$ can be factored out of the integral as $\Gamma(t)$ since $t_a > t_b$ and t is large. The resulting approximation introduces only a subleading error, similar to the previous case.

In the original van Kampen cumulants, integrals containing two or three $\Delta\Gamma$ terms exhibited no growth due to the rapid decay of the BCF. However, in our case, where the correla-

tion function follows a power-law decay, the late-time growth induced by the time-ordered integral is mitigated, though not necessarily eliminated. When growth persists, we must perform resummations of the leading growth terms.

Thus, tracking the occurrences of $\Delta\Gamma$s while carefully considering their time ordering allows us to identify and collect the fastest-growing cumulants. Equations (92) through (94) each contain a single correlation $\Delta\Gamma$, thereby exhibiting leading growth behavior. However, it is important to note that not all $\Delta\Gamma$ terms suppress secular growth. For instance, in Eq. (88), the term

$$\Delta\Gamma(t - t_b, -t_b) = \Gamma(t - t_b) + \Gamma^\star(t_b) \qquad (98)$$

remains asymptotically nonzero and therefore does not contribute to growth suppression. Consequently, Eq. (88) also exhibits leading growth.

C. Late-time growth and growth algebra

The extent of late-time growth in the TCL generator depends on the bath correlation function, which determines how quickly $\Delta\Gamma(t, t')$ in Eq. (84) decays to zero. Understanding this asymptotic behavior in the TCL_4 generator is crucial, as it informs our extension to higher orders, such as TCL_6. Our focus in this section is to classify distinct late-time growth patterns, which arise at both nonzero and zero Bohr frequencies. We begin with the nonzero-frequency case.

Growth at nonzero frequency. Examining Eq. (73), we extract the prefactor $\Gamma^T(t)$ from the integral, as justified in Sec. V B. The remaining integral is well defined and gives rise to a key algebraic structure we term the growth algebra:

$$\int_0^t dt_a [\Gamma_\omega(t) - \Gamma_\omega(t - t_a)] e^{i\omega' t_a} = e^{i\omega' t} \frac{\Gamma_\omega(t) - \Gamma_{\omega-\omega'}(t)}{i\omega'}. \qquad (99)$$

Here, ω and ω' represent distinct Bohr frequencies or their sums. This result follows directly from integration by parts, using $\int u\,dv = uv - \int v\,du$ with $dv = e^{i\omega' t_a} dt_a$. The most significant growth occurs at $\omega' = 0$, where differentiation with respect to ω produces

$$\lambda^2 \int_0^t dt_a [\Gamma_\omega(t) - \Gamma_\omega(t - t_a)]$$
$$= -i\lambda^2 \frac{\partial \Gamma_\omega(t)}{\partial \omega} \sim \lambda^4 t \frac{e^{i\omega t}}{(1 + i\omega_c t)^{s+1}}. \qquad (100)$$

The explicit t prefactor indicates linear time enhancement, amplifying oscillations in the generator rather than leading to divergence for $s > 0$.

For a general spectral density, including at nonzero temperature, the integral can be rewritten as

$$-i\lambda^2 \frac{\partial \Gamma_\omega(t)}{\partial \omega} = \lambda^2 \int_0^t d\tau\, \tau e^{i\omega\tau} C_\beta(\tau) \equiv \lambda^2 \frac{\langle t e^{i\omega t}\rangle_t}{\tau_{\mathrm{SB}}}, \quad (101)$$

where the characteristic system-bath relaxation time is defined as $\tau_{\mathrm{SB}}^{-1} = \int_0^\infty d\tau |C_\beta(\tau)|$ (it is also known as the shortest tion time permitted by the bath [43,46]. The first-order time moment $\langle t e^{i\omega t}\rangle_t$ increases as s decreases. Notably, for $s = 1$ and $\omega = 0$, this moment diverges logarithmically with time, though this divergence cancels out in the TCL_4 generator, as shown in Ref. [20].

Growth in TCL_6. Now, we analyze late-time growth in the TCL_6 generator. Referring to Eq. (92), which falls within the leading growth category, we again extract $\Gamma^T(t_b)$ and $\Gamma(t - t_a)$ as prefactors when t is large. This leaves a double integral, which we evaluate using the growth algebra:

$$\int_0^t dt_a\, e^{i\omega' t_a} \int_0^{t_a} dt_b\, [\Gamma_\omega(t) - \Gamma_\omega(t - t_b)] e^{i\omega'' t_b} \qquad (102)$$

$$= \int_0^t dt_b\, [\Gamma_\omega(t) - \Gamma_\omega(t - t_b)] e^{i\omega'' t_b} \int_{t_b}^t dt_a\, e^{i\omega' t_a} \quad (103)$$

$$= \frac{1}{i\omega'} \left\{ e^{i\omega' t} \int_0^t dt_b\, [\Gamma_\omega(t) - \Gamma_\omega(t - t_b)] e^{i\omega'' t_b} \right.$$
$$\left. - \int_0^t dt_b\, [\Gamma_\omega(t) - \Gamma_\omega(t - t_b)] e^{i(\omega'+\omega'') t_b} \right\} \quad (104)$$

$$= \frac{1}{i\omega'} \left\{ \frac{e^{i(\omega'+\omega'')t}}{i\omega''} [\Gamma_\omega(t) - \Gamma_{\omega-\omega''}(t)] \right.$$
$$\left. - \frac{e^{i(\omega'+\omega'')t}}{i(\omega'+\omega'')} [\Gamma_\omega(t) - \Gamma_{\omega-\omega'-\omega''}(t)] \right\}. \qquad (105)$$

The strongest growth occurs when $\omega' = \omega'' = 0$, yielding the second derivative:

$$\lambda^4 \int_0^t dt_a \int_0^{t_a} dt_b\, [\Gamma_\omega(t) - \Gamma_\omega(t - t_b)]$$
$$= -\frac{\lambda^4}{2!} \frac{\partial^2 \Gamma_\omega(t)}{\partial \omega^2} \sim \lambda^6 \frac{t^2}{2!} \frac{e^{i\omega t}}{(1 + i\omega_c t)^{s+1}}, \quad t \gg \tau_c. \quad (106)$$

For $s \neq 1$, the amplitude of oscillations in the generator scales as $\lambda^6 t^{1-s}$, leading to growth for $s < 1$ and suppression for $s > 1$. The Ohmic bath ($s = 1$) marks the critical boundary, where the generator remains finite but oscillates indefinitely. Thus, TCL_6 serves as a critical master equation for Ohmic environments.

To estimate the asymptotic populations and coherences with precision $O(\lambda^{2n})$, it is necessary to determine the matrix elements of the asymptotic $\mathrm{TCL}_{2(n+1)}$ and TCL_{2n} generators, respectively [38]. Consequently, the asymptotic populations to precision $O(\lambda^4)$ are nonexistent in the Ohmic bath, as the corrections to the asymptotic populations require the asymptotic TCL_6 generator, which does not exist. As a result, the asymptotic population correction of order $O(\lambda^4)$ does not exist. TCL_4 is the highest-order master equation for the Ohmic bath that generates a semigroup at late times.

Higher-order growth. To understand late-time behavior at higher orders, we extend our analysis to the TCL_{2n} generator. Since time-ordered cumulants exclude disconnected time pairings, the leading growth is determined by a unique correlation $\Delta\Gamma$ between the initial and final time arguments in the iterated time-ordered integral. Similar to our approach for

the TCL$_4$ and TCL$_6$ generators, additional values of Γ can be factored out as prefactors, while the remaining integrals can be computed using the algebra established in previous sections.

In Appendix E, we derive the following identity:

$$\int \cdots \int_{\leftarrow}^{t} dt_{1\ldots n-1}[\Gamma_\omega(t) - \Gamma_\omega(t - t_{n-1})] = \frac{(-i)^{n-1}}{(n-1)!} \frac{\partial^{n-1}\Gamma_\omega(t)}{\partial \omega^{n-1}}. \tag{107}$$

Since the TCL$_{2n}$ generator matrix elements contain the $(n-1)$st derivative of $\Gamma_\omega(t)$, the oscillations in the generator scale as

$$\lambda^{2n} t^{n-1} e^{i\omega t} / (1 + i\omega_c t)^{s+1} \propto t^{n-s-2}. \tag{108}$$

Thus, for a fixed s, there exists a critical order $n_{\max}$ beyond which the TCL$_{2n}$ master equation ceases to generate a valid semigroup at late times.

For a general bath correlation function, including at nonzero temperature, the generator matrix elements are proportional to the time moments

$$\lambda^{2n-2} \langle t^{n-1} e^{i\omega t} \rangle_t / [(n-1)! \tau_{SB}]. \tag{109}$$

As n increases, the system memory time extends, raising the order of relevant moments in the master equation. For large n and small s, the moment $\langle t^{n-1} e^{i\omega t} \rangle_t$ ceases to be well defined in the $t \to \infty$ limit. This motivates the following lemma regarding environments with algebraically decaying BCFs:

TCL$_{2n}$ precision lemma. The maximum precision of an asymptotic TCL2n generator is $O(\lambda^{\lceil 2s+2 \rceil})$, while the asymptotic state has a maximum precision of $O(\lambda^{2\lceil s \rceil})$. Here $\lceil \rceil$ is the ceiling function.

Growth at zero frequency. At zero frequency, the derivatives of $\Gamma_\omega(t)$ obey

$$\lim_{\omega \to 0} \frac{\partial^k \Gamma_\omega(t)}{\partial \omega^k} = i^k \int_0^t dt_1 C(t_1) t_1^k \propto t^{k-s}. \tag{110}$$

Since the TCL$_{2n}$ generator involves the $(n-1)$th frequency derivative, its growth at zero frequency scales as

$$\lambda^{2n} t^{n-s-1}. \tag{111}$$

Compared to nonzero frequency growth [Eq. (107)], this contains an extra factor of t, leading to an apparent divergence $\propto t^{1-s}$ for sub-Ohmic baths ($s < 1$). This was previously identified in our analysis of TCL$_4$ [20]. However, infrared effects complicate the interpretation of this divergence, as the number of radiated soft photons also scales as t^{1-s} [80–82].

The relative significance of zero-frequency versus nonzero-frequency growth depends on their response to partial resummations. In the limit $t \to \infty$, we shall see that late-time growth at nonzero frequency dominates, despite appearing to follow a weaker power law at fixed n. We will revisit this topic at the end of the next section.

VI. PARTIAL RESUMMATIONS

In this section, we demonstrate that summing Eq. (107) across all orders of λ^2 corresponds to a partial Taylor expansion of the TCL generator, which can thus be resummed. Ideally, we would aggregate all first- and second-order frequency derivatives in the TCL$_4$ and TCL$_6$ generators, respectively. By juxtaposing these terms, we aim to uncover the initial structure of a multivariable Taylor series expansion. Such an analysis was successfully carried out for the TCL$_4$ generator in Ref. [20]. However, an equivalent deconstruction of the TCL$_6$ generator remains an open technical challenge due to the sheer number of terms involved. While computationally demanding, this endeavor could yield significant insights (see Appendix F).

To illustrate the key ideas, we select a representative term from the TCL$_4$ generator, specifically, the contribution labeled Eq. (73). We then identify its corresponding term in the TCL$_6$ generator and investigate its embedding within the TCL$_2$ and TCL$_4$ frameworks.

A. Identifying growth terms in TCL$_4$

Consider the matrix element $\langle n | \ldots | m \rangle$ from Eq. (73), focusing on terms where ϱ appears exclusively on the right-hand side:

$$\langle n | L^4(t) \varrho(t) | m \rangle = \int_0^t dt_a \langle n | \hat{0}[\hat{a}, (\hat{0} \circ \Delta \Gamma^T(t, t - t_a))](\hat{a} \circ \Gamma^T(t_a)) \hat{\varrho} | m \rangle + \cdots. \tag{112}$$

Expanding the integral over frequency indices, we obtain

$$= \sum_{ksqij} \int_0^t dt_a A_{nk} e^{i\omega_{nk}t} \left\{ A_{ks} e^{i\omega_{ks}t_a} A_{sq} e^{i\omega_{sq}t} [\Gamma_{qs}(t) - \Gamma_{qs}(t - t_a)] \right. \tag{113}$$

$$\left. - A_{ks} e^{i\omega_{ks}t} [\Gamma_{sk}(t) - \Gamma_{sk}(t - t_a)] A_{sq} e^{i\omega_{sq}t_a} \right\} A_{qi} e^{i\omega_{qi}t_a} \Gamma_{iq}(t) \varrho_{ij}(t) \delta_{jm} + \cdots. \tag{114}$$

Here, the spectral density $\Gamma^T(t_a)$ in Eq. (112) maps to the matrix element $\Gamma_{iq}(t)$ in Eq. (114), allowing it to be factored out of the integral as discussed previously.

Transitioning to the Schrödinger picture, we multiply the expression by $e^{-i\omega_{nm}t}$ and substitute $\varrho_{ij}(t) = e^{i\omega_{ij}t} \rho_{ij}(t)$. Since the integral structure aligns with Eq. (99), the result can be expressed using the growth algebra.

B. Peak growth and frequency conditions

The dominant growth occurs at $\omega' = 0$. For the integrals in Eqs. (113) and (114), the peak growth conditions correspond to

$$\omega' = \omega_{ks} + \omega_{qi}, \tag{115}$$

$$\omega' = \omega_{sq} + \omega_{qi} = \omega_{si}. \tag{116}$$

From these conditions, we identify three distinct types of growth, corresponding to different subsets of indices:

(1) $k = s, q = i$.
(2) $k = i, q = s$.
(3) $s = i$.

Substituting these constraints and computing the integrals using Eq. (99), we obtain the respective contributions

$$\int_0^t dt_a \{\ldots\}_{nm} = i \sum_k A_{nk} A_{ki} \frac{\partial \Gamma_{\omega_{ik}}}{\partial \omega_{ik}} \left[A_{kk} A_{ii} \Gamma_0 \right. \tag{117}$$

$$\left. - \sum_q |A_{iq}|^2 \Gamma_{iq} \right] \delta_{jm} \tag{118}$$

$$+ i \sum_s A_{ni} |A_{is}|^2 A_{ss} \Gamma_{is} \frac{\partial \Gamma_\omega}{\partial \omega}\bigg|_{\omega=0} \delta_{jm} + \cdots . \tag{119}$$

C. Avoiding double counting

To ensure accuracy, we must prevent double counting arising from overlapping index subsets. Specifically, all indices in Eq. (118) are explicitly summed over and repeated indices appearing in Eqs. (117) and (119) are excluded to avoid redundancy. For clarity, we suppress the explicit time dependence of the spectral density $\Gamma(t)$ in these expressions to reduce notational clutter.

D. Identifying growth terms in TCL$_6$

Now, we turn our attention to Eq. (92) of the TCL$_6$ generator, which arises from the cumulative correlation term $\langle 04 \rangle \langle 12 \rangle \langle 35 \rangle$. One of the terms will include δ_{jm}, allowing us to identify the matching components in the TCL$_2$ and TCL$_4$ generators. We examine the matrix element nm of Eq. (92) and isolate the δ_{jm} term:

$$\langle n | L^6(t) \varrho(t) | m \rangle = \iint_{\leftarrow}^t dt_{ab} \langle n | \hat{O}[\hat{b}, (\hat{O} \circ \Delta \Gamma^T(t, t-t_b))](\hat{b} \circ \Gamma^T(t_b))(\hat{a} \circ \Gamma(t-t_a)) \hat{a} \varrho | m \rangle + \cdots \tag{120}$$

$$= \sum_{kqsuvij} \iint_{\leftarrow}^t dt_{ab} \{ A_{nk} e^{i\omega_{nk}t} \left[A_{kq} e^{i\omega_{kq}t_b} A_{qs} e^{i\omega_{qs}t} [\Gamma_{sq}(t) - \Gamma_{sq}(t-t_b)] \right. \tag{121}$$

$$\left. - A_{kq} e^{i\omega_{kq}t} [\Gamma_{qk}(t) - \Gamma_{qk}(t-t_b)] A_{qs} e^{i\omega_{qs}t_b} \right] \tag{122}$$

$$\times A_{su} e^{i\omega_{su}t_b} \Gamma_{us} A_{uv} e^{i\omega_{uv}t_a} \Gamma_{uv} A_{vi} e^{i\omega_{vi}t_a} \varrho_{ij} \delta_{jm} \} \cdots . \tag{123}$$

As with the TCL$_4$ case, we substitute the time arguments of Γ_{us} and Γ_{uv} with t, making their time dependence implicit. This expression is then converted into the Schrödinger picture, following the same approach used for the TCL$_4$ generator.

By comparing the result with Eqs. (102)–(105), we identify the conditions for leading growth: $\omega' = \omega_{uv} + \omega_{vi} = \omega_{ui}$, and either $\omega'' = \omega_{kq} + \omega_{su}$ or $\omega'' = \omega_{qs} + \omega_{su} = \omega_{qu}$. The prevailing growth occurs when $\omega' = \omega'' = 0$, leading to the condition for dominant growth:

$$\{u = i \text{ and } [(k = u \text{ and } q = s) \text{ or } (k = q \text{ and } u = s)]\} \text{ or } (u = i \text{ and } q = u). \tag{124}$$

Next, we compute the double time-ordered integral in the algebra, resulting in

$$\iint_{\leftarrow}^t dt_{ab} \{\ldots\}_{nm} = \frac{-1}{2!} \sum_{ij} \left\{ A_{ni} \sum_q A_{qq} |A_{iq}|^2 \Gamma_{iq} \sum_v |A_{iv}|^2 \Gamma_{iv} \frac{\partial^2 \Gamma_\omega}{\partial \omega^2}\bigg|_0 \right. \tag{125}$$

$$+ A_{ii} \Gamma_{ii} \sum_q A_{nq} A_{qq} A_{qi} \sum_v |A_{iv}|^2 \Gamma_{iv} \frac{\partial^2 \Gamma_\omega}{\partial \omega_{iq}^2} \tag{126}$$

$$\left. - \sum_k A_{nk} A_{ki} \frac{\partial^2 \Gamma_\omega}{\partial \omega_{ik}^2} \left(\sum_s |A_{is}|^2 \Gamma_{is} \right)^2 \right\} \rho_{ij} \delta_{jm} \cdots . \tag{127}$$

Just as with the TCL$_4$ case, we enumerate all terms on Eq. (127) and exclude any repeated terms from the previous lines.

Recall the TCL$_2$ generator from Eq. (71), which contains a single sum over k:

$$\sum_{ij} L_{nm,ij}^2(t) \rho_{ij} = \sum_{ij} \left[A_{ni} A_{jm} \Gamma_{in}(t) \rho_{ij} - \sum_{k=1}^N A_{nk} A_{ki} \Gamma_{ik} \rho_{ij} \delta_{jm} \right]. \tag{128}$$

Equations (125) and (126) cannot be directly incorporated into the Bloch-Redfield generator due to the presence of double sums over q and v. However, the final term on (127), which involves a square of a single sum, can be smoothly integrated into the Bloch-Redfield generator.

Similarly, the term in Eq. (118) can be included in the relaxation term of the TCL$_2$ generator. This results in a renormalization of the spectral density to order $O(\lambda^6)$, as shown by

$$\Gamma_{\omega_{ik}} \mapsto \Gamma_{\omega_{ik}} + \frac{-i}{1!} \frac{\partial \Gamma_{\omega_{ik}}(t)}{\partial \omega_{ik}} \left[\sum_q |A_{iq}|^2 \Gamma_{iq}(t) \right]$$

$$+ \frac{(-i)^2}{2!} \frac{\partial^2 \Gamma_\omega(t)}{\partial \omega_{ik}^2} \left[\sum_s |A_{iq}|^2 \Gamma_{iq}(t) \right]^2. \tag{129}$$

This suggests that the sequence in Eq. (129) represents the first three terms of a Taylor expansion, which can then be resummed to all orders in λ^2:

$$\sum_{n=0}^{\infty} \frac{(-i)^n}{n!} \frac{\partial^n \Gamma_{\omega_{ik}}(t)}{\partial \omega_{ik}^n} \left[\sum_q |A_{iq}|^2 \Gamma_{iq}(t) \right]^n$$
$$= \Gamma_{\omega_{ik} - i \sum_q |A_{iq}|^2 \Gamma_{iq}(t)}(t). \tag{130}$$

Thus, the result of the resummation is obtained by renormalizing the Bohr frequencies as

$$\omega_{ik} \mapsto \omega_{ik} - i \sum_q |A_{iq}|^2 \Gamma_{iq}(t). \tag{131}$$

To this point, the analysis has been conducted using only the first three terms of the generator, one for each TCL_{2n}, where $n \in 1, 2, 3$. This procedure must be repeated for the remaining terms. To facilitate this, we will examine all spectral density derivatives in the TCL_4 generator and identify which can be embedded into the structure of the TCL_2 generator via the linear term in the multivariable Taylor expansion. This procedure is detailed in Appendix G, with the final result as follows.

There are two categories of spectral density derivatives: embeddable and nonembeddable. The embeddable derivatives are incorporated into the TCL_2 generator via a renormalization of the spectral density:

$$\Gamma_{ik}(t) \mapsto \Gamma_{ik}(t) - i \frac{\partial \Gamma_{\omega}(t)}{\partial \omega_{ik}} \left[\sum_c (|A_{ic}|^2 \Gamma_{ic}(t) - |A_{kc}|^2 \Gamma_{kc}(t)) \right.$$
$$\left. + 2 J_0(t) A_{jj}(A_{kk} - A_{ii}) \right], \tag{132}$$

which leads to the spectral density in Eq. (37) in the rTCL_4 master equation.

This procedure begins the Taylor expansion of the time-dependent spectral density with respect to frequency, as given by Eq. (32). The term linear in the frequency shift reproduces Eq. (132), while higher-order terms include the quadratic term in Eq. (129) and higher-order terms in Eq. (130).

E. Two distinct divergences

The resummation process leads to a frequency renormalization, introducing an imaginary component to a nonzero Bohr frequency, as shown in Eq. (130). At long timescales, this imaginary part can be negative, resulting in an exponential growth in the time-dependent spectral density $\Gamma_\omega(t)$ when $t \gg \tau_c$. This exponential growth is evident in Eqs. (21) and (25) for cases where $\text{Im}\,\omega < 0$, provided the bath correlation function (BCF) exhibits algebraic decay, as expressed in Eq. (21).

This phenomenon is unique to TCL and represents a novel type of divergence in open quantum system theory, which we term *secular inflation*. A key feature distinguishing secular inflation is its restriction to nonzero Bohr frequencies, a characteristic we explore in subsequent sections. As the generator incorporates exponential growth, the evolution of the density matrix elements, governed by Eq. (49), follows a superexponential trajectory, defined by an exponentiated exponential function. In contrast, *infrared divergence* occurs in the limit of zero Bohr frequency [20]. When $\omega_{ik} = 0$ at zero

temperature ($T = 0$), Eq. (132) simplifies to $\Gamma_{ik}(t) \mapsto \Gamma_{ik}(t)$ for $t \gg \tau_c$, rendering the frequency shift negligible at long times. As the renormalization of zero frequency vanishes, no partial derivatives $\partial^k \Gamma_\omega(t)/\partial \omega^k$ at zero frequency contribute to the rTCL_{2n} ME. Consequently, the rTCL does not exhibit infrared divergence.

Previous studies have shown that the TCL_4 generator does exhibit infrared divergence [20]. The absence of this divergence in rTCL arises from the selective inclusion of leading cumulants. Specifically, in Appendix G, we demonstrate that certain nonembeddable leading cumulants of order $O(\lambda^4)$ are excluded from the rTCL generator. These nonembeddable terms can be expressed through the Liouvillian as

$$\tilde{L}_{nm,ij}^{r4}(t) = -2i\delta_{ij} \sum_k A_{nk} A_{km} \left(|A_{im}|^2 J_{im}(t) \frac{\partial \Gamma_\omega(t)}{\partial \omega_{mk}} \right.$$
$$\left. - |A_{ik}|^2 J_{ik}(t) \frac{\partial \Gamma_\omega(t)}{\partial \omega_{kn}} \right)$$
$$- 2i A_{nm} A_{ji} \frac{\partial \Gamma_\omega(t)}{\partial \omega_{ij}} (|A_{jn}|^2 J_{jn}(t) - |A_{jm}|^2 J_{jm}(t))$$
$$+ \text{r.H.c.} \tag{133}$$

As discussed earlier, we must exclude the indices in this expression that have already been counted in the embeddable terms that are included in rTCL. Preventing this double counting is a time-consuming process, and symbolic math tools are often helpful for managing it efficiently. In the case of a qubit, the final result for $\tilde{L}_{nm,ij}^{r4}(t)$ is provided in Eq. (G24).

In contrast to rTCL, the nonembeddable cumulants in Eq. (133) do contain derivatives of the spectral density at zero frequency, which exhibit infrared divergence with enhanced late-time growth exponents. In the TCL_4 generator, the infrared divergences were isolated and expressed as what we refer to as the infrared divergence generator (IDG), as shown in Ref. [20, Eqs. (54)–(56)]:

$$\text{IDG}_{nm,ij}(t) = 4i A_{nm} \delta_{ij} \frac{\partial J_\omega(t)}{\partial \omega}\Big|_0 [|A_{im}|^2 J_{im}(t)(A_{ii} - A_{mm})$$
$$- |A_{in}|^2 J_{in}(t)(A_{ii} - A_{nn})]. \tag{134}$$

Analysis of the nonembeddable cumulants in Eq. (133) shows that the IDG is fully included within these cumulants. However, in the examples discussed in the following sections, which largely involve the unbiased spin-boson model (SBM), we have $\text{IDG}_{nm,ij} = 0$. Therefore, the study of infrared divergence can be postponed for a future project, where the IDG will serve as the foundational cumulant for subsequent partial resummations. Renormalizing the IDG presents a significant challenge, requiring the deconstruction of all cumulants in Appendix F and identifying the embeddings into the IDG. Such an endeavor may have relevance to the black hole information loss paradox [83–85].

In summary, the resummation mechanism responsible for generating inflation-deflation pairs is absent at zero frequency. However, infrared divergence persists in cumulants that cannot be embedded within the rTCL structure. According to Ref. [73], infrared divergence does not occur in the

super-Ohmic bath, as the number of emitted soft photons, which decay as t^{1-s}, remains finite. Consequently, we do not anticipate infrared divergence in TCL for super-Ohmic baths.

This contrasts with secular inflation, which emerges in any bath with algebraic decay in the bath correlation function, including the super-Ohmic case. When both secular inflation and infrared divergence are present, such as when nonembeddable cumulants are incorporated into rTCL, the former represents a more severe divergence. Secular inflation leads to superexponential growth in the reduced density matrix, surpassing the enhanced power-law behavior of the generator observed at zero frequency.

VII. RESULTS AND DISCUSSION OF RESUMMATION

This section examines the results obtained from two open quantum system models: the resummed (rTCL) and renormalized (rTCL$_{2n}$) master equations (MEs). It is important to note that these formulations are not intended to replace the standard TCL and TCL$_{2n}$ approaches, if they were fully known. Instead, they serve as conceptual tools to explore the limits of master equations and their connections to other open-system methods and theories.

In particular, rTCL$_2$ is equivalent to the TCL$_2$-Bloch-Redfield ME, while rTCL$_4$ represents an improved weak-coupling theory that resolves several shortcomings of TCL$_2$. It closely resembles the canonically consistent ME [49], but with the key distinction that it is derived from a microscopic framework. The general rTCL formulation resums embeddable leading cumulants at all orders of λ^2.

A. General properties of rTCL

To gain insight into the properties of rTCL, let us first examine the frequency shifts in Eq. (32), ignoring terms involving $J_0(t)$. A useful example is the unbiased spin-boson model, where all diagonal elements of A vanish. In this case, the frequency shifts can be directly interpreted as time-dependent eigenenergy shifts:

$$E_n \mapsto E'_n(t) = E_n - i \sum_c |A_{nc}|^2 \Gamma_{\beta,nc}(t), \quad (135)$$

where the renormalized transition frequencies are given by $\omega'_{in}(t) = E'_i(t) - E'_n(t)$. At long times ($t \gg \tau_c \equiv 1/\omega_c$), the shifts in Eqs. (32) and (135) converge to finite asymptotic values, representing the effective energy of quasiparticle states.

The real part of the shift, $\sum_c |A_{nc}|^2 S_{\beta,nc}$, corresponds to the Lamb shift and includes the temperature-independent reorganization energy $A_{nn}^2 S_0 < 0$. The imaginary part represents the quasiparticle width, given by $-i \sum_c |A_{nc}|^2 J_{\beta,nc}$, which corresponds to half of the Fermi's golden rule (FGR) rate. Since all imaginary components are negative, the effective quasiparticle wave function $\exp(-iE'_n t)$ undergoes exponential decay over time. At zero temperature, the ground-state quasiparticle exhibits zero width, as all transition frequencies are nonpositive, resulting in a vanishing spectral density. However, at finite temperature, even the ground state acquires a finite width due to thermal relaxation.

1. Renormalized Bohr frequencies and inflation-deflation pairs

Open quantum system dynamics are fundamentally governed by the Liouvillian and Bohr frequencies, rather than the Hamiltonian eigenvalues. This allows for frequency-dependent width terms that can assume either sign. In the asymptotic limit $t \gg \tau_c$, the renormalized Bohr frequencies take the form

$$\omega'_{in} = \omega_{in} + \tilde{\omega}_{in} - i \sum_c \left(|A_{ic}|^2 J_{\omega_{ic},\beta} - |A_{nc}|^2 J_{\omega_{nc},\beta} \right), \quad (136)$$

where

$$\tilde{\omega}_{in} = \sum_c \left(|A_{ic}|^2 S_{\omega_{ic},\beta} - |A_{nc}|^2 S_{\omega_{nc},\beta} \right) \quad (137)$$

is the frequency-dependent Lamb shift. Extracting the contributions where $c = i$ or n and applying the Kubo-Martin-Schwinger (KMS) condition $J_{\beta,\omega} - J_{\beta,-\omega} = \text{sgn}(\omega)J_{|\omega|} \equiv \tilde{J}_\omega$ eliminates the temperature dependence in the direct transition width. This results in

$$\omega'_{in} = \omega_{in} + \tilde{\omega}_{in} - i|A_{in}|^2 \tilde{J}_{\omega_{in}} - i\left(A_{ii}^2 - A_{nn}^2\right)J_{0,\beta} \quad (138)$$

$$- i \sum_{c \neq i,n} \left(|A_{ic}|^2 J_{\omega_{ic},\beta} - |A_{nc}|^2 J_{\omega_{nc},\beta} \right). \quad (139)$$

Since $\omega'_{in} = -\omega'_{ni}$, the imaginary shifts introduce symmetric pairs of exponential growth and decay, termed *inflation and deflation*.

At zero temperature, this exponential time dependence arises directly from the substitution of ω'_{in} into the asymptotic spectral density [Eq. (25)]. The temperature-independent term $-i|A_{in}|^2 \tilde{J}_{\omega_{in}}$ implies that for transitions where energy decreases ($\omega_{in} > 0$) the imaginary part of ω'_{in} is negative, leading to secular inflation. To ensure the validity of this framework, a Bogoliubov–van Hove–type time limit should be imposed, analogous to that used in justifying the secular approximation [21]. This underscores that the late-time open quantum system dynamics is inherently unstable.

2. Spectral overlap and nonlocal effects

The full frequency shift in Eq. (32) contains an additional term proportional to $J_0(t)$, which is purely imaginary. Unlike the previous terms, this component does not correspond to any standard reorganization energy or Lamb shift. The presence of nonlocal terms involving A_{jj} and A_{ii} prevents us from articulating the shifts as being due to imaginary energy shifts of quasiparticles. This is analogous to Hartree-Fock potentials in many-body quantum theory: the Hartree term represents a well-defined effective potential, whereas the exchange (Fock) potential only has meaning within the self-consistent Hartree-Fock equation due to its dependence on the wave function. Similarly, here the spectral overlap is influenced by *all* diagonal matrix elements of the interaction, rather than just those associated with individual transitions.

3. Definitions of decoherence and dephasing

To clarify terminology in this work, *decoherence* refers specifically to the loss of phase coherence due to relaxation, and *dephasing* (or pure dephasing) describes the loss of phase coherence arising from inhomogeneous broadening of the
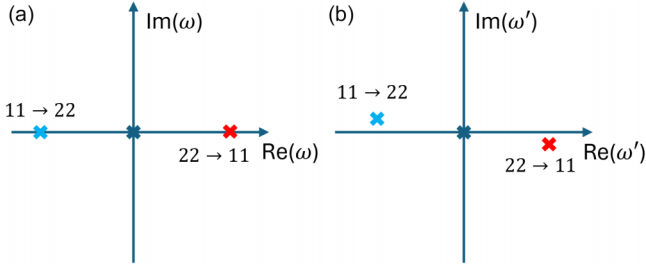
FIG. 4. Renormalization of Bohr frequencies in the spin-boson model at positive temperature. (a) Isolated qubit Bohr frequencies ($E_1 < E_2$). (b) Qubit coupled to the bath without dephasing. The shift in the imaginary part is the decoherence rate at zero temperature.

diagonal elements of A. This distinction is crucial when analyzing the asymptotic behavior of open quantum systems and their divergence properties.

B. Resummation dynamics in the spin-boson model

As an example, we examine the spin-boson model, which represents a qubit immersed in a bosonic bath. The qubit has a Bohr frequency $\Delta > 0$ and the coupling operator is given by

$$A = \begin{pmatrix} A_{11} & A_{12} \\ A_{21} & A_{22} \end{pmatrix} = \sin\theta \frac{\sigma_z}{2} + \cos\theta \frac{\sigma_x}{2}, \quad (140)$$

where $\sigma_{x,z}$ are the Pauli matrices. For a transition characterized by a nonzero Bohr frequency ω_{in}, the renormalized frequency at time t is obtained from the equation

$$\omega'_{in}(j, t) = \omega_{in} + \tilde{\omega}_{\beta,in}(t) - iv_{\beta,2}(t) - 2iJ_{\beta,0}(t)A_{jj}(A_{nn} - A_{ii}). \quad (141)$$

Here $\tilde{\omega}_{\beta,in}(t) = |A_{12}|^2[S_{\beta,\omega_{in}}(t) - S_{\beta,\omega_{ni}}(t)]$ and $v_{\beta,2}(t) = |A_{12}|^2[J_{\beta,\omega_{in}}(t) - J_{\beta,\omega_{ni}}(t)]$ represent the Lamb and decoherence shifts, respectively. For a timescale $t \gg 1/\omega_c$, we can apply the KMS condition $J_{\beta,\omega} - J_{\beta,-\omega} = \tilde{J}_\omega$, leading to the following simplified expression for the frequencies:

$$\omega'_{in}(j) = \omega_{in} + \tilde{\omega}_{\beta,in} - i\,\text{sgn}(\omega_{in})v_2 - 2iJ_{\beta,0}A_{jj}(A_{nn} - A_{ii}). \quad (142)$$

Here v_2 is the decoherence rate at zero temperature, given by $v_2 = 1/T_2 = 1/(2T_1) = |A_{12}|^2 J_\Delta$. In the absence of the spectral overlap (i.e., when $A_{11} = A_{22} = 0$), the inflation rate is independent of temperature. The frequency shifts are antisymmetric, as shown in Fig. 4(b).

Effective bath correlation function and spectral density

Substituting the expression for ω'_{in} from Eq. (142) into the expression for $\Gamma_{\beta,\omega'_{in}}(t)$ [given in Eq. (21)], and assuming $t \gg \tau_c$, we obtain the following:

$$\Gamma_{\beta,\omega'_{in}}(t) = \int_0^t dt_1 \big[C_\beta(t_1)e^{\text{sgn}(\omega_{in})v_2 t_1}\big]e^{i(\omega_{in}+\tilde{\omega}_{\beta,in})t_1}, \quad (143)$$

where the square brackets represent the effective BCF. If $C_\beta(t)$ decays algebraically, the effective BCF exhibits inflation for $\omega_{in} > 0$. In this case, regardless of how small the coupling constant is (as long as it is nonzero), the generator will diverge
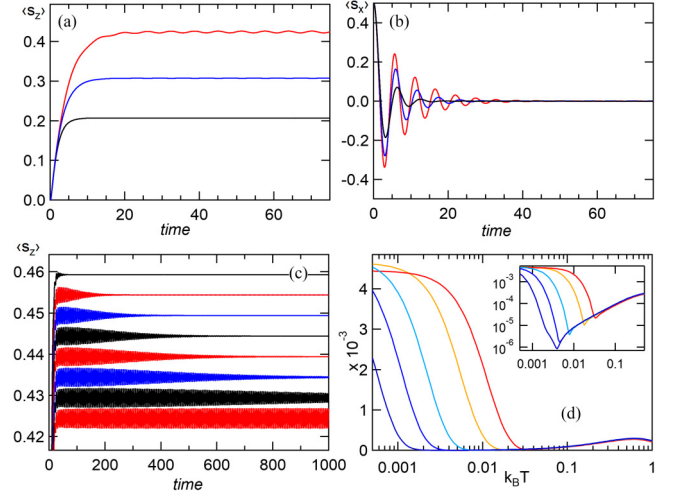

FIG. 5. rTCL$_6$ in the unbiased SBM. (a), (b) $\langle s_z(t)\rangle$ and $\langle s_x(t)\rangle$ at $k_B T = 0$ (red), 0.5 (blue), and 1 (black). (c) Zoomed in $\langle s_z(t)\rangle$ over an expanded timescale. $k_B T = 0$, 0.0005, 0.001, 0.0015, 0.002, 0.003, 0.005, and 0.1, bottom to top. Data at positive temperatures offset for clarity. (d) Peak-to-peak amplitude of $\langle s_z(t)\rangle$ versus temperature, at $t = 50$, 100, 250, 500, and 1000, right to left. Inset: The same as (d) on log-log scale. $\Delta = 1$, $\lambda^2 = 0.1$, and $\omega_c = 10$.

in the infinite time limit, preventing a Markovian approximation from being valid as $t \to \infty$.

Conversely, when $\omega_{in} < 0$, the effective BCF decays exponentially. This leads to a positive spectral density at the negative real part of ω at zero temperature, which is equivalent to an effective temperature. As a result, there will be a nonzero population in the excited state, even at zero temperature.

C. rTCL$_6$ in Ohmic environment

This subsection investigates the unbiased spin-boson model using the rTCL$_6$ master equation (ME). As discussed in Sec. V C, in the context of an Ohmic environment at zero temperature:
  (i) TCL$_4$ exhibits the proper Markovian limit.
  (ii) TCL$_6$ corresponds to the critical master equation.
  (iii) TCL$_8$ is associated with linear late-time growth.

1. Longitudinal and perpendicular magnetization dynamics

Figures 5(a) and 5(b) illustrate the time evolution of the longitudinal [$\langle s_z(t)\rangle$] and perpendicular [$\langle s_x(t)\rangle$] magnetization components, obtained by solving the rTCL$_6$ ME. In these figures, $s_z(t)\rangle = \frac{1}{2} - \rho_{22}(t)$ corresponds to the population dynamics, and $s_x(t)\rangle = \text{Re}\,\rho_{12}(t)$ corresponds to the coherence dynamics. The initial condition is $\rho(0) = (1 + \sigma_x)/2$, which corresponds to a qubit initially oriented along the positive x direction, in the energy eigenbasis of the isolated qubit. This orientation is aligned with the pointer basis.

The analysis aligns with typical relaxation and decoherence processes observed in qubits. However, while the perpendicular magnetization tends toward an asymptotic value of zero, the longitudinal magnetization exhibits indefinite oscillations, which is nonstandard behavior. The coherence dynamics is decoupled from the population dynamics due to the unbiased nature of the SBM.

The oscillations in the longitudinal magnetization persist because of the second derivative of the time-dependent spectral density, which does not tend to a limit as $t \to \infty$. The peak-to-peak amplitude of the oscillations is proportional to λ^6. We also verified that at late times, $\langle s_z(t) \rangle$ becomes independent of the initial state, to a high degree of precision. Therefore, the dynamics loses the Markovian limit not by retaining memory of the initial state but by remembering the initial time when the system and environment were initialized in a factorized state.

2. Temperature dependence of longitudinal magnetization

Figure 5(c) presents a detailed view of $\langle s_z(t) \rangle$ across extended timescales, particularly at low temperatures where $k_B T \ll \Delta$. At zero temperature ($T = 0$), the oscillations are permanent, as previously analyzed. At nonzero temperature, the oscillations decay over time but never fully converge, even as $t \to \infty$. The late-time behavior is highly sensitive to temperature in this range, despite the average populations remaining mostly constant.

Figure 5(d) shows the relationship between the peak-to-peak amplitude of the oscillations and temperature, recorded at various time intervals. As time increases (moving from right to left: red to orange to blue), the curves converge toward a singular temperature dependence. This indicates that the peak-to-peak amplitude becomes independent of time but is significantly suppressed at nonzero temperatures compared to $T = 0$.

There exists a broad minimum in the temperature range, where the oscillation amplitudes are strongly suppressed. The inset in Fig. 5(d) illustrates the suppression on a log-log scale, showing that the minimum amplitude undergoes exponential suppression as the temperature decreases. The results suggest that the asymptotic state is approached in the limit $T \to 0^+$, even though the oscillations remain permanent at exactly $T = 0$.

3. Criticality of rTCL$_6$ and potential consequences

Our observations highlight the inherently critical character of rTCL$_6$ in the Ohmic environment at low temperatures. In particular, the persistent non-Markovian dynamics it captures may give rise to weak violations of ergodicity at extended timescales. Further investigations, potentially using tensor network methods, are necessary to fully understand the physical ramifications of these effects.

D. rTCL in Ohmic environment

We now explore the inflationary behavior in rTCL, which provides a time limit on the validity of master equations (MEs). This is important because, while physical inflation is not possible in practice, it establishes a reliable time limit. In contrast, weak ergodicity may still arise as a potential outcome [86], although whether it truly occurs remains inconclusive. The results are shown in Fig. 6. The exponential fit in Fig. 6(a) gives a relaxation rate of $\nu_1 = 0.071$, which agrees with the FGR rates within 0.16%.

In the TCL$_2$ method, no correction to $\langle s_z \rangle$ is observed in the asymptotic state compared to the ground-state value of
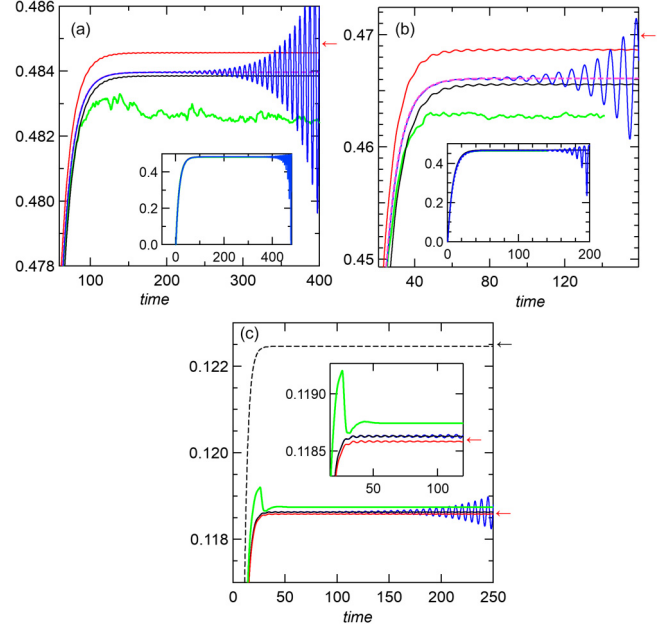

FIG. 6. Time evolution of $\langle s_z(t) \rangle$ in the unbiased SBM. (a), (b) Results at zero temperature for $\lambda^2 = 0.025$ and 0.05, respectively. Different methods are compared: TCL$_4$ (solid red, top), rTCL (solid blue, second from the top), mrTCL (dashed pink), rTCL$_4$ (black, third from the top), and TEMPO (green, bottom). The red arrows indicate the ground-state values obtained using second-order Rayleigh-Schrödinger perturbation theory. (c) $\langle s_z(t) \rangle$ in the unbiased SBM at temperature $T = 2$ and $\lambda^2 = 0.025$. Results are shown for TCL$_2$ (black dashed line), TEMPO (green), rTCL$_4$ (black), rTCL (blue), and TCL$_4$ (red). The black arrow indicates the thermal value, while the red arrow marks the mean-force Gibbs state values. $\Delta = 1$ and $\omega_c = 10$.

the isolated qubit ($\langle s_z \rangle = \frac{1}{2}$; not shown). In contrast, TCL$_4$ computes a population correction that is close to the ground-state value. These corrected values of $\langle s_z \rangle$, obtained from second-order Rayleigh-Schrödinger perturbation theory, are 0.4848 and 0.4696, for Figs. 6(a) and 6(b), respectively [see Eq. (156) for details]. These values are indicated by the red arrows on the vertical axes.

As λ^2 increases from Figs. 6(a) to 6(b), the discrepancy between TCL$_4$, rTCL$_4$, rTCL, mrTCL, and TEMPO [1] methods and the ground state also grows. However, when the asymptotic states of the MEs are computed perturbatively to $O(\lambda^2)$ using the perturbative generator, they precisely match the ground or thermal state at that level of precision (see Sec. VII F and Ref. [20]). We also performed TEMPO simulations using publicly available code from Ref. [1], with parameters set to $K = 500$, $\Delta t = 0.05$, and pp = 70.

At late times, three distinct behaviors are observed:

(1) rTCL: Displays inflationary oscillations.

(2) TCL$_4$ and rTCL$_4$: Both methods converge to unique values without further late-time oscillations.

(3) TEMPO: Fails to settle into a unique state and shows late-time fluctuations in $\langle s_z(t) \rangle$, likely due to time and bond discretizations.

Despite these differences, the average populations remain consistent across all methods.

E. Time limit of rTCL

As shown in Fig. 6, the magnetization computed using rTCL exhibits oscillations that increase in amplitude over extended time periods. This behavior violates the unitary dynamics of the system as a whole, showing the existence of a time limit beyond which rTCL is no longer valid. In this section, we will evaluate this time limit and relate it to the precision limits of asymptotic perturbative generators, as derived in Sec. V C.

1. Nature of the time limit

Since neither TCL$_2$ nor TCL$_4$ exhibit late-time growth (as shown in Fig. 6), the existence of the time limit does not suggest that a master equation cannot be applied at arbitrary times. Rather, the time limit signifies that the accuracy of the asymptotic states becomes imprecise beyond a certain time. In other words, the asymptotic states do not exist with arbitrary precision.

For TCL$_2$ and TCL$_4$, the master equations do not show late-time growth, and the accuracy is preserved at all time. However, for rTCL$_6$, the late-time semigroup behavior is lost in the Ohmic bath, as detailed in Sec. VII C, while rTCL$_8$ shows late-time growth and becomes invalid at late time.

2. Markovian and non-Markovian dynamics

In Figs. 6(a) and 6(b), we observe that the oscillations obtained from solving rTCL are initially symmetric around the asymptotic solution of the Markovian version (mrTCL). This suggests that the rTCL resummation dynamics has an approximate Markovian regime, but it is not merely a continuation of the non-Markovian dynamics.

Typically, non-Markovian master equations offer better accuracy for early-time dynamics compared to Markovian equations [37]. However, at large times, the non-Markovian equations begin to exhibit late-time growth, reversing the initial trend. As a result, there exists a time, denoted t_L, when the accuracy of the Markovian and non-Markovian equations intersects. This defines the time limit beyond which the non-Markovian master equation becomes invalid. After this time, the Markovian approximation should be applied to maintain accuracy, even though the dynamics may remain non-Markovian at arbitrary timescales, as seen in rTCL$_6$.

3. Defining the time limit

In practice, we recommend solving both the rTCL and mrTCL equations, limiting the rTCL calculations to a specific duration. This ensures that a slight discontinuity is introduced between the two equations at the timescale where the oscillation amplitude reaches its minimum. To quantify the time limit, we compare the solutions of the rTCL and mrTCL master equations in the interaction picture:

$$\frac{\partial x}{\partial t} = L^{\mathrm{mr}}(t)x, \tag{144}$$

$$\frac{\partial y}{\partial t} = L^{\mathrm{mr}}(t)y + \mathcal{E}^r(t)y. \tag{145}$$

Here, L^{mr} is the mrTCL generator [from Eq. (34)], and the time dependence arises due to the interaction picture. At

$T = 0$, the term $\mathcal{E}^r$ is derived from L^{mr} by replacing Γ_ω with $\Gamma_\omega(t) - \Gamma_\omega$, which simplifies to

$$\Gamma_\omega(t) - \Gamma_\omega \approx G_\omega(t) = \frac{-2i\lambda^2\Gamma(s+1)\omega_c^2}{\omega}\frac{e^{i\omega t}}{(1+i\omega_c t)^{1+s}} \tag{146}$$

for $t \gg \tau_c$ [see Eq. (25)]. Only $\omega = \Delta - i\nu_2$ needs to be considered, as $G_\omega(t)$ vanishes for $\mathrm{Re}(\omega) \leqslant 0$ and for $t \gg \tau_c$ [because, in that case $\mathrm{Im}(\omega) \geqslant 0$].

4. Weak-coupling regime and time limit

In the weak-coupling regime $\tau_c \ll T_2 = 1/\nu_2$, with a factor of several hundred in our examples. When inflation begins at a timescale of order T_2, we enter the asymptotic regime where $\Gamma_\omega(t) - \Gamma_\omega \approx G_\omega(t)$. The term $|G_\omega(t)| \sim e^{\nu_2 t}/(\omega_c t)^{s+1}$ reaches a minimum at $t_L = (s+1)T_2$. This defines the characteristic timescale above which the distance between the non-Markovian and Markovian generators increases. Both x and y initially relax toward equilibrium at the decoherence rates, but $\mathcal{E}^r(t)$ grows at the decoherence rate ν_2, with an additional power-law decay factor $(\omega_c t)^{-1-s}$.

The state will relax close to equilibrium before inflation prevents it from reaching equilibrium further. This is consistent with the Bogoliubov–van Hove scaling [21], and in the Ohmic bath at at $T = 0$ K, $t_L \approx 4T_1$, roughly in agreement with Figs. 6(a)–6(c).

5. Minimum distance between generators

The minimum distance between the Markovian and non-Markovian generators occurs at $t = t_L$ and is approximately $\approx \|\mathcal{E}^r(t_L)\|$. At this time, we have

$$|G_{t_L}| \sim \lambda^2 e^{s+1}/(\omega_c T_2)^{s+1} = O(\lambda^{2s+4}) \tag{147}$$

and

$$\|\mathcal{E}^r(t_L)\|/\|L^{mr2}\| = O(\lambda^{2s+2}). \tag{148}$$

The error scales continuously with s, compared to the $O(\lambda^{2\lceil s\rceil+2})$ of the TCL$_{2n_{\max}}$ [see the TCL$_{2n}$ precision lemma below Eq. (107)]. While the time limit results in lower precision for small λ and noninteger values s, the precision obtained by the two methods is consistent for integer values of s.

6. Temperature dependence and precision

At nonzero temperature, the relaxation rate is given by

$$\nu_{\beta,1} = 2|A_{12}|^2(J_{\beta,\Delta} + J_{\beta,-\Delta})$$
$$= 2|A_{12}|^2 J_\Delta \coth\frac{\beta\Delta}{2} = \nu_1 \coth\frac{\beta\Delta}{2}. \tag{149}$$

The inflation rate $\nu_2 = \nu_1/2$ is independent of temperature. Therefore, the system can return much closer to equilibrium compared to the zero-temperature case, enhancing the late-time precision of $\langle s_z(t)\rangle$ by a factor of

$$\exp[-(s+1)\nu_2 T_{\beta,1}] = \exp\left[-2(s+1)\coth\frac{\beta\Delta}{2}\right]. \tag{150}$$

This dependence on temperature shows that the precision limit of the asymptotic dynamics has a strong temperature dependence.

7. Comparison to the Bogoliubov–van Hove limit

The time limit is analogous to the Bogoliubov–van Hove ("$\lambda^2 t$") limit, which states that the trace distance between the exact and approximate solutions approaches zero as $\lambda \to 0$, with $t\lambda^2$ being constant. We will now investigate the approach to the ground state and the return to equilibrium in mrTCL, demonstrating a slight improvement over the Bogoliubov–van Hove limit. Specifically, we will show that the asymptotic states of mrTCL exhibit precision $O(\lambda^2)$ relative to standard perturbation theory, while Davies' master equation, valid in the Bogoliubov–van Hove limit, provides an asymptotic state with lower precision of $O(\lambda^0)$ [21].

F. Approach to ground state and return to equilibrium

In this section, we analyze the approach to the ground state and return to equilibrium for an open quantum system. Building on previous results, we extend the analysis to the resummed time-convolutionless (rTCL) master equation in the Markovian regime and confirm that it retains the quadratic accuracy of the asymptotic state in the system-bath coupling strength, λ.

1. Zero-temperature analysis

At zero temperature, the real part of the spectral density at zero frequency vanishes. Consequently, the dephasing rate remains zero upon renormalization, ensuring that the renormalized frequencies in the Markovian equation remain local, even for nonuniform diagonal elements of A. The steady-state excited-state population is derived using Bloch-Redfield theory, incorporating renormalized transition frequencies:

$$\rho_{22} = \frac{\operatorname{Re}\Gamma_{\omega'_{12}}}{\operatorname{Re}\Gamma_{\omega'_{12}} + \operatorname{Re}\Gamma_{\omega'_{21}}}. \quad (151)$$

Applying a Taylor expansion, we express the transition rates as

$$\operatorname{Re}\Gamma_{\omega'_{12}} = \operatorname{Re}\left[\Gamma_{-\Delta} - i\frac{\partial\Gamma_\omega}{\partial\omega}\bigg|_{-\Delta}|A_{12}|^2(\Gamma_{-\Delta} - \Gamma_\Delta)\right] + O(\lambda^6) \quad (152)$$

$$= -|A_{12}|^2\frac{\partial S_\omega}{\partial\omega}\bigg|_{-\Delta}J_\Delta + O(\lambda^6) \quad (153)$$

using the conditions $J_{-\Delta} = 0$ and $dJ_{-\Delta}/d\Delta = 0$ at $T = 0$. Similarly, at positive frequency,

$$\operatorname{Re}\Gamma_{\omega'_{21}} = \operatorname{Re}\left[\Gamma_\Delta - i\frac{\partial\Gamma_\omega}{\partial\omega}\bigg|_\Delta|A_{12}|^2(\Gamma_\Delta - \Gamma_{-\Delta})\right] + O(\lambda^6) \quad (154)$$

$$= J_\Delta + O(\lambda^4). \quad (155)$$

Substituting Eqs. (153) and (155) into (151) and expanding in λ, we obtain

$$\rho_{22} = -|A_{12}|^2\frac{\partial S_\omega}{\partial\omega}\bigg|_{-\Delta} + O(\lambda^4), \quad (156)$$

which matches the second-order Rayleigh-Schrödinger perturbation theory result [20,87].

2. Nonzero temperature analysis

At nonzero temperatures, the dynamics becomes more intricate. As demonstrated in Appendix H, the steady state of the qubit depends on the presence of dephasing:

(i) *Case without dephasing.* If dephasing is absent (i.e., $A_{11} = A_{22}$), the steady state coincides exactly with the mean-force Gibbs state to precision $O(\lambda^2)$. However, this requires inclusion of the nonembeddable leading growths, explicitly accounted for in the rTCL$_4$ master equation as $\tilde{L}$.

(ii) *Case with dephasing.* In the presence of dephasing, the steady state deviates from the mean-force Gibbs state at order $O(\lambda^2)$. Despite this, the TCL$_4$ master equation remains accurate, ensuring that the mean-force Gibbs state is still reproduced at this order. Notably, dephasing does not affect the steady-state populations of the asymptotic qubit state [87].

Thus, we have demonstrated that the rTCL dynamics in the Markovian approximation maintains quadratic accuracy in λ for the approach to the ground state. At zero temperature, the steady state follows second-order Rayleigh-Schrödinger perturbation theory, while at nonzero temperature, the accuracy depends on the presence of dephasing. These results reinforce the accuracy of the rTCL$_4$ master equation in describing open quantum system dynamics.

G. Baths with exponentially relaxing BCFs

A well-known example of a bath with an exponentially relaxing bath correlation function (BCF) is the Ohmic bath with a Drude-Lorentz cutoff in the spectral density, given by

$$J_\omega^{\mathrm{DL}} = 2\pi\lambda^2\frac{\omega\omega_c^2}{\omega^2 + \omega_c^2}\Theta(\omega). \quad (157)$$

The corresponding BCF takes the form

$$C_\beta(t) = \pi\lambda^2\omega_c^2\left[\sum_{n=1}^\infty \frac{8\pi n}{4\pi^2 n^2 - (\beta\omega_c)^2}e^{-n\omega_M t}\right.$$
$$\left. + \left(\cot\frac{\beta\omega_c}{2} - i\right)e^{-\omega_c t}\right]. \quad (158)$$

The imaginary part of $C_\beta(t)$, which remains temperature independent in the Kubo-Martin-Schwinger (KMS) reference state, decays exponentially with a rate of ω_c. Similarly, the real part exhibits exponential decay at finite temperatures, with the decay rate determined by the Matsubara frequency $\omega_M = 2\pi/\beta$.

By substituting $C_\beta(t)$ into Eq. (143), we find that the system exhibits a critical coupling threshold $\lambda_0(T)$, below which the effective BCF ceases to grow exponentially. In the absence of dephasing, this threshold is defined by the condition

$$\nu_2 = \inf(2\pi k_B T, \omega_c). \quad (159)$$

In the limit of large ω_c, the critical coupling simplifies to

$$\lambda_0^2(T) = kT/(\Delta|A_{12}|^2). \quad (160)$$

For couplings satisfying $\lambda < \lambda_0(T)$, the resummed master equation retains a valid Markovian limit. However, as the
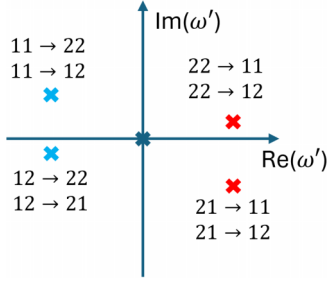
FIG. 7. Renormalization of Bohr frequencies in the spin-boson model at strong dephasing. Both out-of-population transfers are relaxing, while out-of-coherence transfers experience inflation.

temperature approaches zero, the critical coupling $\lambda_0(T)$ vanishes, implying that even weak-coupling strengths can lead to unstable non-Markovian dynamics in the system. This result closely aligns with findings from dynamical resonance theory, as discussed by Merkli [88].

H. Strongly dephasing qubits and the Försters model

So far, we have considered the unbiased spin-boson model (SBM). Now, we shift our focus to the strongly biased SBM, where the dephasing rate significantly exceeds the relaxation rate. As an example, we analyze a dimer composed of two adjacent pigments within a biomolecule, where each qubit state corresponds to an exciton localized at an atomic site. In this scenario, dephasing dominates over relaxation, corresponding to the limit $\theta \to \pi/2^-$ in the coupling operator [Eq. (140)]. Such strongly dephasing qubits are crucial in various biochemical energy transfer processes, particularly in photosynthesis.

Theoretical frameworks for this regime are well established, with Förster's resonant energy transfer (FRET) model serving as a cornerstone [30,31]. This model has been extended into the modified Redfield theory [62], nonequilibrium Förster and modified Redfield approaches [89], and the strong decoherence limit of master equations (ME) [63]. The relationship between the time-convolutionless (TCL) expansion of order $2n$ and these theories is complex. However, we demonstrate that the resummed TCL (rTCL) approach preserves a key feature of the Förster model: *the spectral overlap*.

1. Renormalized frequencies and effective dynamics

When pure dephasing is introduced into the qubit model from the previous section, additional frequency splitting occurs, leading to four renormalized Bohr frequencies instead of two. These are illustrated in Fig. 7. The relevance of each frequency depends on the process under consideration:

(i) Population-to-population and population-to-coherence transitions involve frequencies $\omega_{in}(i)$ and $\omega_{ni}(n)$.

(ii) In this regime, dephasing introduces a positive imaginary frequency shift of $4iJ_0A_{ii}^2$, in addition to the temperature-independent decoherence shift $i\nu_2$.

(iii) If $4J_0A_{ii}^2 > \nu_2$ (i.e., in the strong dephasing regime), the effective BCFs for both population transitions exhibit exponential decay. Consequently, *both* $11 \to 22$ *and* $22 \to 11$

transitions experience deflation, unlike the pure relaxation regime (previous section), where only $22 \to 11$ rates inflated.

On the other hand, coherence-related transitions $\omega_{in}(n)$ and $\omega_{ni}(i)$ experience the opposite frequency shift, $-4iJ_0A_{ii}^2$. These shifts occur in coherence-to-population and coherence-to-coherence transfers. In the strong dephasing limit, this leads to an instability in the resummed dynamics, as coherence transfers become inflated. The time limit (t_L) also differs from the pure relaxation regime due to an additional imaginary shift proportional to $J_{\beta,0}$ in Eq. (142). The bath correlation function decays as t^{-s-1}, with a characteristic timescale:

$$t_L \approx (s+1)/(4J_{\beta,0}|A_{11}|^2) \tag{161}$$

which is inversely proportional to temperature and can be significantly reduced compared to the pure relaxation regime.

2. Comparison between rTCL and Förster theory

For the relaxation transition $ii \to nn$, the rTCL population transfer rate is given by

$$R_{nn,ii}^{\text{rTCL}} = 2|A_{12}|^2 \text{Re} \int_0^\infty dt\, C_\beta(t) \exp\left([i(\omega_{in} + \tilde{\omega}_{\beta,in})\right.$$
$$\left. + \text{sgn}(\omega_{in})\nu_2 - 4A_{11}^2 J_{\beta,0}]t\right), \tag{162}$$

which resembles the Förster transfer rate

$$R_{nn,ii}^{\text{FRET}} = \frac{1}{2}\left|\frac{A_{12}}{A_{11}}\right|^2 \Delta^2 \text{Re} \int_0^\infty dt\, \exp\left(i\omega_{in}t + 4iA_{11}^2 \int_0^t dt_1\right.$$
$$\left. \times [S_0 - S_0(t_1)] - 4A_{11}^2 \int_0^t J_{\beta,0}(t_1)dt_1\right). \tag{163}$$

A detailed derivation of Eq. (163) is provided in Appendix I. Asymptotically at large t, both expressions share the *same spectral overlap* $4|A_{11}|^2 J_{\beta,0}$.

However, significant differences exist between Eqs. (162) and (163):

(1) Prefactor differences ("attempt" frequencies):

(a) rTCL depends on the bath correlation function (BCF), whereas FRET depends on the isolated qubit energy splitting.

(b) This distinction arises because rTCL treats bath interactions as a perturbation, while FRET uses the qubit Hamiltonian's off-diagonal terms in the pointer basis (eigenbasis of A).

(c) Consequently, in the Förster model, transfer rates decrease with increasing λ^2, whereas in rTCL, rates saturate due to the explicit λ^2 prefactor in the BCF.

(2) Role of reorganization energy:

(a) The Förster model incorporates a time-dependent reorganization energy shift $S_0 - S_0(t)$, whereas rTCL instead relies on the Lamb shift at nonzero frequency.

(b) Notably, by setting $A_{11} = -A_{22}$ (which can always be achieved through a unitary transformation of the total Hamiltonian), rTCL does not include a reorganization energy contribution. This contrasts with Förster's theory,

which depends solely on the reorganization energy component of the Lamb shift.

(3) Reference states:

(a) The Förster model assumes *fully displaced thermal states* for the bath [90].

(b) In contrast, rTCL uses the *KMS state* as the reference state.

Conclusion. Despite the above differences, rTCL and the Förster model both capture the essential spectral overlap feature in energy transfer processes. This holds for both downhill and uphill energy transfer directions. This confirms that our resummation scheme correctly reproduces the exponents found in Förster's theory, while also allowing for an investigation of *dephasing-assisted transport.* Future work will explore the mrTCL approach [Eq. (34)]. A key advantage of mrTCL over Förster's theory is that it captures both coherence and population dynamics, including nonsecular transitions, whereas the Förster model only describes population dynamics.

VIII. DISCUSSION AND CONCLUSION

In this study, we present a resummation method for perturbative master equations in open quantum systems, offering a simple, accurate, and intuitive approach to describing system dynamics across a wide range of timescales. Our resummation master equation demonstrates that the Markovian limit for the reduced system dynamics holds at all timescales when bath correlations relax exponentially over time and when the system-bath coupling constant remains below a specific threshold. However, even when bath correlations decay algebraically with time, leading to inflation in the resummation generator, we still obtain a highly accurate Markovian master equation. In fact, the results are often consistent with canonical steady states to an accuracy of $O(\lambda^2)$, addressing a long-standing challenge in open quantum systems theory.

Despite the benefits of exponential decay, nature often resists exponential relaxation at the fundamental scales of the system, particularly at low temperatures. Many physical systems exhibit Ohmic behavior, characterized by quadratic decay in bath correlations. This is prevalent in systems such as electromagnetic and gravitational fields, thermally accelerated qubits, spin baths, phonon baths with defects, and more. In these cases, the resummation of late-time growth in all orders of the coupling constant leads to inflation in the time-convolutionless (TCL) generator. Mathematically, this inflation arises from the pairing of equal but opposite Bohr frequencies. If one Bohr frequency develops a width due to the resummation, leading to exponential decay, the opposite frequency will mirror that width but with exponential growth instead of decay. Without pure dephasing, the timescale of this growth is proportional to $s + 1$ times the decoherence time at zero temperature. The larger the parameter s, the more closely the system can approach the steady state before the growth invalidates the resummation dynamics. The absence of a Markovian limit in the resummation suggests that the dynamics cannot be exactly captured by the perturbative master equation. The precision of the asymptotic states is ultimately constrained by the perturbative order at which late-time growth begins to dominate.

Looking ahead, we see three potential directions for further investigation into the late-time behavior of open quantum systems:

(1) *Infrared divergence in the spin-boson model.* Further exploration of the problem of infrared divergence in the spin-boson model is a natural next step. The upper bound on the number of soft quanta emitted during the relaxation process scales as t^{1-s} [20,73], which mirrors the late-time growth at zero frequency observed in TCL$_4$. A partial resummation of the zero-frequency growth is necessary, but it will not result in secular inflation, as zero-frequency renormalizes to zero frequency (i.e., without involving imaginary components that give rise to inflation).

(2) *Nonlocality in spectral overlap and dephasing-assisted transport.* Another area of interest is the nonlocal characteristics of the spectral overlap revealed through our resummation method. It would be insightful to explore whether nonlocality enhances dephasing-assisted transport over large spatial distances, as seen in works such as Refs. [91–94]. Understanding this could have significant implications for biological and quantum information processing systems.

(3) *Mapping cumulant expansions to influence function networks.* Lastly, the equivalence between TCL, cumulant expansions, and influence function methods [95] suggests a promising avenue for mapping the leading cumulants into networks of influence functions. Tensor networks have recently emerged as powerful models for efficiently evaluating the influence functional over long timescales [15–19]. These networks offer advantages over cumulant expansions by directly performing partial traces of unitary dynamics, thereby mitigating the issue of inflation. Mapping cumulants to influence function networks could lead to the development of more efficient tensor network methods for simulating the late-time dynamics of open quantum systems.

DATA AVAILABILITY

The data that support the findings of this article are not publicly available. The data are available from the authors upon reasonable request.

APPENDIX A: PROOF OF THE HADAMARD IDENTITY (68)

For the first equation in (68), we have

$$\int_{t_i}^{t_f} dt_a \, \hat{A}(t_a) C(t_a - t_b)$$

$$= \int_{t_i}^{t_f} dt_a \, C(t_a - t_b) A_{nm} e^{i\omega_{nm}t_a}$$

$$= A_{nm} e^{i\omega_{nm}t_b} \int_{t_i-t_b}^{t_f-t_a} d\tilde{t} \, C(\tilde{t}) e^{i\omega_{nm}\tilde{t}}$$

now defining $\tilde{t} \equiv t_a - t_b$. Next, we utilize the relation between the bath correlation function and the timed spectral density

$$A_{nm} e^{i\omega_{nm}t_b} \int_{t_i-t_b}^{t_f-t_b} d\tilde{t} \, C(\tilde{t}) e^{i\omega_{nm}\tilde{t}}$$

$$= A_{nm} e^{i\omega_{nm}t_k}[\Gamma_{nm}(t_f - t_b) - \Gamma_{nm}(t_i - t_b)]$$

$$= \hat{A}(t_b) \circ [\Gamma(t_f - t_b) - \Gamma(t_i - t_b)]$$

$$= \hat{b} \circ [\Gamma(t_f - t_b) - \Gamma(t_i - t_b)].$$

The proof of the second equation in (68) follows from the same steps and justifications as the last:

$$\int_{t_i}^{t_f} dt_a \hat{A}(t_a) C(t_b - t_a) = \int_{t_i}^{t_f} dt_a C(t_b - t_a) A_{nm} e^{i\omega_{nm}t_a}$$

$$= A_{nm} e^{i\omega_{nm}t_b} \int_{t_b-t_f}^{t_b-t_i} d\tilde{t} \, C(\tilde{t}) e^{i\omega_{mn}\tilde{t}},$$

where $\tilde{t} \equiv t_b - t_a$. Again, we utilize the relation between the bath correlation function and the timed spectral density:

$$A_{nm} e^{i\omega_{nm}t_b} \int_{t_b-t_f}^{t_b-t_i} d\tilde{t} \, C(\tilde{t}) e^{i\omega_{mn}\tilde{t}}$$

$$= A_{nm} e^{i\omega_{nm}t_b}[\Gamma_{mn}(t_b - t_i) - \Gamma_{mn}(t_b - t_f)]$$

$$= A_{nm} e^{i\omega_{nm}t_b}[\Gamma_{nm}^T(t_b - t_i) - \Gamma_{nm}^T(t_b - t_f)]$$

$$= \hat{b} \circ [\Gamma^T(t_b - t_i) - \Gamma^T(t_b - t_f)].$$

APPENDIX B: INTEGRATION BOUNDS FOR TIME-ORDERED INTEGRALS

In this and the following Appendixes only, we identify $t \to t_{2n}$ *and* $t_0 \to 0$ *so we will have* $0 = t_0 < t_1 < t_2 < \cdots < t_{2n} = t$ *for* TCL$_{2n}$. This is unconventional, but as we shall see, this will be a huge notational convenience. Assume we have a time-ordered iterated integral of the form

$$\int_0^{t_k} dt_{k-1} \int_0^{t_{k-1}} dt_{k-2} \ldots \int_0^{t_2} dt_1, \tag{B1}$$

and we want to rewrite this integral in the arbitrary order

$$\int dt_{\alpha_1} \int dt_{\alpha_2} \ldots \int dt_{\alpha_{k-1}}, \tag{B2}$$

where the α_i's give a permutation of $\{1, \ldots, k-1\}$. We now detail a simple algorithm for determining the bounds on this arbitrary rearrangement of the time-ordered integral.

For each $1 \leqslant i \leqslant k$, define the lesser child of α_i to be

$$l_i := \sup(\{0\} \cup \{\alpha_j : j < i \text{ and } \alpha_j < \alpha_i\})$$

and define the greater child of α_i to be

$$g_i := \inf(\{k\} \cup \{\alpha_j : j < i \text{ and } \alpha_j > \alpha_i\}).$$

Alternatively, write the numbers 0 and k and then α_1 through α_{k-1} sequentially:

$$0 \, k \quad \alpha_1 \, \alpha_2 \, \ldots \, \alpha_i \, \alpha_{i+1} \, \ldots \, \alpha_{k-1}. \tag{B3}$$

The lesser child of α_i is then the greatest number written to the left of α_i in Eq. (B3) that is also less than α_i, and the greater child of α_i is the smallest number written to the left of α_i in Eq. (B3) that is also greater than α_i. This visualization will be quite useful later. The bounds on the integrals in Eq. (B2) are then given by

$$\int_{t_{l_1}}^{t_{g_1}} dt_{\alpha_1} \int_{t_{l_2}}^{t_{g_2}} dt_{\alpha_2} \ldots \int_{t_{l_{k-1}}}^{t_{g_{k-1}}} dt_{\alpha_{k-1}}, \tag{B4}$$

where we adopt the convention $t_0 = 0$, as before. That is, the integral corresponding to t_{α_j} has lower bound t_{l_j} and upper bound g_{l_j}.

The intuition for this result is that the space we are integrating over is given by

$$0 < t_1 < t_2 < \cdots < t_{k-1} < t_k, \tag{B5}$$

where (for the sake of our integration) 0 and t_k are fixed. So one can imagine picking $k - 1$ numbers $t_1, t_2, \ldots, t_{k-1}$, on a number line, in order, such that they satisfy Eq. (B5). The set of all possible ways to do this corresponds to the integration region given by Eq. (B1). To find the bounds on a rearrangement of these integrals, we need only ask how we can choose these $k - 1$ numbers out of order (in particular, in the order $t_{\alpha_1}, t_{\alpha_2}, \ldots, t_{\alpha_{k-1}}$) such that we scan the same space: our numbers still satisfy Eq. (B5) and, moreover, every ordered $(k - 1)$-tuple of numbers t_1 through t_{k-1} that satisfies Eq. (B5) is achievable by our new method of picking our numbers out of order. With this in mind, the reader may want to consider playing with an example ordering to illuminate why Eq. (B4) is correct.

We can prove Eq. (B4) is correct rigorously via induction. Note that a series of iterated integrals of the form in Eq. (B1) can always be rearranged into a series of iterated integrals of the form in Eq. (B2) through a series of finite "swaps": exchanging the order between two neighboring integrals. Since Eq. (B1) is of the form given by Eq. (B4), we need only show that performing a "swap" on a series of integrals of the form given by Eq. (B4) returns a series of integrals which are still in the form (B4), with only α_1 through α_{k-1} potentially changing value.[2] That is, after performing a swap, the bounds on each integral remain the lesser and greater children of the *new* permutation of $\{1, 2, \ldots, k - 1\}$, in accordance with Eq. (B4).

---

[2]Performing a swap is equivalent to transposing α_i and α_{i+1} for some $1 \leqslant i \leqslant k - 2$.

To wit, say we swap the integrals corresponding to α_i and α_{i+1} for some $1 \leqslant i \leqslant k-2$. We want to show

$$\int_{t_{l_1}}^{t_{g_1}} dt_{\alpha_1} \ldots \int_{t_{l_i}}^{t_{g_i}} dt_{\alpha_i} \int_{t_{l_{i+1}}}^{t_{g_{i+1}}} dt_{\alpha_{i+1}} \ldots \int_{t_{l_{k-1}}}^{t_{g_{k-1}}} dt_{\alpha_{k-1}} f(\mathbf{t})$$
$$= \int_{t_{l'_1}}^{t_{g'_1}} dt_{\alpha_1} \ldots \int_{t_{l'_{i+1}}}^{t_{g'_{i+1}}} dt_{\alpha_{i+1}} \int_{t_{l'_i}}^{t_{g'_i}} dt_{\alpha_i} \ldots \int_{t_{l'_{k-1}}}^{t_{g'_{k-1}}} dt_{\alpha_{k-1}} f(\mathbf{t}),$$
(B6)

where $f(\mathbf{t})$ is an arbitrary test function, and $\mathbf{t} = (t_1, t_2, \ldots, t_k)$. We have denoted the greater and lesser children of α_j in the *swapped* permutation by g'_j and l'_j, respectively. In the language of Eq. (B3), l'_j and g'_j are the lesser and greater children of α_j in the following string:

$$0 \, k \ \ \alpha_1 \, \alpha_2 \, \ldots \, \alpha_{i+1} \, \alpha_i \, \ldots \, \alpha_{k-1}. \tag{B7}$$

If Eq. (B6) holds, then (B4) gives the correct bounds on a rearrangement of the time-ordered integral (B1).

To prove Eq. (B6), first consider what happens when we swap the t_{α_i} and $t_{\alpha_{i+1}}$ integrals on the left-hand side of (B6). Note that the bounds only change for the two integrals over t_{α_i} and $t_{\alpha_{i+1}}$. Hence, if Eq. (B6) is to hold, we need that $g_j = g'_j$ and $l_j = l'_j$ for $j < i$ or $j > i+1$. But this is simple to show: if $j < i$, then the numbers to the left of α_j are the same in Eqs. (B3) and in (B7), so the greater and lesser children of α_j will be the same. Similarly, if $j > i+1$, the numbers to the left of α_j are the same in both equations: they are just in a different order, which is irrelevant to determining lesser and greater children.

Now all that is left to show is that the bounds on the two swapped integrals are correct. That is, we need only show

$$\int_{t_{l_i}}^{t_{g_i}} dt_{\alpha_i} \int_{t_{l_{i+1}}}^{t_{g_{i+1}}} dt_{\alpha_{i+1}} h(\mathbf{t}) = \int_{t_{l'_{i+1}}}^{t_{g'_{i+1}}} dt_{\alpha_{i+1}} \int_{t_{l'_i}}^{t_{g'_i}} dt_{\alpha_i} h(\mathbf{t}) \tag{B8}$$

for an arbitrary test function $h(\mathbf{t})$.[3] There are three cases:

(1) $g_{i+1} \neq \alpha_i$ and $l_{i+1} \neq \alpha_i$. In this case the integration region in Eq. (B8) is a rectangular one, so the bounds do not change after swapping the integrals. Hence, we must show $g_i = g'_i$, $h_i = h'_i$, $g_{i+1} = g'_{i+1}$, $h_{i+1} = h'_{i+1}$. Because $g_{i+1} \neq \alpha_i$, we know the greater child of α_{i+1} in Eq. (B3) lies to the left of α_i; so after swapping, the greater child of α_{i+1} remains the same in Eq. (B7). The same applies for the lesser child of α_{i+1}. Hence, $g_{i+1} = g'_{i+1}$ and $h_{i+1} = h'_{i+1}$ both hold. Without loss of generality, assume $\alpha_i < \alpha_{i+1}$. Then $l_{i+1} \neq \alpha_i$ implies there exists a $j < i$ such that $\alpha_i < \alpha_j < \alpha_{i+1}$. Then in Eq. (B7), the greater child of α_i cannot be α_{i+1}, and therefore the greater child does not change after swapping. Moreover, the lesser child of α_i in Eq. (B7) cannot be α_{i+1} because $\alpha_{i+1} > \alpha_i$, so the lesser child of α_i remains the same after swapping. Hence, $g_i = g'_i$ and $h_i = h'_i$ both hold. The logic is similar if $\alpha_i > \alpha_{i+1}$.

(2) $g_{i+1} = \alpha_i$ and $l_{i+1} \neq \alpha_i$. Note this implies $\alpha_{i+1} < \alpha_i$, and therefore $l_{i+1} = l_i$. In this case the integration region in

Eq. (B8) is triangular, so we have

$$\int_{t_{l_i}}^{t_{g_i}} dt_{\alpha_i} \int_{t_{l_{i+1}}}^{t_{g_{i+1}}} dt_{\alpha_{i+1}} h(\mathbf{t}) = \int_{t_{l_i}}^{t_{g_i}} dt_{\alpha_i} \int_{t_{l_i}}^{t_{\alpha_i}} dt_{\alpha_{i+1}} h(\mathbf{t})$$
$$= \int_{t_{l_i}}^{t_{g_i}} dt_{\alpha_{i+1}} \int_{t_{\alpha_{i+1}}}^{t_{g_i}} dt_{\alpha_i} h(\mathbf{t}).$$

So we need to show that $g'_{i+1} = g_i$, $l'_{i+1} = l_i$, $g'_i = g_i$, $l'_i = \alpha_{i+1}$. Because $g_{i+1} = \alpha_i$, we know that for all $j < i$, we must either have $\alpha_j > \alpha_i > \alpha_{i+1}$ or $\alpha_i > \alpha_{i+1} > \alpha_j$. Focus on the first case. After swapping the integrals, the greater child of α_{i+1} in Eq. (B7) will therefore be the *second* smallest number greater than α_{i+1} to the left of α_{i+1} in Eq. (B3), which is thus the first smallest number to the left of α_i in Eq. (B7), that is, g_i. Hence, $g'_{i+1} = g_i$. Similarly, the second case implies $l'_{i+1} = l_i$. Because $\alpha_i > \alpha_{i+1}$, the greater child of α_i does not change when we swap the integrals, so $g'_i = g_i$. Moreover, we know there does not exist a $j < i$ satisfying $\alpha_i > \alpha_j > \alpha_{i+1}$, which implies the lesser child of α_i in Eq. (B7) is α_{i+1}. Hence, $l'_i = \alpha_{i+1}$.

(3) $l_{i+1} = \alpha_i$ and $g_{i+1} \neq \alpha_i$. This implies $\alpha_{i+1} > \alpha_i$, and thus $g_{i+1} = g_i$. Again, we get a triangular integration region, and the logic hereon is essentially identical to the previous case, just swapping the roles of the lesser children and the greater children.

Hence, Eq. (B6) is true and then, by induction, Eq. (B4) gives the correct bounds for an arbitrary rearrangement of the time-ordered integral (B1).

APPENDIX C: HADAMARD TRICK FOR ITERATED INTEGRALS

We can generalize Eq. (68) for iterated integrals, which we inevitably encounter in TCL$_{2n}$. Take TCL$_6$, for example. Our superoperator is now $\mathcal{B}(\hat{1}, \ldots, \hat{6}): L(\mathcal{H})^6 \to L(\mathcal{H})$, a multilinear superoperator, linear in each component. We have five integrals, three correlation functions. For each of these correlation functions we can eliminate one integral using the Hadamard trick. For TCL$_{2n}$, we have n correlation functions and $2n - 1$ integrals. Ideally, we could perform the Hadamard trick n times to reduce our $(2n - 1)$-dimensional integral to a $(n - 1)$-dimensional integral. However, our integrals need to satisfy certain rules for the Hadamard trick to be performed n times consecutively.

1. Sufficient conditions to perform the iterated Hadamard trick

Let us work through a specific example for TCL$_4$ to discover these rules. We will start with the time-ordered integral

$$\int_0^{t_4} dt_3 \int_0^{t_3} dt_2 \int_0^{t_2} dt_1 \, \mathcal{B}(\hat{1}, \hat{2}, \hat{3}, \hat{4}) \langle 43 \rangle \langle 21 \rangle. \tag{C1}$$

Since $\langle 43 \rangle$ is a constant with respect to t_2 and t_3, it can be ignored for the innermost integral, and we can then perform the Hadamard trick on the integral over t_1 to obtain

$$\int_0^{t_4} dt_3 \int_0^{t_3} dt_2 \, \mathcal{B}(\hat{2} \circ \Gamma^T(t_2), \hat{2}, \hat{3}, \hat{4}) \langle 43 \rangle,$$

noting that $\Gamma(0) = 0$.

---

[3]To be precise, we can take $h(\mathbf{t}) = \int_{t_{l_{i+2}}}^{t_{g_{i+2}}} dt_{\alpha_{i+2}} \ldots \int_{t_{l_{k-1}}}^{t_{g_{k-1}}} dt_{\alpha_{k-1}} f(\mathbf{t})$.

At this point, we would like to perform the Hadamard trick a second time to eliminate the integral over t_2. However, we encounter a problem: the correlation function involving t_2 has already been used up, and therefore we cannot perform the Hadamard trick to eliminate the integral over t_2. This problem occurred because one of our correlation terms was $\langle 21 \rangle$: this correlation term involved two times that were among the integrating variables in the innermost two integrals. When we integrated over one of these times (t_1 in this instance), we lost the correlation term for the other time (t_2 in this instance). This gives us our first condition if we are to utilize the Hadamard trick n times: none of the innermost n integration variables can be paired up together in a single correlation term. Or, equivalently, note the following:

Condition 1. Each correlation term must involve exactly one time in the innermost n integration variables in the iterated integral expression.

Let us next satisfy this condition. We cannot change our correlation terms, but we can rearrange the order of our integrals appropriately, so that each correlation term involves exactly one time in the innermost n integrals, and one time in the outermost $n-1$ integrals (or t_{2n}). We can adopt this condition into our string notation presented in Eq. (B3). Since we are working in TCL$_{2n}$, our permutation goes from α_1 to α_{2n-1} (we have $2n-1$ integrals). Draw a vertical bar between α_{n-1} and α_n. Condition 1 says that each correlation pair should have exactly one number to the left of the vertical bar, and one number to the right of the vertical bar. We can visualize this by connecting correlation pairs together in the string. Take our current example given by Eq. (C1). The corresponding string for that equation would be

$$0\,\overset{\frown}{4\ 3}\,|\,\overset{\frown}{2\,1},$$

where we have used Wick contraction-style notation to denote correlation pairs. Rearranging the integrals allows us to change the order of the α_i's: everything except the 0 and 4. When rearranging, the vertical bar stays fixed such that there are $n+1$ numbers (total) to the left of the bar and n numbers to the right of the bar. Again, our goal is to rearrange the three rightmost digits such that each pair lies on opposite sides of the vertical bar. There are several ways to do this; one such (unintelligent, as we will soon see) way is

$$0\,\overset{\frown}{4\ \overset{\frown}{1}\,|\,3}\,2.\tag{C2}$$

According to Appendix B, this string corresponds to the following rearrangement of Eq. (C1):

$$\int_0^{t_4} dt_1 \int_{t_1}^{t_4} dt_3 \int_{t_1}^{t_3} dt_2\, \mathcal{B}(\hat{1}, \hat{2}, \hat{3}, \hat{4}) \langle 43 \rangle \langle 21 \rangle.$$

We can use the Hadamard trick to eliminate the innermost integral:

$$\int_0^{t_4} dt_1 \int_{t_1}^{t_4} dt_3\, \mathcal{B}(\hat{1}, \hat{1} \circ \Gamma(t_3 - t_1), \hat{3}, \hat{4}) \langle 43 \rangle.$$

Again, we would like to use the Hadamard trick to eliminate the integral over t_3, but this time we encounter a different problem: the dependence of the integrand on t_3 is not just through $\hat{3}$ and $\langle 43 \rangle$: there is also a dependence from the second

component of $\mathcal{B}$, through the $\Gamma(t_3 - t_1)$ term. The Hadamard trick, as listed in Eq. (68), is not applicable here. The problem was that when we applied the Hadamard trick to eliminate the integral over t_2, we introduced an additional dependence on t_3 because the upper bound on the integral over t_2 was t_3. Indeed, for TCL$_{2n}$, any time our integration bounds on the innermost n integrals involve any of the innermost n integration variables, we are at risk of encountering this problem. To avoid this problem, we need to ensure the bounds on the innermost integrals are only dependent on the outermost integration variables. In the language of Appendix B, this gives us our second condition:

Condition 2. The greater and lesser child of each of the innermost n integration variables cannot be any of the innermost n integration variables.

Referring to our string paradigm, Condition 2 can be rephrased as follows: the lower and greater child of each of the numbers to the right of the vertical bar must lie to the left of the vertical bar. With this in mind, we can see why the string in Eq. (C2) fails to work: the upper neighbor of 2 (which is 3) lies to the right of the vertical bar.

It hopefully is intuitively clear that Conditions 1 and 2, taken together, are sufficient to perform the Hadamard trick n times to eliminate the innermost n integrals in a TCL$_{2n}$ expression.[4] Condition 1 ensures that an appropriate correlation term is available for each of the n applications of the Hadamard trick, and Condition 2 ensures that the only time dependence of $\mathcal{B}$ on the innermost integration variable t_a is through $\hat{a}$.

2. Integral rearrangement algorithm

The question now becomes if it is always possible to find a rearrangement of a string of the form given by Eq. (B4) that satisfies Conditions 1 and 2. The answer is no. Take the following example:

$$0\,\overset{\frown}{6\ \overset{\frown}{5\ 4}\,|\,\overset{\frown}{3\ 2}\,1}.\tag{C3}$$

There is no rearrangement of these digits that satisfies Conditions 1 and 2. Note that, since 6 is fixed to the left of the vertical bar, Condition 1 forces the 2 to lie to the right of the vertical bar. Moreover, Condition 1 forces one of the 1 or 3 to be to the right of the vertical bar. Suppose the 1 is to the right of the vertical bar. If the 1 is placed to the right of the 2, then the greater child of 1 lies to the right of the vertical bar, which violates Condition 2. If the 1 is placed to the left of 2, then the lesser child of 2 lies to the right of the vertical bar, which violates Condition 2. A similar problem occurs if the 3 is placed to the right of the vertical bar instead. Hence, there is no rearrangement of these symbols that satisfies both Conditions 1 and 2.

The situation is not hopeless because we can loosen the required conditions on our rearrangement by splitting an

---

[4]Note it may not be the case that these two conditions are *necessary* to perform the Hadamard trick n times, although although this may be the case that they are.

integral into two: we can write

$$\int_{t_i}^{t_f} dt_a\, f(\mathbf{t}) = \int_0^{t_f} dt_a\, f(\mathbf{t}) - \int_0^{t_i} f(\mathbf{t})$$

and, as a result, we have, for any $1 \leqslant i \leqslant k$,

$$
\begin{aligned}
\int dt_1 & \ldots \int_{t_i}^{t_f} dt_i \ldots \int dt_k\, f(\mathbf{t}) \\
&= \int dt_1 \ldots \int_0^{t_f} dt_i \ldots \int dt_k\, f(\mathbf{t}) \\
&\quad - \int dt_1 \ldots \int_0^{t_i} dt_i \ldots \int dt_k\, f(\mathbf{t}),
\end{aligned}
\tag{C4}
$$

where the bounds on the other integrals are arbitrary. This is useful to us because it allows us to loosen Condition 2: for each of the two integrals on the right-hand side of Eq. (C4), we only have to worry about *one* of the greater or lesser children for t_i, because the other bound is now 0, and thus will not introduce an incompatible time dependence. For the first integral, we only need to satisfy Condition 2 for the *greater* child of t_i, and for the second integral, we only need to satisfy Condition 2 for the *lesser* child of t_i.

However, we need to rearrange our iterated integrals once we have split them. The method outlined in Appendix B no longer works because neither of the integrals' expressions on the right-hand side of Eq. (C4) is necessarily in the form of Eq. (B4), so as of now we have no idea what the bounds on a rearrangement of either these integral expressions would be. However, we avoid this issue by *only rearranging integrals to the left of the integral we have split.* In Eq. (C4), for example, after splitting, we would only rearrange the integrals corresponding to t_1 through t_{i-1}. Because the bounds on $\int dt_j$ are only dependent on the bounds on the integrals to its left[5] (i.e., $\int dt_1$ through $\int dt_{j-1}$), we are free to rearrange any of the integrals to the left of a split integral, and the bounds on these integrals are still given by their greater and lesser children as in Appendix B. The same applies to the integrals to the right of our split integral, but the integral rearrangement algorithm explained below does not utilize this fact.

Returning to our string notation, we will indicate an integral expression that has been split using a subscript or superscript asterisk. A subscript asterisk next to a digit indicates that we only need to satisfy Condition 2 for the lesser child of said digit, and a superscript asterisk next to a digit indicates that we only need to satisfy Condition 2 for the greater child of said digit. For example, the integral expression

$$\int_0^{t_4} dt_2 \int_0^{t_4} dt_3 \int_0^{t_2} dt_1\, f(\mathbf{t}) - \int_0^{t_4} dt_2 \int_0^{t_2} dt_3 \int_0^{t_2} dt_1\, f(\mathbf{t})$$

corresponds to the strings

$$0\,4\;\;2\,|\,3^*\,1 - 0\,4\;\;2\,|\,3_*\,1.$$

Now let us use this splitting technique to find a valid set of arrangements to perform the Hadamard trick three times for the integral expression corresponding to Eq. (C3). We will soon

---

generalize this logic into a recursive integral rearrangement algorithm for TCL_{2n}.

First, move the digit paired with 6 all the way to the right:

$$0\,6\;\;5\,4\,|\,3\,1\,2.$$

Then, split the integral corresponding to the digit paired with 6:

$$0\,6\;\;5\,4\,|\,3\,1\,2^* - 0\,6\;\;5\,4\,|\,3\,1\,2_*$$

Focusing on the first string, we need the greater child of 2 (which is 3) to be to the left of the vertical bar, so we move the 3 all the way to the left. For the second string, we need the lesser child of 2 (which is 1) to be to the left of the vertical bar, so we move the 1 all the way to the left:

$$0\,6\;\;3\,5\,|\,4\,1\,2^* - 0\,6\;\;1\,5\,|\,4\,3\,2_*.$$

This completes the first recursion in the algorithm. At this point, we fix the rightmost and (excluding the 0 and 6) leftmost digits, and iterate this process with the three remaining digits (the 5, 4, 1 in the first string, and the 5, 4, 3 in the second string). Note we have essentially just reduced a TCL_6 problem into two TCL_4 problems:

$$0\,3\;\;5\,|\,4\,1 \quad \text{and} \quad 0\,1\;\;5\,|\,4\,3 \tag{C5}$$

Next, we handle each of these TCL_4 problems separately. Our first step would be to shift the number paired with the leftmost (nonzero) digit all the way to the right, but this is already the case, so we can skip that step.

Next, focus on the second string in Eq. (C5). The greater and lesser children of 3 in the second string are 4 and 1, respectively. 1 is already *fixed* to the left of the vertical bar, so we do not need to split the 3. Essentially, we can act as though we have already split the 3, and only worry about satisfying Condition 2 for the greater child of 3 (you can imagine there is a 3^* there instead of a 3). At this point, we just repeat the same process we used to reduce our TCL_6 problem into TCL_4 problems: take the greater child of 3 (a 4), and move it as far left as possible. We find our final string to be

$$0\,1\;\;4\,|\,5\,3.$$

Now that the conditions on the 3 are satisfied, we have reduced our TCL_4 problem into a TCL_2 problem:

$$0\,4\;\;|\,5,$$

which always satisfies Conditions 1 and 2 without further rearrangement.

Looking at the first string and noting the lesser child of 1 is 0, which is already fixed to the left of the vertical bar, we move the greater child of 1 as far right as possible. The lesser child of 1 is 3, which is already moved as far left as possible, so we do not actually have to change anything about this second string. Hence, our final, valid, TCL_6 expression is given by

the right-hand side of the following "equality":

$$06\ 54\,|\,321 = 06\ 35\,|\,412_* - 06\ 14\,|\,532_*.$$

The great thing about this string notation is that it only takes seconds to check that the two strings on the right-hand side satisfy both conditions. Written out as integrals, these strings correspond to the following equality[6]:

$$\int_0^{t_6} dt_5 \int_0^{t_5} dt_4 \int_0^{t_4} dt_3 \int_0^{t_3} dt_2 \int_0^{t_2} dt_1\, \mathcal{B}(\hat{1}, \hat{2}, \hat{3}, \hat{4}, \hat{5}, \hat{6})\langle 62\rangle\langle 54\rangle\langle 31\rangle$$

$$= \int_0^{t_6} dt_3 \int_{t_3}^{t_6} dt_5 \int_{t_3}^{t_5} dt_4 \int_0^{t_3} dt_1 \int_0^{t_3} dt_2\, \mathcal{B}(\hat{1}, \hat{2}, \hat{3}, \hat{4}, \hat{5}, \hat{6})\langle 62\rangle\langle 54\rangle\langle 31\rangle$$

$$- \int_0^{t_6} dt_1 \int_{t_1}^{t_6} dt_4 \int_{t_4}^{t_6} dt_5 \int_{t_1}^{t_4} dt_3 \int_0^{t_1} dt_2\, \mathcal{B}(\hat{1}, \hat{2}, \hat{3}, \hat{4}, \hat{5}, \hat{6})\langle 62\rangle\langle 54\rangle\langle 31\rangle. \tag{C6}$$

We can then apply the Hadamard trick [Eq. (68)] three times for each integral expression on the right-hand side of this equation to obtain

$$\int_0^{t_6} dt_5 \int_0^{t_5} dt_4 \int_0^{t_4} dt_3 \int_0^{t_3} dt_2 \int_0^{t_2} dt_1\, \mathcal{B}(\hat{1}, \hat{2}, \hat{3}, \hat{4}, \hat{5}, \hat{6})\langle 62\rangle\langle 54\rangle\langle 31\rangle$$

$$= \int_0^{t_6} dt_3 \int_{t_3}^{t_6} dt_5\, \mathcal{B}(\hat{3} \circ [\Gamma^T(t_3)], \hat{6} \circ [\Gamma^T(t_6) - \Gamma^T(t_6 - t_3)], \hat{3}, \hat{5} \circ \Gamma^T(t_5 - t_3), \hat{5}, \hat{6})$$

$$- \int_0^{t_6} dt_1 \int_{t_1}^{t_6} dt_4\, \mathcal{B}(\hat{1}, \hat{6} \circ [\Gamma^T(t_6) - \Gamma^T(t_6 - t_1)], \hat{1} \circ \Gamma(t_4 - t_1), \hat{4}, \hat{4} \circ \Gamma(t_6 - t_4), \hat{6}).$$

We have reduced a quintuple integral into two double integrals.

The general algorithm follows naturally from this example. Start with a general TCL$_{2n}$ string:

$$0\,2n\ \alpha_1\,\alpha_2\,\ldots\,\alpha_{n-1}\,|\,\alpha_n\,\ldots\,\alpha_{2n-1}. \tag{C7}$$

We have omitted the Wick contraction pairings for the sake of clarity. We will instead explicitly state which digits are paired together by correlation terms. The general algorithm is as follows:

(1) Label r the rightmost *fixed* digit that is to the left of the vertical bar. Take the digit paired with r and call it s. Move s as far right as possible, without passing it through any fixed digits. Fix s at this position.

(2) Label g_s and l_s the greater and lesser children of s (in its newly fixed position), respectively. If neither of g_s or l_s are already fixed to the left of the vertical bar, then split s into the difference of two strings, the first with s^* in the place of s, and the second with s_* in the place of s. Otherwise, do not split s.

We now introduce the label "*relevant child.*" The relevant child of s^* is g_s, the relevant child of s_* is l_s, and the relevant child of s, if the string has not been split, is the child of s that is not fixed to the left of the vertical bar. Label the relevant child of s as c_s.

(3) Move c_s as far left as possible, without passing it through any fixed digits. Fix c_s at this position. You have reduced a TCL$_{2n}$ string into either one or two TCL$_{2n-2}$ string(s), each with some ancillary fixed digits.

(4) Repeat steps 1 through 3 on each of these strings (now with $n \to n - 1$) until you are left with strings that only have one nonfixed digit (TCL$_2$ strings), at which point stop. You should have a sum of strings which all adhere to Conditions 1 and 2, and therefore the Hadamard

trick can be performed on each of these strings n times systematically.

Some notes on the algorithm:

(i) By the nature of the algorithm, s should never be fixed at the start of step 1.

(ii) In step 2, you may worry that we would have to split s if g_s and l_s are paired together. This is a valid concern, but, again by the nature of the algorithm, this can only occur if neither g_s nor l_s are fixed to the left of the vertical bar, so it is, logically speaking, a superfluous concern. This is because if, for example, g_s was fixed to the left of the vertical bar and g_s was paired with l_s, then l_s would be fixed to the right of s, and therefore l_s could not be the lesser child of s, a contradiction.

(iii) Also in step 2, if both children of s are already fixed to the left of the vertical bar, then s does not have a relevant child. In this case, you can choose any nonfixed digit as c_s. There might be some room for optimization here by choosing an ideal digit for c_s that would reduce the number of times we have to split our integrals after moving c_s in step 3.

(iv) Be sure to account for the signs of each string via the distributive property when splitting strings.

(v) Because this algorithm recursively splits each integral, the number of "Hadamardable" strings generated for an initial "seed" string grows exponentially with n for TCL$_{2n}$ (see Appendix D). Still, the cost of computing to find the integrals remains the bottleneck. If N is the number of sample points, and n is the number of integrals, then the computational

---

[6]Note the order of the correlation pairs is left ambiguous by the string notation, as for example the pairs $\langle 62\rangle$ and $\langle 26\rangle$ are denoted identically with string notation. However, as long as the ordering of each correlation term is consistent on both sides of the equation, the equality holds, as the integrand does not change when rearranging the integrals.

complexity grows as $\sim N^n$. The Hadamard trick cuts the number of integrals in half, $2n - 1 \rightarrow n - 1$, reducing the computational complexity by a factor of N^n (which is huge). The number of integrals generated grows as $2^{n/2}$. So in total the complexity is divided by $(N/\sqrt{2})^n$, and since $N \gg \sqrt{2}$, the algorithm always provides exponential speedup for any n. This is very significant.

APPENDIX D: ESTIMATION OF THE NUMBER OF $(n-1)$-DIMENSIONAL INTEGRALS GENERATED PER $(2n-1)$-DIMENSIONAL INTEGRAL

We can use a heuristic argument to approximate how many $(n-1)$-dimensional integrals are generated from a single TCL$_{2n}$ expression. Equivalently, given a TCL$_{2n}$ string of the form given by Eq. (C7), what is the expected value of the number of "Hadamardable" strings we generated after completing the algorithm from Appendix C 2? We will call this the "multiplicity," m_n, of our algorithm.

The number of strings generated after the kth recursion can be modeled as a branching process. Let $X_{n,j}$ be a random variable which denotes the number of strings generated after the jth recursion of our algorithm with initial seed a random TCL$_{2n}$ string. Denote

$$\mu_{n,j} = \mathbb{E}\left(\frac{X_{n,j}}{X_{n,j-1}}\right).$$

That is, $\mu_{n,j}$ is the number of "offspring" generated in the jth recursive step of our algorithm *per string in the $(j-1)$th step of our algorithm.* It is the number of expected children we get per string in the jth recursion of our algorithm. If we now start with a TCL$_{2n}$ string, the expected number of strings generated total after the kth recursion is thus

$$q_{n,k} := \prod_{j=1}^{k} \mu_{n,j},$$

and then the expected number of "Hadamardable" strings generated after completing the algorithm is

$$m_n := q_{n,n} = \prod_{j=1}^{n} \mu_{n,j}, \tag{D1}$$

since there are n recursive steps total. All we have to do is find the value of $\mu_{n,j}$.

To find the value of $\mu_{n,j}$, we just need to find the probability that we must split a random string at the jth recursion. To do this, we count the number of fixed and nonfixed digits for a given string at the start of step 2 of the jth recursion of our algorithm. If we freeze one of our strings at this level of recursion, it will look roughly like this:

$$0\,2n\,\overbrace{\beta_1 \ldots \beta_{j-1}}^{j-1 \text{ fixed digits}}|\overbrace{\beta_j \ldots \beta_{n-1}|\beta_n \ldots \beta_{2n-j-1}}^{2n-2j \text{ nonfixed digits}}|s\,\overbrace{\beta_{2n-j+1} \ldots \beta_{2n-1}}^{j \text{ fixed digits}}..$$

We know g_s and l_s lie somewhere among $\beta_1, \beta_2, \ldots, \beta_{2n-j-1}$. We will assume (without justification) that g_s and l_s are equally likely to be any one of these digits. Then the probability we need to split this string at this recursion is the probability that both the g_s and l_s are amongst the $2n - 2j$ nonfixed digits[7]:

$$p_{n,j} := \frac{2n-2j}{(2n-2j)+(j-1)} \cdot \frac{2n-2j-1}{(2n-2j)+(j-1)-1} = \frac{(2n-2j)(2n-2j-1)}{(2n-j-1)(2n-j-2)}.$$

We then have

$$\mu_{n,j} = 1(1-p_{n,j}) + 2p_{n,j} = 1 + p_{n,j},$$

and then from Eq. (D1) the multiplicity of our algorithm is given by

$$m_n = \prod_{j=1}^{n}\left(1 + \frac{(2n-2j)(2n-2j-1)}{(2n-j-1)(2n-j-2)}\right), \tag{D2}$$

valid for $n \geqslant 3$ (see Footnote 7). Plotting $(n, \log_2(m_n))$ for $3 \leqslant n \leqslant 200$, and performing a linear regression, we find that m_n grows as

$$m_n \sim 2^{-0.133685} \times 2^{0.506474n} \approx 0.911 \times 1.42^n.$$

Hence, to a good approximation, m_n grows with n as $2^{n/2}$. This is exponentially better than a worst case of 2^n, but still, the number of terms grows exponentially with n.

APPENDIX E: PROOF OF THE IDENTITY (107)

Let us evaluate the integral

$$\int_0^{t_n} dt_{n-1} \int_0^{t_{n-1}} dt_{n-2} \cdots \int_0^{t_2} dt_1 [\Gamma_\omega(t_n) - \Gamma_\omega(t_n - t_1)]. \tag{E1}$$

---

[7]We end up dividing by 0 if $n = j = 2$. Otherwise, this expression is valid.

For the string (B7), we use

$$0\,n\,1\,2\,\ldots\,n-1, \tag{E2}$$

and change the order following the algorithm described in Appendix B, resulting in

$$\int_0^{t_n} dt_1 [\Gamma_\omega(t_n) - \Gamma_\omega(t_n - t_1)] \int_{t_1}^{t_n} dt_2 \cdots \int_{t_{n-2}}^{t_n} dt_{n-1} = \int_0^{t_n} dt_1 \frac{(t_n - t_1)^{n-2}}{(n-2)!} [\Gamma_\omega(t) - \Gamma_\omega(t_n - t_1)] \tag{E3}$$

$$= \frac{1}{(n-2)!} \int_0^{t_n} dt_1\, t_1^{n-2} \int_{t_1}^{t_n} C(\tau) e^{i\omega\tau} = \frac{1}{(n-2)!} \int_0^{t_n} d\tau\, C(\tau) e^{i\omega\tau} \int_0^\tau dt_1 t_1^{n-2} \tag{E4}$$

$$= \frac{1}{(n-1)!} \int_0^{t_n} d\tau\, \tau^{n-1} C(\tau) e^{i\omega\tau} = \frac{(-i)^{n-1}}{(n-1)!} \frac{\partial^{n-1}}{\partial\omega^{n-1}} \int_0^{t_n} d\tau\, C(\tau) e^{i\omega\tau} = \frac{(-i)^{n-1}}{(n-1)!} \frac{\partial^{n-1}\Gamma_\omega(t)}{\partial\omega^{n-1}}. \tag{E5}$$

∎

APPENDIX F: COMPLETE TCL$_6$ GENERATOR

The cumulative correlation terms were calculated by unnesting the commutator of the Liouvillians, applying Wick's theorem, and renesting the operators to reduce the number of terms. Further details are accessible in [96]. The terms were derived by scripts and human labor, resulting in agreement:

$$L^6\varrho = -\left[\hat{0}, \int_0^t dt_1 \int_0^{t_1} dt_2 \int_0^{t_2} dt_3 \int_0^{t_3} dt_4 \int_0^{t_4} dt_5 \right(\tag{F1}$$

$$+ \langle 02\rangle\langle 14\rangle\langle 35\rangle([\hat{1},\hat{2}][\hat{3},\hat{4}]\hat{5}\varrho) + \langle 02\rangle\langle 14\rangle\langle 53\rangle(-[\hat{1},\hat{2}][\hat{3},\hat{4}]\varrho\hat{5}) + \langle 02\rangle\langle 41\rangle\langle 35\rangle(-[\hat{1},\hat{2}]\hat{5}\varrho[\hat{3},\hat{4}]) \tag{F2}$$

$$+ \langle 02\rangle\langle 41\rangle\langle 53\rangle([\hat{1},\hat{2}]\varrho\hat{5}[\hat{3},\hat{4}]) + \langle 02\rangle\langle 15\rangle\langle 34\rangle([\hat{1},\hat{2}]([\hat{3},\hat{4}\hat{5}\varrho] - \hat{5}[\hat{3},\hat{4}\varrho])) \tag{F3}$$

$$+ \langle 02\rangle\langle 15\rangle\langle 43\rangle(-[\hat{1},\hat{2}][\hat{3},\hat{5}]\varrho\hat{4}) + \langle 02\rangle\langle 51\rangle\langle 34\rangle(-[\hat{1},\hat{2}]\hat{4}\varrho[\hat{3},\hat{5}]) + \langle 02\rangle\langle 51\rangle\langle 43\rangle([\hat{1},\hat{2}]([\hat{3},\varrho\hat{5}\hat{4}] - [\hat{3},\varrho\hat{4}]\hat{5})) \tag{F4}$$

$$+ \langle 03\rangle\langle 14\rangle\langle 25\rangle(-\hat{3}[\hat{1},[\hat{2},\hat{4}]\hat{5}\varrho] - [\hat{1},[\hat{3}\hat{4},\hat{2}]\hat{5}\varrho] - [\hat{2},\hat{3}]\hat{5}[\hat{1},\hat{4}\varrho]) \tag{F5}$$

$$+ \langle 03\rangle\langle 14\rangle\langle 52\rangle(\hat{3}[\hat{1},[\hat{2},\hat{4}]\varrho\hat{5}] - [\hat{1},[\hat{2},\hat{3}\hat{4}]\varrho\hat{5}] + [\hat{2},\hat{3}][\hat{1},\hat{4}\varrho]\hat{5}) \tag{F6}$$

$$+ \langle 03\rangle\langle 41\rangle\langle 25\rangle(-[\hat{1},[\hat{2},\hat{3}]\hat{5}]\varrho\hat{4} - [\hat{1},\hat{3}]\hat{5}\varrho[\hat{2},\hat{4}]) + \langle 03\rangle\langle 41\rangle\langle 52\rangle([\hat{1},\hat{3}]\varrho\hat{5}[\hat{2},\hat{4}] + [\hat{1},[\hat{2},\hat{3}]\varrho\hat{5}\hat{4}] - [\hat{2},\hat{3}][\hat{1},\varrho\hat{4}]\hat{5}) \tag{F7}$$

$$+ \langle 03\rangle\langle 15\rangle\langle 24\rangle([\hat{1},[\hat{2},\hat{3}]\hat{4}]\hat{5}\varrho + [\hat{1},\hat{3}][\hat{2},\hat{4}\hat{5}\varrho] - [\hat{1},\hat{3}]\hat{5}[\hat{2},\hat{4}\varrho]) \tag{F8}$$

$$+ \langle 03\rangle\langle 15\rangle\langle 42\rangle(\hat{3}[\hat{1},[\hat{2},\hat{5}]\varrho\hat{4}] - [\hat{1},[\hat{2},\hat{3}\hat{5}]\varrho\hat{4}] + [\hat{2},\hat{3}][\hat{1},\hat{5}\varrho]\hat{4}) + \langle 03\rangle\langle 51\rangle\langle 24\rangle(-[\hat{1},\hat{3}]\hat{4}\varrho[\hat{2},\hat{5}] - [\hat{1},[\hat{2},\hat{3}]\hat{4}]\varrho\hat{5}) \tag{F9}$$

$$+ \langle 03\rangle\langle 51\rangle\langle 42\rangle(-\hat{3}[\hat{1},[\hat{2},\varrho\hat{5}\hat{4}]] - [\hat{1},\hat{3}][\hat{2},\varrho\hat{4}]\hat{5} - [\hat{2},\hat{3}][\hat{1},\varrho\hat{5}]\hat{4} + [\hat{1},[\hat{2},\hat{3}\varrho\hat{5}\hat{4}]]) \tag{F10}$$

$$+ \langle 04\rangle\langle 12\rangle\langle 35\rangle(-[\hat{3},\hat{4}]\hat{5}[\hat{1},\hat{2}\varrho] + [\hat{1},\hat{2}[\hat{3},\hat{4}]\hat{5}\varrho]) + \langle 04\rangle\langle 12\rangle\langle 53\rangle([\hat{3},\hat{4}][\hat{1},\hat{2}\varrho]\hat{5} - [\hat{1},\hat{2}[\hat{3},\hat{4}]\varrho\hat{5}]) \tag{F11}$$

$$+ \langle 04\rangle\langle 21\rangle\langle 35\rangle(-[\hat{1},[\hat{3},\hat{4}]\hat{5}]\varrho\hat{2}) + \langle 04\rangle\langle 21\rangle\langle 53\rangle(-[\hat{3},\hat{4}][\hat{1},\varrho\hat{2}]\hat{5} + [\hat{1},[\hat{3},\hat{4}]\varrho\hat{5}\hat{2}]) \tag{F12}$$

$$+ \langle 04\rangle\langle 13\rangle\langle 25\rangle(-\hat{4}[\hat{1},[\hat{2},\hat{3}]\hat{5}\varrho] + [\hat{1},[\hat{2},\hat{3}\hat{4}]\hat{5}\varrho] - [\hat{2},\hat{4}]\hat{5}[\hat{1},\hat{3}\varrho]) \tag{F13}$$

$$+ \langle 04\rangle\langle 13\rangle\langle 52\rangle(\hat{4}[\hat{1},[\hat{2},\hat{3}]\varrho\hat{5}] - [\hat{1},[\hat{2},\hat{3}\hat{4}]\varrho\hat{5}] + [\hat{2},\hat{4}][\hat{1},\hat{3}\varrho]\hat{5}) \tag{F14}$$

$$+ \langle 04\rangle\langle 31\rangle\langle 25\rangle(-[\hat{1},[\hat{2},\hat{4}]\hat{5}]\varrho\hat{3} - [\hat{1},\hat{4}]\hat{5}\varrho[\hat{2},\hat{3}]) + \langle 04\rangle\langle 31\rangle\langle 52\rangle([\hat{1},\hat{4}]\varrho\hat{5}[\hat{2},\hat{3}] + [\hat{1},[\hat{2},\hat{4}]\varrho\hat{5}\hat{3}] - [\hat{2},\hat{4}][\hat{1},\varrho\hat{3}]\hat{5}) \tag{F15}$$

$$+ \langle 04\rangle\langle 15\rangle\langle 23\rangle(-[\hat{1},\hat{4}]\hat{5}[\hat{2},\hat{3}\varrho] + \hat{4}[\hat{2},\hat{3}[\hat{1},\hat{5}\varrho]] - \hat{4}[\hat{1},[\hat{2},\hat{3}\hat{5}\varrho]] - [\hat{2},\hat{3}\hat{4}[\hat{1},\hat{5}\varrho]] + [\hat{1},[\hat{2},\hat{3}\hat{4}\hat{5}\varrho]]) \tag{F16}$$

$$+ \langle 04\rangle\langle 15\rangle\langle 32\rangle(\hat{4}[\hat{1},[\hat{2},\hat{5}]\varrho\hat{3}] + [\hat{2},\hat{4}][\hat{1},\hat{5}\varrho]\hat{3} - [\hat{1},[\hat{2},\hat{4}\hat{5}]\varrho\hat{3}]) \tag{F17}$$

$$+ \langle 04\rangle\langle 51\rangle\langle 23\rangle(\hat{4}[\hat{1},\hat{3}\varrho[\hat{2},\hat{5}]] - \hat{4}[\hat{2},\hat{3}[\hat{1},\varrho\hat{5}]] + [\hat{1},\hat{4}[\hat{2},\hat{3}\varrho]\hat{5}] + [\hat{2},\hat{3}\hat{4}[\hat{1},\varrho\hat{5}]] - [\hat{1},[\hat{2},\hat{3}\hat{4}\varrho\hat{5}]]) \tag{F18}$$

$$+ \langle 04\rangle\langle 51\rangle\langle 32\rangle(-[\hat{1},\hat{4}][\hat{2},\varrho\hat{3}]\hat{5} - [\hat{2},\hat{4}][\hat{1},\varrho\hat{5}]\hat{3} - \hat{4}[\hat{1},[\hat{2},\varrho\hat{5}\hat{3}]] + [\hat{1},[\hat{2},\hat{4}\varrho\hat{5}\hat{3}]]) \tag{F19}$$

$$+ \langle 05\rangle\langle 12\rangle\langle 34\rangle(\hat{5}[\hat{3},\hat{4}[\hat{1},\hat{2}\varrho]] - [\hat{1},\hat{2}\hat{5}[\hat{3},\hat{4}\varrho]] + [\hat{1},\hat{2}[\hat{3},\hat{4}\hat{5}\varrho]] - [\hat{3},\hat{4}\hat{5}[\hat{1},\hat{2}\varrho]]) \tag{F20}$$

$$+ \langle 05\rangle\langle 12\rangle\langle 43\rangle([\hat{3},\hat{5}][\hat{1},\hat{2}\varrho]\hat{4} - [\hat{1},\hat{2}[\hat{3},\hat{5}]\varrho\hat{4}]) + \langle 05\rangle\langle 21\rangle\langle 34\rangle(-[\hat{1},[\hat{3}\hat{4},\hat{5}]]\varrho\hat{2} + [\hat{1},[\hat{4},\hat{5}]\varrho\hat{3}\hat{2}] - [\hat{4},\hat{5}][\hat{1},\varrho\hat{2}]\hat{3}) \tag{F21}$$

$$+ \langle 05\rangle\langle 21\rangle\langle 43\rangle(-[\hat{3},\hat{5}][\hat{1},\varrho\hat{2}]\hat{4} + [\hat{1},[\hat{3},\hat{5}]\varrho\hat{4}\hat{2}]) \tag{F22}$$

$$+ \langle 05\rangle\langle 13\rangle\langle 24\rangle(-\hat{5}[\hat{1},[\hat{2},\hat{3}]\hat{4}\varrho] + \hat{5}[\hat{2},\hat{4}[\hat{1},\hat{3}\varrho]] - [\hat{1},\hat{3}\hat{5}[\hat{2},\hat{4}\varrho]] - [\hat{2},\hat{4}\hat{5}[\hat{1},\hat{3}\varrho]] + [\hat{1},[\hat{2},\hat{3}\hat{4}\hat{5}\varrho]]) \tag{F23}$$

$$+ \langle 05 \rangle \langle 13 \rangle \langle 42 \rangle (\hat{5}[\hat{1}, [\hat{2}, \hat{3}]\varrho\hat{4}] + [\hat{2}, \hat{5}][\hat{1}, \hat{3}\varrho]\hat{4} - [\hat{1}, [\hat{2}, \hat{3}\hat{5}]\varrho\hat{4}]) \tag{F24}$$

$$+ \langle 05 \rangle \langle 31 \rangle \langle 24 \rangle (\hat{5}[\hat{1}, \hat{4}\varrho[\hat{2}, \hat{3}]] - \hat{5}[\hat{2}, \hat{4}[\hat{1}, \varrho\hat{3}]] + [\hat{1}, \hat{5}[\hat{2}, \hat{4}\varrho]\hat{3}] + [\hat{2}, \hat{4}\hat{5}[\hat{1}, \varrho\hat{3}]] - [\hat{1}, [\hat{2}, \hat{4}\hat{5}\varrho\hat{3}]]) \tag{F25}$$

$$+ \langle 05 \rangle \langle 31 \rangle \langle 42 \rangle ([\hat{1}, \hat{5}]\varrho\hat{4}[\hat{2}, \hat{3}] + [\hat{1}, [\hat{2}, \hat{5}]\varrho\hat{4}\hat{3}] - [\hat{2}, \hat{5}][\hat{1}, \varrho\hat{3}]\hat{4}) \tag{F26}$$

$$+ \langle 05 \rangle \langle 14 \rangle \langle 23 \rangle (\hat{5}[\hat{1}, \hat{4}[\hat{2}, \hat{3}\varrho]] + \hat{5}[\hat{2}, \hat{3}[\hat{1}, \hat{4}\varrho]] - \hat{5}[\hat{1}, [\hat{2}, \hat{3}\hat{4}\varrho]] - [\hat{1}, \hat{4}\hat{5}[\hat{2}, \hat{3}\varrho]] - [\hat{2}, \hat{3}\hat{5}[\hat{1}, \hat{4}\varrho]] + [\hat{1}, [\hat{2}, \hat{3}\hat{4}\hat{5}\varrho]])$$
$$\tag{F27}$$

$$+ \langle 05 \rangle \langle 14 \rangle \langle 32 \rangle (\hat{5}[\hat{1}, [\hat{2}, \hat{4}]\varrho\hat{3}] + [\hat{2}, \hat{5}][\hat{1}, \hat{4}\varrho]\hat{3} - [\hat{1}, [\hat{2}, \hat{4}\hat{5}]\varrho\hat{3}]) \tag{F28}$$

$$+ \langle 05 \rangle \langle 41 \rangle \langle 23 \rangle (\hat{5}[\hat{1}, \hat{3}\varrho[\hat{2}, \hat{4}]] - \hat{5}[\hat{2}, \hat{3}[\hat{1}, \varrho\hat{4}]] + [\hat{1}, \hat{5}[\hat{2}, \hat{3}\varrho]\hat{4}] + [\hat{2}, \hat{3}\hat{5}[\hat{1}, \varrho\hat{4}]] - [\hat{1}, [\hat{2}, \hat{3}\hat{5}\varrho\hat{4}]]) \tag{F29}$$

$$\left. + \langle 05 \rangle \langle 41 \rangle \langle 32 \rangle (-[\hat{1}, \hat{5}][\hat{2}, \varrho\hat{3}]\hat{4} + [\hat{5}, \hat{2}][\hat{1}, \varrho\hat{4}]\hat{3} - \hat{5}[\hat{1}, [\hat{2}, \varrho\hat{4}\hat{3}]] + [\hat{1}, [\hat{2}, \hat{5}\varrho\hat{4}\hat{3}]]) \right] + \text{H.c.} \tag{F30}$$

The Hadamard trick on the time-ordered cumulants was implemented following the methods described in Appendix C, using scripts and by human labor. Further information is available in [96]. The expansion of TCL$_6$ into time-ordered cumulants after the Hadamard trick is given as follows:

$$L^6(t)\varrho = -\left[\hat{0}, \int_0^t dt_a \int_0^{t_a} dt_b \right. \tag{F31}$$

$$+ [\hat{a}, (\hat{0} \circ \Delta\Gamma^T(t - t_b, t - t_a))][\hat{b}, (\hat{a} \circ \Delta\Gamma^T(t_a, t_a - t_b))](\hat{b} \circ \Gamma^T(t_b))\hat{\varrho} \tag{F32}$$

$$- [\hat{a}, (\hat{0} \circ \Delta\Gamma^T(t, t - t_a))][(\hat{b} \circ \Gamma(t_a - t_b)), (\hat{a} \circ \Delta\Gamma^T(t_a, t_a - t_b))]\hat{b}\hat{\varrho} \tag{F33}$$

$$+ [(\hat{b} \circ \Delta\Gamma(t - t_b, -t_b)), (\hat{0} \circ \Delta\Gamma^T(t, t - t_a))][\hat{a}, \hat{b}](\hat{a} \circ \Gamma^T(t_a - t_b))\hat{\varrho} \tag{F34}$$

$$- [\hat{a}, (\hat{0} \circ \Delta\Gamma^T(t - t_b, t - t_a))][\hat{b}, (\hat{a} \circ \Delta\Gamma^T(t_a, t_a - t_b))]\hat{\varrho}(\hat{b} \circ (-\Gamma(-t_b))) \tag{F35}$$

$$- [(\hat{b} \circ \Delta\Gamma(t - t_b, -t_b)), (\hat{0} \circ \Delta\Gamma^T(t, t - t_a))][\hat{a}, \hat{b}]\hat{\varrho}(\hat{a} \circ (-\Gamma(t_b - t_a))) \tag{F36}$$

$$+ [\hat{a}, (\hat{0} \circ \Delta\Gamma^T(t, t - t_a))][(\hat{b} \circ \Gamma(t_a - t_b)), \hat{b}(\hat{a} \circ \Delta\Gamma^T(t_a, t_a - t_b))\hat{\varrho}] \tag{F37}$$

$$- [\hat{a}, (\hat{0} \circ \Delta\Gamma^T(t, t - t_a))](\hat{a} \circ \Delta\Gamma^T(t_a, t_a - t_b))[(\hat{b} \circ \Gamma(t_a - t_b)), \hat{b}\hat{\varrho}] \tag{F38}$$

$$- [\hat{a}, (\hat{0} \circ \Delta\Gamma^T(t, t - t_b))][\hat{b}, (\hat{b} \circ \Gamma^T(t_b))(\hat{a} \circ \Delta\Gamma^T(t_a, t_a - t_b))\hat{\varrho}] \tag{F39}$$

$$+ [\hat{a}, (\hat{0} \circ \Delta\Gamma^T(t, t - t_b))](\hat{a} \circ \Delta\Gamma^T(t_a, t_a - t_b))[\hat{b}, (\hat{b} \circ \Gamma^T(t_b))\hat{\varrho}] \tag{F40}$$

$$+ [(\hat{b} \circ \Delta\Gamma(t - t_b, t_a - t_b)), (\hat{0} \circ \Delta\Gamma^T(t, t - t_a))][\hat{a}, (\hat{a} \circ \Delta\Gamma^T(t_a, t_a - t_b))\hat{b}\hat{\varrho}] \tag{F41}$$

$$- [(\hat{b} \circ \Delta\Gamma(t - t_b, t_a - t_b)), (\hat{0} \circ \Delta\Gamma^T(t, t - t_a))]\hat{b}[\hat{a}, (\hat{a} \circ \Delta\Gamma^T(t_a, t_a - t_b))\hat{\varrho}] \tag{F42}$$

$$+ [\hat{a}, (\hat{0} \circ \Delta\Gamma^T(t, t - t_b))][\hat{b}, (\hat{a} \circ \Delta\Gamma^T(t_a, t_a - t_b))]\hat{\varrho}(\hat{b} \circ (-\Gamma(-t_b))) \tag{F43}$$

$$- [(\hat{b} \circ \Delta\Gamma(t - t_b, t_a - t_b)), (\hat{0} \circ \Delta\Gamma^T(t, t - t_a))][\hat{a}, \hat{b}]\hat{\varrho}(\hat{a} \circ \Delta\Gamma(t_b - t_a, -t_a)) \tag{F44}$$

$$- [\hat{a}, (\hat{0} \circ \Delta\Gamma^T(t - t_b, t - t_a))](\hat{b} \circ \Gamma^T(t_b))\hat{\varrho}[\hat{b}, (\hat{a} \circ \Delta\Gamma(t_b - t_a, -t_a))] \tag{F45}$$

$$- [(\hat{b} \circ \Delta\Gamma^T(t_b, t_b - t)), (\hat{0} \circ \Delta\Gamma^T(t, t - t_a))](\hat{a} \circ \Gamma^T(t_a - t_b))\hat{\varrho}[\hat{a}, \hat{b}] \tag{F46}$$

$$+ [\hat{a}, (\hat{0} \circ \Delta\Gamma^T(t - t_b, t - t_a))]\hat{\varrho}(\hat{b} \circ (-\Gamma(-t_b)))[\hat{b}, (\hat{a} \circ \Delta\Gamma(t_b - t_a, -t_a))] \tag{F47}$$

$$- [\hat{a}, (\hat{0} \circ \Delta\Gamma^T(t, t - t_a))]\hat{\varrho}\hat{b}[(\hat{b} \circ (-\Gamma^T(t_b - t_a))), (\hat{a} \circ \Delta\Gamma(t_b - t_a, -t_a))] \tag{F48}$$

$$+ [(\hat{b} \circ \Delta\Gamma^T(t_b, t_b - t)), (\hat{0} \circ \Delta\Gamma^T(t, t - t_a))]\hat{\varrho}(\hat{a} \circ (-\Gamma(t_b - t_a)))[\hat{a}, \hat{b}] \tag{F49}$$

$$+ [\hat{a}, (\hat{0} \circ \Delta\Gamma^T(t, t - t_b))](\hat{b} \circ \Gamma^T(t_b))\hat{\varrho}[\hat{b}, (\hat{a} \circ \Delta\Gamma(t_b - t_a, -t_a))] \tag{F50}$$

$$- [(\hat{b} \circ \Delta\Gamma^T(t_b - t_a, t_b - t)), (\hat{0} \circ \Delta\Gamma^T(t, t - t_a))](\hat{a} \circ \Delta\Gamma^T(t_a, t_a - t_b))\hat{\varrho}[\hat{a}, \hat{b}] \tag{F51}$$

$$+ [\hat{a}, (\hat{0} \circ \Delta\Gamma^T(t, t - t_a))][(\hat{b} \circ (-\Gamma^T(t_b - t_a))), \hat{\varrho}(\hat{a} \circ \Delta\Gamma(t_b - t_a, -t_a))\hat{b}] \tag{F52}$$

$$- [\hat{a}, (\hat{0} \circ \Delta\Gamma^T(t, t - t_a))][(\hat{b} \circ (-\Gamma^T(t_b - t_a))), \hat{\varrho}\hat{b}](\hat{a} \circ \Delta\Gamma(t_b - t_a, -t_a)) \tag{F53}$$

$$- [\hat{a}, (\hat{0} \circ \Delta\Gamma^T(t, t - t_b))][\hat{b}, \hat{\varrho}(\hat{a} \circ \Delta\Gamma(t_b - t_a, -t_a))(\hat{b} \circ (-\Gamma(-t_b)))] \tag{F54}$$

$$+ [\hat{a}, (\hat{0} \circ \Delta\Gamma^T(t, t - t_b))][\hat{b}, \hat{\varrho}(\hat{b} \circ (-\Gamma(-t_b)))](\hat{a} \circ \Delta\Gamma(t_b - t_a, -t_a)) \tag{F55}$$

$$+ [(\hat{b} \circ \Delta\Gamma^T(t_b - t_a, t_b - t)), (\hat{0} \circ \Delta\Gamma^T(t, t - t_a))][\hat{a}, \hat{\varrho}\hat{b}(\hat{a} \circ \Delta\Gamma(t_b - t_a, -t_a))] \tag{F56}$$

$$- [(\hat{b} \circ \Delta\Gamma^T(t_b - t_a, t_b - t)), (\hat{0} \circ \Delta\Gamma^T(t, t - t_a))][\hat{a}, \hat{\varrho}(\hat{a} \circ \Delta\Gamma(t_b - t_a, -t_a))]\hat{b} \tag{F57}$$

$$- (\hat{0} \circ \Delta\Gamma^T(t - t_b, t - t_a))[(\hat{b} \circ \Delta\Gamma(t - t_b, t_a - t_b)), [\hat{a}, \hat{b}](\hat{a} \circ \Delta\Gamma^T(t_a, t_a - t_b))\hat{\varrho}] \tag{F58}$$

$$- [(\hat{b} \circ \Delta\Gamma(t - t_b, t_a - t_b)), [(\hat{0} \circ \Delta\Gamma^T(t - t_b, t - t_a))\hat{b}, \hat{a}](\hat{a} \circ \Delta\Gamma^T(t_a, t_a - t_b))\hat{\varrho}] \tag{F59}$$

$$-[\hat{a}, (\hat{0} \circ \Delta\Gamma^T(t - t_b, t - t_a))](\hat{a} \circ \Delta\Gamma^T(t_a, t_a - t_b))[(\hat{b} \circ \Delta\Gamma(t - t_b, t_a - t_b)), \hat{b}\hat{\varrho}] \tag{F60}$$

$$+ (\hat{0} \circ \Delta\Gamma^T(t - t_b, t - t_a))[(\hat{b} \circ \Delta\Gamma(t - t_b, t_a - t_b)), [\hat{a}, \hat{b}]\hat{\varrho}(\hat{a} \circ \Delta\Gamma(t_b - t_a, -t_a))] \tag{F61}$$

$$- [(\hat{b} \circ \Delta\Gamma(t - t_b, t_a - t_b)), [\hat{a}, (\hat{0} \circ \Delta\Gamma^T(t - t_b, t - t_a))\hat{b}]\hat{\varrho}(\hat{a} \circ \Delta\Gamma(t_b - t_a, -t_a))] \tag{F62}$$

$$+ [\hat{a}, (\hat{0} \circ \Delta\Gamma^T(t - t_b, t - t_a))][(\hat{b} \circ \Delta\Gamma(t - t_b, t_a - t_b)), \hat{b}\hat{\varrho}](\hat{a} \circ \Delta\Gamma(t_b - t_a, -t_a)) \tag{F63}$$

$$+ [(\hat{b} \circ \Delta\Gamma(t - t_b, t_a - t_b)), [\hat{a}, (\hat{0} \circ \Delta\Gamma^T(t, t - t_a))](\hat{a} \circ \Gamma^T(t_a - t_b))]\hat{b}\hat{\varrho} \tag{F64}$$

$$+ [(\hat{b} \circ \Delta\Gamma(t - t_b, t_a - t_b)), (\hat{0} \circ \Delta\Gamma^T(t, t - t_a))][\hat{a}, (\hat{a} \circ \Gamma^T(t_a - t_b))\hat{b}\hat{\varrho}] \tag{F65}$$

$$- [(\hat{b} \circ \Delta\Gamma(t - t_b, t_a - t_b)), (\hat{0} \circ \Delta\Gamma^T(t, t - t_a))]\hat{b}[\hat{a}, (\hat{a} \circ \Gamma^T(t_a - t_b))\hat{\varrho}] \tag{F66}$$

$$- [\hat{a}, [(\hat{b} \circ \Gamma(t_a - t_b)), (\hat{0} \circ \Delta\Gamma^T(t, t - t_b))]\hat{b}](\hat{a} \circ \Delta\Gamma^T(t_a, t_a - t_b))\hat{\varrho} \tag{F67}$$

$$- [\hat{a}, (\hat{0} \circ \Delta\Gamma^T(t, t - t_b))][(\hat{b} \circ \Gamma(t_a - t_b)), \hat{b}(\hat{a} \circ \Delta\Gamma^T(t_a, t_a - t_b))\hat{\varrho}] \tag{F68}$$

$$+ (\hat{0} \circ \Delta\Gamma^T(t, t - t_a))[(\hat{b} \circ \Delta\Gamma(t - t_b, t_a - t_b)), [\hat{a}, \hat{b}]\hat{\varrho}(\hat{a} \circ (-\Gamma(t_b - t_a)))] \tag{F69}$$

$$- [(\hat{b} \circ \Delta\Gamma(t - t_b, t_a - t_b)), [\hat{a}, (\hat{0} \circ \Delta\Gamma^T(t, t - t_a))\hat{b}]\hat{\varrho}(\hat{a} \circ (-\Gamma(t_b - t_a)))] \tag{F70}$$

$$+ [\hat{a}, (\hat{0} \circ \Delta\Gamma^T(t, t - t_a))][(\hat{b} \circ \Delta\Gamma(t - t_b, t_a - t_b)), \hat{b}\hat{\varrho}](\hat{a} \circ (-\Gamma(t_b - t_a))) \tag{F71}$$

$$- [(\hat{b} \circ \Delta\Gamma^T(t_b - t_a, t_b - t)), [\hat{a}, (\hat{0} \circ \Delta\Gamma^T(t - t_b, t - t_a))](\hat{a} \circ \Delta\Gamma^T(t_a, t_a - t_b))]\hat{\varrho}\hat{b} \tag{F72}$$

$$- [(\hat{b} \circ \Delta\Gamma^T(t_b - t_a, t_b - t)), (\hat{0} \circ \Delta\Gamma^T(t - t_b, t - t_a))](\hat{a} \circ \Delta\Gamma^T(t_a, t_a - t_b))\hat{\varrho}[\hat{a}, \hat{b}] \tag{F73}$$

$$+ [(\hat{b} \circ \Delta\Gamma^T(t_b - t_a, t_b - t)), (\hat{0} \circ \Delta\Gamma^T(t - t_b, t - t_a))]\hat{\varrho}(\hat{a} \circ \Delta\Gamma(t_b - t_a, -t_a))[\hat{a}, \hat{b}] \tag{F74}$$

$$+ [(\hat{b} \circ \Delta\Gamma^T(t_b - t_a, t_b - t)), [\hat{a}, (\hat{0} \circ \Delta\Gamma^T(t - t_b, t - t_a))]\hat{\varrho}(\hat{a} \circ \Delta\Gamma(t_b - t_a, -t_a))]\hat{b} \tag{F75}$$

$$- [\hat{a}, (\hat{0} \circ \Delta\Gamma^T(t - t_b, t - t_a))][(\hat{b} \circ \Delta\Gamma^T(t_b - t_a, t_b - t)), \hat{\varrho}\hat{b}](\hat{a} \circ \Delta\Gamma(t_b - t_a, -t_a)) \tag{F76}$$

$$- [(\hat{b} \circ \Delta\Gamma^T(t_b - t_a, t_b - t)), (\hat{0} \circ \Delta\Gamma^T(t, t - t_a))](\hat{a} \circ \Gamma^T(t_a - t_b))\hat{\varrho}[\hat{a}, \hat{b}] \tag{F77}$$

$$- [(\hat{b} \circ \Delta\Gamma^T(t_b - t_a, t_b - t)), [\hat{a}, (\hat{0} \circ \Delta\Gamma^T(t, t - t_a))](\hat{a} \circ \Gamma^T(t_a - t_b))]\hat{\varrho}\hat{b} \tag{F78}$$

$$+ [\hat{a}, (\hat{0} \circ \Delta\Gamma^T(t, t - t_b))]\hat{b}\hat{\varrho}[(\hat{b} \circ \Gamma(t_a - t_b)), (\hat{a} \circ \Delta\Gamma(t_b - t_a, -t_a))] \tag{F79}$$

$$+ [\hat{a}, [(\hat{b} \circ \Gamma(t_a - t_b)), (\hat{0} \circ \Delta\Gamma^T(t, t - t_b))]\hat{b}]\hat{\varrho}(\hat{a} \circ \Delta\Gamma(t_b - t_a, -t_a)) \tag{F80}$$

$$- (\hat{0} \circ \Delta\Gamma^T(t, t - t_a))[(\hat{b} \circ \Delta\Gamma^T(t_b - t_a, t_b - t)), [\hat{a}, \hat{\varrho}\hat{b}(\hat{a} \circ (-\Gamma(t_b - t_a)))]] \tag{F81}$$

$$- [(\hat{b} \circ \Delta\Gamma^T(t_b - t_a, t_b - t)), (\hat{0} \circ \Delta\Gamma^T(t, t - t_a))][\hat{a}, \hat{\varrho}(\hat{a} \circ (-\Gamma(t_b - t_a)))]\hat{b} \tag{F82}$$

$$- [\hat{a}, (\hat{0} \circ \Delta\Gamma^T(t, t - t_a))][(\hat{b} \circ \Delta\Gamma^T(t_b - t_a, t_b - t)), \hat{\varrho}\hat{b}](\hat{a} \circ (-\Gamma(t_b - t_a))) \tag{F83}$$

$$+ [(\hat{b} \circ \Delta\Gamma^T(t_b - t_a, t_b - t)), [\hat{a}, (\hat{0} \circ \Delta\Gamma^T(t, t - t_a))\hat{\varrho}\hat{b}(\hat{a} \circ (-\Gamma(t_b - t_a)))]] \tag{F84}$$

$$- [\hat{b}, (\hat{0} \circ \Delta\Gamma^T(t, t - t_b))](\hat{b} \circ \Gamma^T(t_b))[(\hat{a} \circ \Gamma(t - t_a)), \hat{a}\hat{\varrho}] \tag{F85}$$

$$+ [(\hat{a} \circ \Gamma(t - t_a)), \hat{a}[\hat{b}, (\hat{0} \circ \Delta\Gamma^T(t, t - t_b))](\hat{b} \circ \Gamma^T(t_b))\hat{\varrho}] \tag{F86}$$

$$+ [(\hat{b} \circ \Gamma(t_a - t_b)), (\hat{0} \circ \Delta\Gamma^T(t, t - t_b))]\hat{b}[(\hat{a} \circ \Gamma(t - t_a)), \hat{a}\hat{\varrho}] \tag{F87}$$

$$- [(\hat{a} \circ \Gamma(t - t_a)), \hat{a}[(\hat{b} \circ \Gamma(t_a - t_b)), (\hat{0} \circ \Delta\Gamma^T(t, t - t_b))]\hat{b}\hat{\varrho}] \tag{F88}$$

$$+ [\hat{b}, (\hat{0} \circ \Delta\Gamma^T(t, t - t_b))][(\hat{a} \circ \Gamma(t - t_a)), \hat{a}\hat{\varrho}](\hat{b} \circ (-\Gamma(-t_b))) \tag{F89}$$

$$- [(\hat{a} \circ \Gamma(t - t_a)), \hat{a}[\hat{b}, (\hat{0} \circ \Delta\Gamma^T(t, t - t_b))]\hat{\varrho}(\hat{b} \circ (-\Gamma(-t_b)))] \tag{F90}$$

$$- (\hat{0} \circ \Delta\Gamma^T(t, t - t_b))[(\hat{b} \circ \Delta\Gamma(t - t_b, t_a - t_b)), [\hat{a}, \hat{b}](\hat{a} \circ \Delta\Gamma^T(t_a, t_a - t_b))\hat{\varrho}] \tag{F91}$$

$$+ [(\hat{b} \circ \Delta\Gamma(t - t_b, t_a - t_b)), [\hat{a}, \hat{b}(\hat{0} \circ \Delta\Gamma^T(t, t - t_b))](\hat{a} \circ \Delta\Gamma^T(t_a, t_a - t_b))\hat{\varrho}] \tag{F92}$$

$$- [\hat{a}, (\hat{0} \circ \Delta\Gamma^T(t, t - t_b))](\hat{a} \circ \Delta\Gamma^T(t_a, t_a - t_b))[(\hat{b} \circ \Delta\Gamma(t - t_b, t_a - t_b)), \hat{b}\hat{\varrho}] \tag{F93}$$

$$- [\hat{a}, [(\hat{b} \circ \Delta\Gamma(t_a - t_b, -t_b)), (\hat{a} \circ \Gamma^T(t_a - t_b))(\hat{0} \circ \Delta\Gamma^T(t, t - t_b))]\hat{b}\hat{\varrho}] \tag{F94}$$

$$+ [(\hat{b} \circ \Delta\Gamma(t_a - t_b, -t_b)), (\hat{0} \circ \Delta\Gamma^T(t, t - t_b))]\hat{b}[\hat{a}, (\hat{a} \circ \Gamma^T(t_a - t_b))\hat{\varrho}] \tag{F95}$$

$$+ [(\hat{a} \circ \Gamma(t - t_a)), [(\hat{b} \circ \Delta\Gamma(t_a - t_b, -t_b)), \hat{a}(\hat{0} \circ \Delta\Gamma^T(t, t - t_b))]\hat{b}\hat{\varrho}] \tag{F96}$$

$$- [(\hat{b} \circ \Delta\Gamma(t_a - t_b, -t_b)), (\hat{0} \circ \Delta\Gamma^T(t, t - t_b))]\hat{b}[(\hat{a} \circ \Gamma(t - t_a)), \hat{a}\hat{\varrho}] \tag{F97}$$

$$+ (\hat{0} \circ \Delta\Gamma^T(t, t - t_b))[(\hat{b} \circ \Delta\Gamma(t - t_b, t_a - t_b)), [\hat{a}, \hat{b}]\hat{\varrho}(\hat{a} \circ \Delta\Gamma(t_b - t_a, -t_a))] \tag{F98}$$

$$- [(\hat{b} \circ \Delta\Gamma(t - t_b, t_a - t_b)), [\hat{a}, \hat{b}(\hat{0} \circ \Delta\Gamma^T(t, t - t_b))]\hat{\varrho}(\hat{a} \circ \Delta\Gamma(t_b - t_a, -t_a))] \tag{F99}$$

$$+ [\hat{a}, (\hat{0} \circ \Delta\Gamma^T(t, t - t_b))][(\hat{b} \circ \Delta\Gamma(t - t_b, t_a - t_b)), \hat{b}\hat{\varrho}](\hat{a} \circ \Delta\Gamma(t_b - t_a, -t_a)) \tag{F100}$$

$$+ (\hat{0} \circ \Delta\Gamma^T(t, t - t_b))[(\hat{b} \circ \Gamma(t_a - t_b)), \hat{b}[\hat{a}, (\hat{a} \circ \Delta\Gamma^T(t_a, t_a - t_b))\hat{\varrho}]] \tag{F101}$$

$$- (\hat{0} \circ \Delta\Gamma^T(t, t-t_b))[\hat{a}, [(\hat{b} \circ \Gamma(t_a - t_b)), \hat{b}(\hat{a} \circ \Delta\Gamma^T(t_a, t_a - t_b))\hat{\varrho}]] \tag{F102}$$

$$- [(\hat{b} \circ \Gamma(t_a - t_b)), \hat{b}(\hat{0} \circ \Delta\Gamma^T(t, t-t_b))[\hat{a}, (\hat{a} \circ \Delta\Gamma^T(t_a, t_a - t_b))\hat{\varrho}]] \tag{F103}$$

$$+ [\hat{a}, [(\hat{b} \circ \Gamma(t_a - t_b)), \hat{b}(\hat{0} \circ \Delta\Gamma^T(t, t-t_b))(\hat{a} \circ \Delta\Gamma^T(t_a, t_a - t_b))\hat{\varrho}]] \tag{F104}$$

$$+ [(\hat{b} \circ \Delta\Gamma^T(t - t_b, t_a - t_b)), (\hat{0} \circ \Delta\Gamma^T(t, t-t_b))]\hat{b}[\hat{a}, (\hat{a} \circ \Gamma^T(t_a - t_b))\hat{\varrho}] \tag{F105}$$

$$- [(\hat{b} \circ \Delta\Gamma^T(t - t_b, t_a - t_b)), [\hat{a}, (\hat{a} \circ \Gamma^T(t_a - t_b))(\hat{0} \circ \Delta\Gamma^T(t, t-t_b))\hat{b}\hat{\varrho}]] \tag{F106}$$

$$+ [(\hat{b} \circ \Delta\Gamma^T(t - t_b, t_a - t_b)), [\hat{a}, (\hat{0} \circ \Delta\Gamma^T(t, t-t_b))\hat{b}]\hat{\varrho}(\hat{a} \circ (-\Gamma(t_b - t_a)))] \tag{F107}$$

$$- [(\hat{a} \circ (-\Gamma^T(t_a - t))), [\hat{b}, (\hat{0} \circ \Delta\Gamma^T(t, t-t_b))](\hat{b} \circ \Gamma^T(t_b))]\hat{\varrho}\hat{a} \tag{F108}$$

$$+ [(\hat{a} \circ (-\Gamma^T(t_a - t))), [(\hat{b} \circ \Gamma(t_a - t_b)), (\hat{0} \circ \Delta\Gamma^T(t, t-t_b))]\hat{b}]\hat{\varrho}\hat{a} \tag{F109}$$

$$- [\hat{b}, (\hat{0} \circ \Delta\Gamma^T(t, t-t_b))][(\hat{a} \circ (-\Gamma^T(t_a - t))), \hat{\varrho}\hat{a}](\hat{b} \circ (-\Gamma(-t_b))) \tag{F110}$$

$$+ [(\hat{a} \circ (-\Gamma^T(t_a - t))), [\hat{b}, (\hat{0} \circ \Delta\Gamma^T(t, t-t_b))]\hat{\varrho}(\hat{b} \circ (-\Gamma(-t_b)))\hat{a} \tag{F111}$$

$$- [(\hat{b} \circ \Delta\Gamma^T(t_b - t_a, t_b - t)), [\hat{a}, (\hat{0} \circ \Delta\Gamma^T(t, t-t_b))](\hat{a} \circ \Delta\Gamma^T(t_a, t_a - t_b))]\hat{\varrho}\hat{b} \tag{F112}$$

$$- [(\hat{b} \circ \Delta\Gamma^T(t_b - t_a, t_b - t)), (\hat{0} \circ \Delta\Gamma^T(t, t-t_b))](\hat{a} \circ \Delta\Gamma^T(t_a, t_a - t_b))\hat{\varrho}[\hat{a}, \hat{b}] \tag{F113}$$

$$+ [\hat{a}, [(\hat{b} \circ \Delta\Gamma(t_a - t_b, -t_b)), (\hat{0} \circ \Delta\Gamma^T(t, t-t_b))]\hat{b}]\hat{\varrho}(\hat{a} \circ (-\Gamma(t_b - t_a))) \tag{F114}$$

$$+ [\hat{a}, (\hat{0} \circ \Delta\Gamma^T(t, t-t_b))\hat{b}\hat{\varrho}[(\hat{b} \circ \Delta\Gamma(t_a - t_b, -t_b)), (\hat{a} \circ (-\Gamma(t_b - t_a)))] \tag{F115}$$

$$- [(\hat{a} \circ (-\Gamma^T(t_a - t))), [(\hat{b} \circ \Delta\Gamma(t_a - t_b, -t_b)), (\hat{0} \circ \Delta\Gamma^T(t, t-t_b))]\hat{b}]\hat{\varrho}\hat{a} \tag{F116}$$

$$- [(\hat{a} \circ (-\Gamma^T(t_a - t))), (\hat{0} \circ \Delta\Gamma^T(t, t-t_b))]\hat{b}\hat{\varrho}[(\hat{b} \circ \Delta\Gamma(t_a - t_b, -t_b)), \hat{a}] \tag{F117}$$

$$+ [(\hat{b} \circ \Delta\Gamma^T(t_b - t_a, t_b - t)), (\hat{0} \circ \Delta\Gamma^T(t, t-t_b))]\hat{\varrho}(\hat{a} \circ \Delta\Gamma(t_b - t_a, -t_a))[\hat{a}, \hat{b}] \tag{F118}$$

$$+ [(\hat{b} \circ \Delta\Gamma^T(t_b - t_a, t_b - t)), [\hat{a}, (\hat{0} \circ \Delta\Gamma^T(t, t-t_b))]\hat{\varrho}(\hat{a} \circ \Delta\Gamma(t_b - t_a, -t_a))\hat{b}] \tag{F119}$$

$$- [\hat{a}, (\hat{0} \circ \Delta\Gamma^T(t, t-t_b))][(\hat{b} \circ \Delta\Gamma^T(t_b - t_a, t_b - t)), \hat{\varrho}\hat{b}](\hat{a} \circ \Delta\Gamma(t_b - t_a, -t_a)) \tag{F120}$$

$$+ (\hat{0} \circ \Delta\Gamma^T(t, t-t_b))[\hat{a}, \hat{b}\hat{\varrho}[(\hat{b} \circ \Gamma(t_a - t_b)), (\hat{a} \circ \Delta\Gamma(t_b - t_a, -t_a))]] \tag{F121}$$

$$- (\hat{0} \circ \Delta\Gamma^T(t, t-t_b))[(\hat{b} \circ \Gamma(t_a - t_b)), \hat{b}[\hat{a}, \hat{\varrho}(\hat{a} \circ \Delta\Gamma(t_b - t_a, -t_a))]] \tag{F122}$$

$$+ [\hat{a}, (\hat{0} \circ \Delta\Gamma^T(t, t-t_b))[(\hat{b} \circ \Gamma(t_a - t_b)), \hat{b}\hat{\varrho}](\hat{a} \circ \Delta\Gamma(t_b - t_a, -t_a))] \tag{F123}$$

$$+ [(\hat{b} \circ \Gamma(t_a - t_b)), \hat{b}(\hat{0} \circ \Delta\Gamma^T(t, t-t_b))[\hat{a}, \hat{\varrho}(\hat{a} \circ \Delta\Gamma(t_b - t_a, -t_a))]] \tag{F124}$$

$$- [\hat{a}, [(\hat{b} \circ \Gamma(t_a - t_b)), \hat{b}(\hat{0} \circ \Delta\Gamma^T(t, t-t_b))\hat{\varrho}(\hat{a} \circ \Delta\Gamma(t_b - t_a, -t_a))]] \tag{F125}$$

$$+ [\hat{a}, (\hat{0} \circ \Delta\Gamma^T(t, t-t_b))][(\hat{b} \circ \Delta\Gamma^T(t_b - t_a, t_b - t)), \hat{\varrho}\hat{b}](\hat{a} \circ (-\Gamma(t_b - t_a))) \tag{F126}$$

$$+ (\hat{0} \circ \Delta\Gamma^T(t, t-t_b))[(\hat{b} \circ \Gamma(t_a - t_b)), \hat{b}[(\hat{a} \circ \Gamma(t - t_a)), \hat{a}\hat{\varrho}]] \tag{F127}$$

$$- [(\hat{a} \circ \Gamma(t - t_a)), \hat{a}(\hat{0} \circ \Delta\Gamma^T(t, t-t_b))[(\hat{b} \circ \Gamma(t_a - t_b)), \hat{b}\hat{\varrho}]] \tag{F128}$$

$$+ [(\hat{a} \circ \Gamma(t - t_a)), \hat{a}[(\hat{b} \circ \Gamma(t_a - t_b)), \hat{b}(\hat{0} \circ \Delta\Gamma^T(t, t-t_b))\hat{\varrho}]] \tag{F129}$$

$$- [(\hat{b} \circ \Gamma(t_a - t_b)), \hat{b}(\hat{0} \circ \Delta\Gamma^T(t, t-t_b))[(\hat{a} \circ \Gamma(t - t_a)), \hat{a}\hat{\varrho}]] \tag{F130}$$

$$+ (\hat{0} \circ \Delta\Gamma^T(t, t-t_b))[(\hat{b} \circ \Delta\Gamma(t_a - t_b, -t_b)), \hat{b}[\hat{a}, (\hat{a} \circ \Gamma^T(t_a - t_b))\hat{\varrho}]] \tag{F131}$$

$$- [\hat{a}, (\hat{a} \circ \Gamma^T(t_a - t_b))(\hat{0} \circ \Delta\Gamma^T(t, t-t_b))[(\hat{b} \circ \Delta\Gamma(t_a - t_b, -t_b)), \hat{b}\hat{\varrho}]] \tag{F132}$$

$$- [(\hat{b} \circ \Delta\Gamma(t_a - t_b, -t_b)), \hat{b}(\hat{0} \circ \Delta\Gamma^T(t, t-t_b))[\hat{a}, (\hat{a} \circ \Gamma^T(t_a - t_b))\hat{\varrho}]] \tag{F133}$$

$$+ [\hat{a}, [(\hat{b} \circ \Delta\Gamma(t_a - t_b, -t_b)), (\hat{a} \circ \Gamma^T(t_a - t_b))\hat{b}(\hat{0} \circ \Delta\Gamma^T(t, t-t_b))\hat{\varrho}]] \tag{F134}$$

$$- (\hat{0} \circ \Delta\Gamma^T(t, t-t_b))[(\hat{b} \circ \Delta\Gamma(t_a - t_b, -t_b)), \hat{b}[(\hat{a} \circ \Gamma(t - t_a)), \hat{a}\hat{\varrho}]] \tag{F135}$$

$$+ [(\hat{a} \circ \Gamma(t - t_a)), \hat{a}(\hat{0} \circ \Delta\Gamma^T(t, t-t_b))[(\hat{b} \circ \Delta\Gamma(t_a - t_b, -t_b)), \hat{b}\hat{\varrho}]] \tag{F136}$$

$$+ [(\hat{b} \circ \Delta\Gamma(t_a - t_b, -t_b)), \hat{b}(\hat{0} \circ \Delta\Gamma^T(t, t-t_b))[(\hat{a} \circ \Gamma(t - t_a)), \hat{a}\hat{\varrho}]] \tag{F137}$$

$$- [(\hat{a} \circ \Gamma(t - t_a)), [(\hat{b} \circ \Delta\Gamma(t_a - t_b, -t_b)), \hat{a}\hat{b}(\hat{0} \circ \Delta\Gamma^T(t, t-t_b))\hat{\varrho}]] \tag{F138}$$

$$+ (\hat{0} \circ \Delta\Gamma^T(t, t-t_b))[(\hat{b} \circ \Delta\Gamma(t - t_b, t_a - t_b)), \hat{b}[\hat{a}, (\hat{a} \circ \Gamma^T(t_a - t_b))\hat{\varrho}]] \tag{F139}$$

$$- [(\hat{b} \circ \Delta\Gamma(t - t_b, t_a - t_b)), \hat{b}(\hat{0} \circ \Delta\Gamma^T(t, t-t_b))[\hat{a}, (\hat{a} \circ \Gamma^T(t_a - t_b))\hat{\varrho}]] \tag{F140}$$

$$+ [(\hat{b} \circ \Delta\Gamma(t - t_b, t_a - t_b)), [\hat{a}, (\hat{a} \circ \Gamma^T(t_a - t_b))\hat{b}(\hat{0} \circ \Delta\Gamma^T(t, t-t_b))\hat{\varrho}]] \tag{F141}$$

$$- [(\hat{b} \circ \Delta\Gamma(t - t_b, t_a - t_b)), [\hat{a}, \hat{b}(\hat{0} \circ \Delta\Gamma^T(t, t-t_b))]\hat{\varrho}(\hat{a} \circ (-\Gamma(t_b - t_a)))] \tag{F142}$$

$$- [(\hat{a} \circ (-\Gamma^T(t_a - t))), [(\hat{b} \circ \Gamma(t_a - t_b))\hat{b}, (\hat{0} \circ \Delta\Gamma^T(t, t-t_b))]]\hat{\varrho}\hat{a} \tag{F143}$$

$$+ [(\hat{a} \circ (-\Gamma^T(t_a - t))), [\hat{b}, (\hat{0} \circ \Delta\Gamma^T(t, t - t_b))]\hat{\varrho}(\hat{b} \circ \Gamma(t_a - t_b))\hat{a}] \tag{F144}$$

$$- [\hat{b}, (\hat{0} \circ \Delta\Gamma^T(t, t - t_b))][(\hat{a} \circ (-\Gamma^T(t_a - t))), \hat{\varrho}\hat{a}](\hat{b} \circ \Gamma(t_a - t_b)) \tag{F145}$$

$$+ (\hat{0} \circ \Delta\Gamma^T(t, t - t_b))[\hat{a}, \hat{b}\hat{\varrho}[(\hat{b} \circ \Delta\Gamma(t_a - t_b, -t_b)), (\hat{a} \circ (-\Gamma(t_b - t_a)))]] \tag{F146}$$

$$- (\hat{0} \circ \Delta\Gamma^T(t, t - t_b))[(\hat{b} \circ \Delta\Gamma(t_a - t_b, -t_b)), \hat{b}[\hat{a}, \hat{\varrho}(\hat{a} \circ (-\Gamma(t_b - t_a)))]] \tag{F147}$$

$$+ [\hat{a}, (\hat{0} \circ \Delta\Gamma^T(t, t - t_b))[(\hat{b} \circ \Delta\Gamma(t_a - t_b, -t_b)), \hat{b}\hat{\varrho}](\hat{a} \circ (-\Gamma(t_b - t_a))) \tag{F148}$$

$$+ [(\hat{b} \circ \Delta\Gamma(t_a - t_b, -t_b)), \hat{b}(\hat{0} \circ \Delta\Gamma^T(t, t - t_b))[\hat{a}, \hat{\varrho}(\hat{a} \circ (-\Gamma(t_b - t_a)))]] \tag{F149}$$

$$- [\hat{a}, [(\hat{b} \circ \Delta\Gamma(t_a - t_b, -t_b)), \hat{b}(\hat{0} \circ \Delta\Gamma^T(t, t - t_b))\hat{\varrho}(\hat{a} \circ (-\Gamma(t_b - t_a)))]] \tag{F150}$$

$$- (\hat{0} \circ \Delta\Gamma^T(t, t - t_b))[(\hat{a} \circ (-\Gamma^T(t_a - t))), \hat{b}\hat{\varrho}[(\hat{b} \circ \Delta\Gamma(t_a - t_b, -t_b)), \hat{a}]] \tag{F151}$$

$$+ (\hat{0} \circ \Delta\Gamma^T(t, t - t_b))[(\hat{b} \circ \Delta\Gamma(t_a - t_b, -t_b)), \hat{b}[(\hat{a} \circ (-\Gamma^T(t_a - t))), \hat{\varrho}\hat{a}]] \tag{F152}$$

$$- [(\hat{a} \circ (-\Gamma^T(t_a - t))), (\hat{0} \circ \Delta\Gamma^T(t, t - t_b))[(\hat{b} \circ \Delta\Gamma(t_a - t_b, -t_b)), \hat{b}\hat{\varrho}]\hat{a}] \tag{F153}$$

$$- [(\hat{b} \circ \Delta\Gamma(t_a - t_b, -t_b)), \hat{b}(\hat{0} \circ \Delta\Gamma^T(t, t - t_b))[(\hat{a} \circ (-\Gamma^T(t_a - t))), \hat{\varrho}\hat{a}]] \tag{F154}$$

$$+ [(\hat{a} \circ (-\Gamma^T(t_a - t))), [(\hat{b} \circ \Delta\Gamma(t_a - t_b, -t_b)), \hat{b}(\hat{0} \circ \Delta\Gamma^T(t, t - t_b))\hat{\varrho}\hat{a}]] \tag{F155}$$

$$+ [(\hat{0} \circ \Delta\Gamma^T(t, t - t_b)), \hat{a}][(\hat{b} \circ \Delta\Gamma^T(t_b - t_a, t_b - t)), \hat{\varrho}\hat{b}](\hat{a} \circ (-\Gamma(t_b - t_a))) \tag{F156}$$

$$\Bigg] + \text{H.c.} \tag{F157}$$

APPENDIX G: CLASSIFICATION OF $\omega_1 + \omega_2 + \omega_3 = 0$ TCL$_4$ TERMS

The analysis starts with the distilled TCL$_4$ generator, as established in Ref. [20]. For one linear-harmonic bath, the generator is simplified as

$$L^4_{nm,ij}(t) = \sum_{a,b,c} A_{na}A_{ab}A_{bc}A_{ci}\delta_{jm}[\mathsf{F}_{cb,ci,ac}(t) - \mathsf{R}_{cb,ab,bi}(t) - \mathsf{F}_{ba,ci,ac}(t) + \mathsf{R}_{ic,ab,bi}(t)] \tag{G1}$$

$$+ \sum_{a,b} \Big\{ A_{na}A_{ab}A_{bi}A_{jm}[-\mathsf{F}_{ba,bi,nb}(t) + \mathsf{R}_{ba,na,ai}(t) + \mathsf{F}_{an,bi,nb}(t) - \mathsf{R}_{ib,na,ai}(t)] \tag{G2}$$

$$+ A_{na}A_{ab}A_{bi}A_{jm}[\mathsf{C}_{ba,jm,ai}(t) + \mathsf{R}_{ba,jm,ai}(t) - \mathsf{C}_{ib,jm,ai}(t) - \mathsf{R}_{ib,jm,ai}(t)] \tag{G3}$$

$$+ A_{na}A_{ai}A_{jb}A_{bm}[-\mathsf{C}_{an,jb,ni}(t) - \mathsf{R}_{an,jb,ni}(t) + \mathsf{C}_{ia,jb,ni}(t) + \mathsf{R}_{ia,jb,ni}(t)] \Big\} + \text{r.H.c.} \tag{G4}$$

Here we introduced the bath spectral density functions

$$\mathsf{F}_{\omega_1\omega_2\omega_3}(t) = \tilde{\mathsf{F}}_{\omega_1\omega_2\omega_3}(t) + i\Gamma^T_{\omega_2}(t)\frac{\Gamma_{-\omega_2-\omega_3}(t) - \Gamma_{\omega_1}(t)}{\omega_1 + \omega_2 + \omega_3}, \tag{G5}$$

$$\mathsf{C}_{\omega_1\omega_2\omega_3}(t) = \tilde{\mathsf{C}}_{\omega_1\omega_2\omega_3}(t) + i\Gamma^\star_{\omega_2}(t)\frac{\Gamma_{-\omega_2-\omega_3}(t) - \Gamma_{\omega_1}(t)}{\omega_1 + \omega_2 + \omega_3}, \tag{G6}$$

$$\mathsf{R}_{\omega_1\omega_2\omega_3}(t) = \tilde{\mathsf{R}}_{\omega_1\omega_2\omega_3}(t) + i\Gamma_{\omega_2}(t)\frac{\Gamma_{-\omega_2-\omega_3}(t) - \Gamma_{\omega_1}(t)}{\omega_1 + \omega_2 + \omega_3}, \tag{G7}$$

which display the following irreducible integrals:

$$\tilde{\mathsf{F}}_{\omega_1\omega_2\omega_3}(t) = -\int_0^t d\tau \, \Delta\Gamma_{\omega_1}(t, \tau)\Delta\Gamma^T_{\omega_2}(t, t - \tau)e^{-i(\omega_1+\omega_2+\omega_3)\tau}, \tag{G8}$$

$$\tilde{\mathsf{C}}_{\omega_1\omega_2\omega_3}(t) = -\int_0^t d\tau \, \Delta\Gamma_{\omega_1}(t, \tau)\Delta\Gamma^\star_{\omega_2}(t, t - \tau)e^{-i(\omega_1+\omega_2+\omega_3)\tau}, \tag{G9}$$

$$\tilde{\mathsf{R}}_{\omega_1\omega_2\omega_3}(t) = -\int_0^t d\tau \, \Delta\Gamma_{\omega_1}(t, \tau)\Delta\Gamma_{\omega_2}(t, \tau)e^{-i(\omega_1+\omega_2+\omega_3)\tau}. \tag{G10}$$

They are irreducible in the sense that they introduce new functions, which cannot be analytically expressed in terms of the BCF or Γ. Given that $\tilde{\mathsf{F}}$, $\tilde{\mathsf{C}}$, and $\tilde{\mathsf{R}}$ incorporate two correlation functions, their growths are suppressed relative to the algebraic terms in Eqs. (G5)–(G7), which are in the growth algebra of Sec. V C. The suppression of growth in $\tilde{\mathsf{F}}$, $\tilde{\mathsf{C}}$, and $\tilde{\mathsf{R}}$ was analyzed in Ref. [20] and further discussion of such terms will not be pursued, as they are subleading. However, they may need to be revisited for other resummations in future.

When the sum $\omega_\Sigma = \omega_1 + \omega_2 + \omega_3$ in the algebraic terms in (G5)–(G7) equals zero, it becomes essential to examine the limit $\omega_\Sigma \to 0$, which introduces the derivative $\partial\Gamma_\omega(t)/\partial\omega$. The analysis proceeds by imposing the condition $\omega_1 + \omega_2 + \omega_3 = 0$ across the 16 instances of F, C, or R in Eqs. (G1)–(G4), followed by the collection and organization of the resulting terms.

Take the initial occurrence of $\mathsf{F}_{cb,ci,ac}(t)$ found on Eq. (G1). The condition being enforced is $\omega_{cb} + \omega_{ci} + \omega_{ac} = \omega_{cb} + \omega_{ai} = 0$. Two sets of indices exist: ($c = b$ and $a = i$) or ($c = i$ and $b = a$). The intersections of the sets must be counted once. The resulting growth term is

$$\delta_{jm} \sum_b (A_{ni}|A_{ib}|^2 A_{bb} \mathsf{F}_{bb,bi,ib} + A_{nb} A_{bi} A_{bb} A_{ii} \mathsf{F}_{ib,ii,bi}) \tag{G11}$$

$$= -i\delta_{jm} \sum_b \left(A_{nb} A_{bi} A_{bb} A_{ii} \Gamma_0 \frac{\partial \Gamma}{\partial \omega_{ib}} + A_{ni} |A_{ib}|^2 A_{bb} \Gamma_{ib} \frac{\partial \Gamma}{\partial \omega} \bigg|_{\omega=0} \right). \tag{G12}$$

All the derivatives from line G1 and G2 result in the net contribution of

$$\text{Line } G1 + G2 = i\delta_{jm} \sum_k A_{nk} A_{ki} \frac{\partial \Gamma}{\partial \omega_{ik}} \sum_c [|A_{ic}|^2 \Gamma_{ic} - |A_{kc}|^2 \Gamma_{kc}] \tag{G13}$$

$$- i A_{ni} A_{jm} \frac{\partial \Gamma}{\partial \omega_{in}} \sum_c [|A_{ic}|^2 \Gamma_{ic} - |A_{nc}|^2 \Gamma_{nc}]. \tag{G14}$$

We follow up with the similar analysis in the subsequent lines, which will include a larger variety of terms:

$$\text{Line } G3 = \delta_{jm} \sum_k A_{nk} A_{ki} A_{jj} (A_{kk} - A_{ii}) 2i J_0 \frac{\partial \Gamma}{\partial \omega_{ik}} \tag{G15}$$

$$- \delta_{ij} |A_{im}|^2 \sum_k A_{nk} A_{km} 2i J_{im} \frac{\partial \Gamma}{\partial \omega_{mk}} \tag{G16}$$

$$+ A_{nm} A_{ji} |A_{jm}|^2 2i J_{jm} \frac{\partial \Gamma}{\partial \omega_{ij}}, \tag{G17}$$

$$\text{Line } G4 = -A_{ni} A_{jm} A_{jj} (A_{nn} - A_{ii}) 2i J_0(t) \frac{\partial \Gamma}{\partial \omega_{in}} \tag{G18}$$

$$+ \delta_{ij} \sum_k |A_{ik}|^2 A_{nk} A_{km} 2i J_{ik} \frac{\partial \Gamma}{\partial \omega_{kn}} \tag{G19}$$

$$- |A_{jn}|^2 A_{nm} A_{ji} 2i J_{jn} \frac{\partial \Gamma}{\partial \omega_{ij}}. \tag{G20}$$

Reflecting on the Bloch-Redfield generator in Eq. (71), $L^2_{nm,ij}(t) = A_{ni} A_{jm} \Gamma_{in}(t) - \sum_{k=1}^N A_{nk} A_{ki} \Gamma_{ik} \delta_{jm} + \text{r.H.c.}$, allows us to incorporate Eqs. (G15) and (G18) into Eqs. (G13) and (G14), respectively. The result is a shift in the spectral density

$$\Gamma_{ik} \mapsto \Gamma_{ik} - i \frac{\partial \Gamma}{\partial \omega_{ik}} \left[\sum_c (|A_{ic}|^2 \Gamma_{ic} - |A_{kc}|^2 \Gamma_{kc}) + 2J_0(t) A_{jj}(A_{kk} - A_{ii}) \right]. \tag{G21}$$

The remaining terms are not embeddable, as indicated in Eqs. (G16), (G17), (G19), and (G20). The nonembeddable terms have the following Liouvillian:

$$\tilde{L}^2_{nm,ij} = -2i\delta_{ij} \sum_k A_{nk} A_{km} \left(|A_{im}|^2 J_{im} \frac{\partial \Gamma}{\partial \omega_{mk}} - |A_{ik}|^2 J_{ik} \frac{\partial \Gamma}{\partial \omega_{kn}} \right) \tag{G22}$$

$$- 2i A_{nm} A_{ji} \frac{\partial \Gamma}{\partial \omega_{ij}} (|A_{jn}|^2 J_{jn} - |A_{jm}|^2 J_{jm}) + \text{r.H.c.} \tag{G23}$$

For one qubit, we prevent double or triple counting using symbolic math, leading to

$$\tilde{L}^2_{nm,ij} = 2i|A_{12}|^2 \begin{pmatrix} |A_{12}|^2 J_{12} \frac{\partial \Gamma}{\partial \omega_{21}} & 0 & 0 & -|A_{12}|^2 J_{21} \frac{\partial \Gamma}{\partial \omega_{12}} \\ A_{21}(A_{22} - A_{11}) J_{12} \frac{\partial \Gamma}{\partial \omega_{11}} & -|A_{12}|^2 J_{12} \frac{\partial \Gamma}{\partial \omega_{21}} & A_{21}^2 J_{21} \frac{\partial \Gamma}{\partial \omega_{12}} & A_{21}(A_{11} - A_{22}) J_{21} \left(\frac{\partial \Gamma}{\partial \omega_{12}} - \frac{\partial \Gamma}{\partial \omega_{11}} \right) \\ A_{12}(A_{11} - A_{22}) J_{12} \left(\frac{\partial \Gamma}{\partial \omega_{11}} - \frac{\partial \Gamma}{\partial \omega_{21}} \right) & A_{12}^2 J_{12} \frac{\partial \Gamma}{\partial \omega_{21}} & -|A_{21}|^2 J_{21} \frac{\partial \Gamma}{\partial \omega_{12}} & A_{12}(A_{11} - A_{22}) J_{21} \frac{\partial \Gamma}{\partial \omega_{11}} \\ -|A_{12}|^2 J_{12} \frac{\partial \Gamma}{\partial \omega_{21}} & 0 & 0 & |A_{12}|^2 J_{21} \frac{\partial \Gamma}{\partial \omega_{12}} \end{pmatrix}$$

$$+ \text{r.H.c.} \tag{G24}$$

APPENDIX H: RETURN TO EQUILIBRIUM

In this Appendix we compute the leading correction to the steady states of the rTCL$_4$-ME. We utilize the perturbation theory of the asymptotic states, as outlined in Refs. [20,38,40]. If the asymptotic generator in the Schrödinger picture is expressed as

$$L = L^0 + L^2 + L^4, \tag{H1}$$

where L^{2k} is proportional to λ^{2k}, then the correction to the steady population of the qubit, to precision $O(\lambda^2)$, is obtained using [20, Eqs. (71) and (75)]:

$$\sum_k L^2_{nn,kk}\rho^2_{kk} = -\sum_k L^4_{nn,kk}\rho^0_{kk} - \sum_{l\neq m} L^2_{nn,lm}\rho^2_{lm} \tag{H2}$$

$$= -\sum_k L^4_{nn,kk}\rho^0_{kk} + i\sum_k \sum_{l\neq m} \frac{L^2_{nn,lm}L^2_{lm,kk}}{\omega_{lm}}\rho^0_{kk}. \tag{H3}$$

Here, ρ^0_{kk} are the zeroth-order thermal populations of the system, and ρ^2_{lm} are the coherences computed in quadratic precision.

From the Bloch-Redfield generator in Eq. (71), we find $L^2_{nn,kk} = 2|A_{nk}|^2 J_{kn} - 2\delta_{kn}\sum_q |A_{nq}|^2 J_{nq}$, so that $L^2_{22,22} = -2|A_{12}|^2 J_{\beta,\Delta}$ and $L^2_{22,11} = 2|A_{12}|^2 J_{\beta,-\Delta}$. In the unbiased SBM, which we shall consider from now on, unless stated otherwise, the second-order generator has neither population-to-coherence nor coherence-to-population transfer matrix elements, so the second terms on the right-hand sides in Eqs. (H2) and (H3) are zero. Moreover, for the qubit we have $\rho^2_{11} + \rho^2_{22} = 0$, leading to the correction

$$\rho^2_{22} = -\frac{\sum_k L^4_{22,kk}\rho^0_{kk}}{L^2_{22,22} - L^2_{22,11}} = \frac{\sum_k L^4_{22,kk}\rho^0_{kk}}{2|A_{12}|^2(J_{\beta,\Delta} + J_{\beta,-\Delta})}. \tag{H4}$$

First, we examine the effect of the embeddable terms, which have the Liouvillian L^4 in the same form as L^2 but with the spectral density $J_{\beta,\pm\Delta}$ replaced by the shift $\delta J_{\beta,\pm\Delta}$ obtained from Eq. (G21). That is, $L^4_{22,22} = -2|A_{12}|^2\delta J_{\beta,\Delta}$, $L^4_{22,11} = 2|A_{12}|^2\delta J_{\beta,-\Delta}$, and

$$\delta J_{\beta,\pm\Delta} = \mathrm{Re}\left[-i\frac{\partial\Gamma_{\beta,\omega}}{\partial\omega}\bigg|_{\pm\Delta} |A_{12}|^2(\Gamma_{\beta,\pm\Delta} - \Gamma_{\beta,\mp\Delta}) \right] \tag{H5}$$

$$= \pm\left(\frac{\partial S_{\beta,\omega}}{\partial\omega}\bigg|_{\pm\Delta} \nu_2 + \frac{\partial J_{\beta,\omega}}{\partial\omega}\bigg|_{\pm\Delta} \tilde{\omega}_{\beta,21} \right). \tag{H6}$$

Inserting into Eq. (H4), and using $\rho^0_{11} = 1 - \rho^0_{22} = J_{\beta,\Delta}/(J_{\beta,\Delta} + J_{\beta,-\Delta})$, we obtain

$$\rho^2_{22} = -\nu_2 \frac{J_{\beta,\Delta}\frac{\partial S_{\beta,\omega}}{\partial\omega}\big|_{-\Delta} + J_{\beta,-\Delta}\frac{\partial S_{\beta,\omega}}{\partial\omega}\big|_{\Delta}}{(J_{\beta,-\Delta} + J_{\beta,\Delta})^2}$$

$$- \tilde{\omega}_{\beta,21} \frac{J_{\beta,\Delta}\frac{\partial J_{\beta,\omega}}{\partial\omega}\big|_{-\Delta} + J_{\beta,-\Delta}\frac{\partial J_{\beta,\omega}}{\partial\omega}\big|_{\Delta}}{(J_{\beta,-\Delta} + J_{\beta,\Delta})^2}. \tag{H7}$$

Applying the KMS conditions $J_{\beta,\Delta} = e^{\beta\Delta}J_{\beta,-\Delta}$ and $J'_{\beta,\Delta} = \beta e^{\beta\Delta}J_{\beta,-\Delta} - e^{\beta\Delta}J'_{\beta,-\Delta}$, where the prime indicates derivative

over frequency, we find

$$\rho^2_{22} = -\frac{\nu_2}{J_{\beta,\Delta} + J_{\beta,-\Delta}}\left[\rho^0_{11}\frac{\partial S_{\beta,\omega}}{\partial\omega}\bigg|_{-\Delta} + \rho^0_{22}\frac{\partial S_{\beta,\omega}}{\partial\omega}\big|_{\Delta} \right]$$

$$- \beta\rho^0_{11}\rho^0_{22}\tilde{\omega}_{\beta,21}. \tag{H8}$$

Subsequently, utilizing $\nu_2 = |A_{12}|^2(J_{\beta,\Delta} - J_{\beta,-\Delta})$ and $\tilde{\omega}_{\beta,21} = |A_{12}|^2(S_{\beta,\Delta} - S_{\beta,-\Delta})$, the population of the excited state becomes

$$\rho_{22} = \rho^0_{22} - |A_{12}|^2\left[\tanh\frac{\beta\Delta}{2}\left(\rho^0_{11}\frac{\partial S_{\beta,\omega}}{\partial\omega}\bigg|_{-\Delta} + \rho^0_{22}\frac{\partial S_{\beta,\omega}}{\partial\omega}\bigg|_{\Delta} \right) \right. \tag{H9}$$

$$\left. + \beta\rho^0_{11}\rho^0_{22}(S_{\beta,\Delta} - S_{\beta,-\Delta}) \right]. \tag{H10}$$

Let us now compute the contribution from the nonemebeddable terms. From Eq. (G24), we have $\tilde{L}^2_{22,22} = -4|A_{12}|^4 J_{\beta,\Delta}\partial S_{\beta,\omega}/\partial\omega|_{-\Delta}$ and $\tilde{L}^2_{22,11} = 4|A_{12}|^4 J_{\beta,-\Delta}\partial S_{\beta,\omega}/\partial\omega|_{\Delta}$. Inserting into Eq. (H4), we obtain the contribution

$$\tilde{\rho}^2_{22} = 2|A_{12}|^2 \frac{J_{\beta,\Delta}J_{\beta,-\Delta}}{(J_{\beta,\Delta} + J_{\beta,-\Delta})^2}\left(\frac{\partial S_{\beta,\omega}}{\partial\omega}\bigg|_{\Delta} - \frac{\partial S_{\beta,\omega}}{\partial\omega}\bigg|_{-\Delta} \right). \tag{H11}$$

Adding to the previous equation, we obtain

$$\rho_{22} = \rho^0_{22} + |A_{12}|^2\left[\left(-\rho^0_{11}\frac{\partial S_{\beta,\omega}}{\partial\omega}\bigg|_{-\Delta} + \rho^0_{22}\frac{\partial S_{\beta,\omega}}{\partial\omega}\bigg|_{\Delta} \right) \right. \tag{H12}$$

$$\left. - \beta\rho^0_{11}\rho^0_{22}(S_{\beta,\Delta} - S_{\beta,-\Delta}) \right]. \tag{H13}$$

Let us transform this following the next equalities:

$$S_{\beta,\omega} = \frac{1}{\pi}P\int_{-\infty}^{\infty} d\omega' \frac{J_{\beta,\omega'}}{\omega - \omega'} \tag{H14}$$

$$= \frac{1}{\pi}P\int_0^{\infty} d\omega' \frac{J_{\omega'}}{\omega^2 - \omega'^2}\left(\omega\coth\frac{\beta\omega'}{2} + \omega' \right) \tag{H15}$$

$$\frac{\partial S_{\beta,\omega}}{\partial\omega} = -\frac{1}{\pi}P\int_0^{\infty} d\omega' \frac{J_{\omega'}}{(\omega^2 - \omega'^2)^2}$$

$$\times \left[(\omega^2 + \omega'^2)\coth\frac{\beta\omega'}{2} + 2\omega\omega' \right]. \tag{H16}$$

With some algebra, we arrive at

$$\rho_{22} = \rho^0_{22} + \frac{|A_{12}|^2}{\pi}P\int_0^{\infty} d\omega' \frac{J_{\omega'}}{(\Delta^2 - \omega'^2)^2}$$

$$\times \left\{ \coth\frac{\beta\omega'}{2}\left[(\Delta^2 + \omega'^2)\tanh\frac{\beta\Delta}{2} \right.\right.$$

$$\left.\left. + \frac{\beta\Delta}{2}(\omega'^2 - \Delta^2)\mathrm{sech}^2\frac{\beta\Delta}{2} \right] - 2\Delta\omega' \right\}, \tag{H17}$$

which is precisely the same as the mean-force Gibbs state correction [87,97].

We have also computed the asymptotic state of the TCL$_4$ master equation at arbitrary temperature, by substituting the

TCL$_4$ generator into Eq. (H1), and find that is is the same as (H17), within at least eight significant digits. This is a remarkable result because the quartic componenet of the rTCL$_4$ generator is a subset of the TCL$_4$ generator terms, picked based on the leading late-time growths. These two tensors have different population-to-population matrix elements, and the relaxation rates of rTCL$_4$ and TCL$_4$ can be different by more than 10%. Nevertheless, they have the same asymptotic states. This exemplifies that canonical consistency can be achieved using different master equations. Since TCL$_4$ is the complete fourth-order generator, and rTCL$_4$ is only a subset, it follows that enforcing canonical consistency does not guarantee accuracy at all timescales, even though the asymptotic states are identical.

We have examined larger systems, with three or four energy levels, and in those systems the rTCL$_4$ master equation does not lead to return to equilibrium at nonzero temperature to quadratic precision [e.g., it returns to equilibrium only to precision $O(\lambda^0)$ like the Davies or TCL$_2$-Bloch-Redfield ME]. Whereas, we find that the TCL$_4$ generator always generates to the mean-force Gibbs state to precision $O(\lambda^2)$ within the numerical precision. As in our previous work [20], the return to equilibrium in TCL$_4$ is proven only numerically, but the reasons for the agreement in arbitrary systems remain a puzzle. Recently, the analytic proof for any qubit (including the biased regime) and in a bath with analytic continuity of the spectral functions in the entire upper complex plane was accomplished in Ref. [98].

In the presence of dephasing, the asymptotic populations of TCL$_4$ remain the same as those given by Eq. (H17), in agreement with the mean-force Gibbs state, but the rTCL$_4$ no longer leads to the equilibrium state to precision $O(\lambda^4)$. To conclude, at zero temperature, all rTCL, rTCL$_4$, and TCL$_4$ approach ground state to precision $O(\lambda^2)$ regardless of the qubit Hamiltonian. But, in the Ohmic bath at positive temperature, rTCL$_4$ will exhibit return to equilibrium to precision $O(\lambda^2)$, only when the diagonal elements of A are zero.

APPENDIX I: FÖRSTER REGIME

We will obtain the Förster rate by mapping to the exciton-in-a-dimer Hamiltonian:

$$H_T = -\frac{\Delta}{2}|1\rangle\langle 1| + \frac{\Delta}{2}|2\rangle\langle 2| + U(|1\rangle\langle 2| + |2\rangle\langle 1|)$$
$$+ |1\rangle\langle 1| \otimes F_1 + |2\rangle\langle 2| \otimes F_2 + H_{B1} + H_{B2}. \quad (I1)$$

Each site is coupled to a local bath characterized by the coupling and bath Hamiltonians F_i and H_{Bi}, respectively given by Eqs. (6) and (9). The baths are independent and the frequencies and form factors of the bath satisfy $\omega_{k1} = \omega_{k2} = \tilde{\omega}_k$ and $g_{k1} = g_{k2} = \tilde{g}_k$. The reorganization energy in each bath is

$$\tilde{E}_r = \int_0^\infty d\omega \frac{\tilde{J}_\omega}{\pi \omega} = -\tilde{S}_0. \quad (I2)$$

The Förster transfer rate is computed treating the system energy U as perturbation, while the reference states are the asymptotic states of the pure-dephasing Hamiltonian. That is, for the exciton at each site, the bath state is taken to be the fully displaced thermal state. The Förster master equation is the Pauli equation in the site or the pointer basis,

in which the coherence dynamics is traced out (as opposed to neglected [99]). The Förster rate is the tunneling rate between sites, obtained in the limit $U \ll \Delta, \tilde{E}_r$, using Ref. [90, Eqs. (18), (21), (22)]:

$$R_{nn,mm}^{\text{FRET}} = 2U^2 \text{Re} \int_0^\infty dt\, e^{i\omega_{mn}t - 2i\tilde{E}_r t - 2g(t)}, \quad (I3)$$

where $g(t)$ is the line-shape broadening function

$$g(t) = \int_0^t dt_1 \int_0^{t_1} dt_1 \tilde{C}_\beta(t_2) dt_2 = \int_0^t dt_1 \tilde{\Gamma}_{\beta,0}(t_1) \quad (I4)$$

$$= \int_0^t dt_1 [\tilde{J}_{\beta,0}(t_1) + i\tilde{S}_0(t_1)] \quad (I5)$$

since $\tilde{S}_{\beta,0}(t)$ is independent of β via Eq. (17). Thus,

$$R_{nn,mm}^{\text{FRET}} = 2U^2 \text{Re} \int_0^\infty dt\, e^{i\omega_{mn}t + 2i\int_0^t dt_1 [\tilde{S}_0 - \tilde{S}_0(t_1)] - 2\int_0^t dt_1 \tilde{J}_{\beta,0}(t_1)}. \quad (I6)$$

The relaxation rate is $\omega_F = R_{11,22}^{\text{FRET}} + R_{22,11}^{\text{FRET}}$, while the asymptotic site population is $\rho_{11} = R_{11,22}^{\text{FRET}}/\omega_R$.

The mapping to the qubit is done in two simple steps. First, the hopping Hamiltonian is mapped into a qubit Hamiltonian by the unitary transformation in the baths:

$$b_k' = \frac{1}{\sqrt{2}}(b_{k1} - b_{k2}), \quad (I7)$$

$$b_k'' = \frac{1}{\sqrt{2}}(b_{k1} + b_{k2}). \quad (I8)$$

Only the b_k' bath is coupled to the system, in terms of which the Hamiltonian is

$$H' = -\frac{\Delta}{2}\sigma_z + U\sigma_x + \frac{1}{2}\sigma_z \otimes \sum_k \sqrt{2}\tilde{g}_k(b_k' + b_k'^\dagger)$$
$$+ \sum_k \tilde{\omega}_k b_k'^\dagger b_k'. \quad (I9)$$

Here, the Pauli matrices operate in the site basis, with $\sigma_z = \pm 1$ corresponding to different sites. TCL$_{2n}$ is expressed in the eigenbasis of the isolated system Hamiltonian. Next, we make the unitary transformation W into the isolated system energy eigenbasis. In the limit $U \ll \Delta$, we have

$$W = \begin{pmatrix} 1 & U/\Delta \\ -U/\Delta & 1 \end{pmatrix}, \quad (I10)$$

and the Hamiltonian

$$H'' = W^\dagger H'W \approx -\frac{\Delta}{2}\sigma_z + A' \otimes F' + \sum_k \tilde{\omega}_k b_k'^\dagger b_k', \quad (I11)$$

where $F' = \sum_k \tilde{g}_k(b_k' + b_k'^\dagger)$ and

$$A' = \frac{1}{\sqrt{2}}\begin{pmatrix} 1 & 2U/\Delta \\ 2U/\Delta & -1 \end{pmatrix}. \quad (I12)$$

This can be identified with the qubit Hamiltonian by scaling, e.g., $A = cA'$, $g_k = \tilde{g}_k/c$, and $\omega_k = \tilde{\omega}_k$. Thus, $c = \sqrt{2}A_{11}$, $U = \Delta A_{12}/(2A_{11})$, and $\tilde{J} = c^2 J = 2A_{11}^2 J$, $\tilde{S} = c^2 S = 2A_{11}^2 S$. Substituting into Eq. (I6) leads to Eq. (163), while in the limit $U \ll \Delta$, the populations in the site and isolated system energy eigenbasis are approximately equal.

[1] A. Strathearn, P. Kirton, D. Kilda, J. Keeling, and B. W. Lovett, Efficient non-Markovian quantum dynamics using time-evolving matrix product operators, Nat. Commun. **9**, 3322 (2018).

[2] R. Hartmann and W. T. Strunz, Exact open quantum system dynamics using the hierarchy of pure states (hops), J. Chem. Theory Comput. **13**, 5834 (2017).

[3] M. R. Jørgensen and F. A. Pollock, Exploiting the causal tensor network structure of quantum processes to efficiently simulate non-Markovian path integrals, Phys. Rev. Lett. **123**, 240602 (2019).

[4] Y. Tanimura, Numerically "exact" approach to open quantum dynamics: The hierarchical equations of motion (heom), J. Chem. Phys. **153**, 020901 (2020).

[5] F. Mascherpa, A. Smirne, A. D. Somoza, P. Fernández-Acebal, S. Donadi, D. Tamascelli, S. F. Huelga, and M. B. Plenio, Optimized auxiliary oscillators for the simulation of general open quantum systems, Phys. Rev. A **101**, 052108 (2020).

[6] S. Milz and K. Modi, Quantum stochastic processes and quantum non-Markovian phenomena, PRX Quantum **2**, 030201 (2021).

[7] I. de Vega and D. Alonso, Dynamics of non-Markovian open quantum systems, Rev. Mod. Phys. **89**, 015001 (2017).

[8] F. Bloch, Nuclear induction, Phys. Rev. **70**, 460 (1946).

[9] A. Redfield, The theory of relaxation processes, in *Advances in Magnetic Resonance*, edited by J. S. Waugh, Advances in Magnetic and Optical Resonance Vol. 1 (Academic Press, New York, 1965), pp. 1–32

[10] N. Van Kampen, A cumulant expansion for stochastic linear differential equations. I, Physica (Amsterdam) **74**, 215 (1974).

[11] N. Van Kampen, A cumulant expansion for stochastic linear differential equations. II, Physica (Amsterdam) **74**, 239 (1974).

[12] G. Schaller and T. Brandes, Preservation of positivity by dynamical coarse graining, Phys. Rev. A **78**, 022106 (2008).

[13] J. Thingna, H. Zhou, and J.-S. Wang, Improved dyson series expansion for steady-state quantum transport beyond the weak coupling limit: Divergences and resolution, J. Chem. Phys. **141**, 194101 (2014).

[14] G. Kaplanek and C. P. Burgess, Hot accelerated qubits: decoherence, thermalization, secular growth and reliable late-time predictions, J. High Energy Phys. 03 (2020) 008.

[15] V. Link, H.-H. Tu, and W. T. Strunz, Open quantum system dynamics from infinite tensor network contraction, Phys. Rev. Lett. **132**, 200403 (2024).

[16] M. Cygorek, J. Keeling, B. W. Lovett, and E. M. Gauger, Sublinear scaling in non-Markovian open quantum systems simulations, Phys. Rev. X **14**, 011010 (2024).

[17] F. Kahlert, V. Link, R. Hartmann, and W. T. Strunz, Simulating the Landau–Zener sweep in deeply sub-ohmic environments, J. Chem. Phys. **161**, 184108 (2024).

[18] H. Nguyen, N. Ng, L. P. Lindoy, G. Park, A. J. Millis, G. K.-L. Chan, and D. R. Reichman, Correlation functions from tensor network influence functionals: The case of the spin-boson model, J. Chem. Phys. **161**, 104111 (2024).

[19] N. Dowling, K. Modi, R. N. Muñoz, S. Singh, and G. A. L. White, Capturing long-range memory structures with tree-geometry process tensors, Phys. Rev. X **14**, 041018 (2024).

[20] E. Crowder, L. Lampert, G. Manchanda, B. Shoffeitt, S. Gadamsetty, Y. Pei, S. Chaudhary, and D. Davidović,

[21] Invalidation of the Bloch-Redfield equation in the sub-Ohmic regime via a practical time-convolutionless fourth-order master equation, Phys. Rev. A **109**, 052205 (2024).

[21] E. B. Davies, Markovian master equations, Commun. Math. Phys. **39**, 91 (1974).

[22] M. Tokuyama and H. Mori, Statistical-mechanical theory of the Boltzmann equation and fluctuations in μ space, Prog. Theor. Phys. **56**, 1073 (1976).

[23] S. Nakajima, On quantum theory of transport phenomena: Steady diffusion, Prog. Theor. Phys. **20**, 948 (1958).

[24] R. Zwanzig, Ensemble method in the theory of irreversibility, J. Chem. Phys. **33**, 1338 (1960).

[25] H.-P. Breuer and F. Petruccione, *The Theory of Open Quantum Systems* (Oxford University Press, Oxford, 2007).

[26] J. Chen, E. Crowder, L. Xiang, and D. Davidovic, Benchmarking TCL4: Assessing the usability and reliability of fourth-order approximations, APL Quantum **2**, 026109 (2025).

[27] Y. Tanimura and R. Kubo, Two-time correlation functions of a system coupled to a heat bath with a Gaussian-Markoffian interaction, J. Phys. Soc. Jpn. **58**, 1199 (1989).

[28] N. N. Bogolyubov, Problems of a dynamical theory in statistical physics (1962).

[29] L. van Hove, Quantum-mechanical perturbations giving rise to a statistical transport equation, Physica (Amsterdam) **21**, 517 (1954).

[30] T. Forster, Energiewanderung und fluoreszenz, Naturwissenschaften **33**, 166 (1946).

[31] T. Förster, Zwischenmolekulare energiewanderung und fluoreszenz, Ann. Phys. **437**, 55 (1948).

[32] V. Gorini, A. Kossakowski, and E. C. G. Sudarshan, Completely positive dynamical semigroups of n-level systems, J. Math. Phys. **17**, 821 (1976).

[33] G. Lindblad, On the generators of quantum dynamical semigroups, Commun. Math. Phys. **48**, 119 (1976).

[34] M. Merkli, Dynamics of open quantum systems I, oscillation and decay, Quantum **6**, 615 (2022).

[35] M. Merkli, Dynamics of open quantum systems II, Markovian approximation, Quantum **6**, 616 (2022).

[36] D. Davidović, Geometric-arithmetic master equation in large and fast open quantum systems, J. Phys. A: Math. Theor. **55**, 455301 (2022).

[37] R. Hartmann and W. T. Strunz, Accuracy assessment of perturbative master equations: Embracing nonpositivity, Phys. Rev. A **101**, 012103 (2020).

[38] C. H. Fleming and N. I. Cummings, Accuracy of perturbative master equations, Phys. Rev. E **83**, 031117 (2011).

[39] J. Thingna, J.-S. Wang, and P. Hänggi, Generalized Gibbs state with modified redfield solution: Exact agreement up to second order, J. Chem. Phys. **136**, 194110 (2012).

[40] D. Tupkary, A. Dhar, M. Kulkarni, and A. Purkayastha, Fundamental limitations in Lindblad descriptions of systems weakly coupled to baths, Phys. Rev. A **105**, 032208 (2022).

[41] T. Colas, J. Grain, and V. Vennin, Benchmarking the cosmological master equations, Eur. Phys. J. C **82**, 1085 (2022).

[42] D. Farina and V. Giovannetti, Open-quantum-system dynamics: Recovering positivity of the Redfield equation via the partial secular approximation, Phys. Rev. A **100**, 012107 (2019).

[43] E. Mozgunov and D. Lidar, Completely positive master equation for arbitrary driving and small level spacing, Quantum **4**, 227 (2020).

[44] T. V. Tscherbul and P. Brumer, Partial secular Bloch-Redfield master equation for incoherent excitation of multilevel quantum systems, J. Chem. Phys. **142**, 104107 (2015).

[45] A. Trushechkin, Unified Gorini-Kossakowski-Lindblad-Sudarshan quantum master equation beyond the secular approximation, Phys. Rev. A **103**, 062226 (2021).

[46] F. Nathan and M. S. Rudner, Universal Lindblad equation for open quantum systems, Phys. Rev. B **102**, 115109 (2020).

[47] D. Davidović, Completely positive, simple, and possibly highly accurate approximation of the Redfield equation, Quantum **4**, 326 (2020).

[48] P. P. Potts, A. A. S. Kalaee, and A. Wacker, A thermodynamically consistent Markovian master equation beyond the secular approximation, New J. Phys. **23**, 123013 (2021).

[49] T. Becker, A. Schnell, and J. Thingna, Canonically consistent quantum master equation, Phys. Rev. Lett. **129**, 200403 (2022).

[50] C. Uchiyama, Dynamics of a quantum interacting system-extended global approach beyond the Born-Markov and secular approximation, arXiv:2303.02926.

[51] M. Winczewski and R. Alicki, Renormalization in the theory of open quantum systems via the self-consistency condition, arXiv:2112.11962.

[52] M. Łobejko, M. Winczewski, G. Suárez, R. Alicki, and M. Horodecki, Towards reconciliation of completely positive open system dynamics with the equilibration postulate, Phys. Rev. E **110**, 014144 (2024).

[53] D. Tupkary, A. Dhar, M. Kulkarni, and A. Purkayastha, Searching for Lindbladians obeying local conservation laws and showing thermalization, arXiv:2301.02146.

[54] A. D'Abbruzzo, V. Cavina, and V. Giovannetti, A time-dependent regularization of the Redfield equation, SciPost Phys. **15**, 117 (2023).

[55] G. Gasbarri and L. Ferialdi, Recursive approach for non-Markovian time-convolutionless master equations, Phys. Rev. A **97**, 022114 (2018).

[56] K. Nestmann and C. Timm, Time-convolutionless master equation: Perturbative expansions to arbitrary order and application to quantum dots, arXiv:1903.05132.

[57] A. Trushechkin, Higher-order corrections to the Redfield equation with respect to the system-bath coupling based on the hierarchical equations of motion, Lobachevskii J. Math. **40**, 1606 (2019).

[58] A. S. Trushechkin, Derivation of the Redfield quantum master equation and corrections to it by the Bogoliubov method, Proc. Steklov Inst. Math. **313**, 246 (2021).

[59] A. Y. Karasev and A. E. Teretenkov, Time-convolutionless master equations for composite open quantum systems, Lobachevskii J. Math. **44**, 2051 (2023).

[60] Z. Xia, J. Garcia-Nila, and D. A. Lidar, Markovian and non-Markovian master equations versus an exactly solvable model of a qubit in a cavity, Phys. Rev. Appl. **22**, 014028 (2024).

[61] A. Caldeira and A. Leggett, Path integral approach to quantum brownian motion, Physica A (Amsterdam) **121**, 587 (1983).

[62] W. M. Zhang, T. Meier, V. Chernyak, and S. Mukamel, Exciton-migration and three-pulse femtosecond optical spectroscopies of photosynthetic antenna complexes, J. Chem. Phys. **108**, 7763 (1998).

[63] A. Trushechkin, Quantum master equations and steady states for the ultrastrong-coupling limit and the strong-decoherence limit, Phys. Rev. A **106**, 042209 (2022).

[64] C. Burgess, R. Holman, G. Tasinato, and M. Williams, EFT beyond the horizon: Stochastic inflation and how primordial quantum fluctuations go classical, J. High Energy Phys. 03 (2015) 090.

[65] D. Boyanovsky, Effective field theory during inflation: Reduced density matrix and its quantum master equation, Phys. Rev. D **92**, 023527 (2015).

[66] D. Boyanovsky, Effective field theory during inflation. II. stochastic dynamics and power spectrum suppression, Phys. Rev. D **93**, 043501 (2016).

[67] C. P. Burgess, R. Holman, and G. Tasinato, Open EFTs, IR effects & late-time resummations: Systematic corrections in stochastic inflation, J. High Energy Phys. 01 (2016) 153.

[68] S. Shandera, N. Agarwal, and A. Kamal, Open quantum cosmological system, Phys. Rev. D **98**, 083535 (2018).

[69] G. Kaplanek, C. P. Burgess, and R. Holman, Qubit heating near a hotspot, J. High Energy Phys. 08 (2021) 132.

[70] S. Chaykov, N. Agarwal, S. Bahrami, and R. Holman, Loop corrections in Minkowski spacetime away from equilibrium. part I. Late-time resummations, J. High Energy Phys. 02 (2023) 093.

[71] S. Chaykov, N. Agarwal, S. Bahrami, and R. Holman, Loop corrections in Minkowski spacetime away from equilibrium. Part II. Finite-time results, J. High Energy Phys. 02 (2023) 094.

[72] T. Colas, J. Grain, G. Kaplanek, and V. Vennin, In-in formalism for the entropy of quantum fields in curved spacetimes, J. Cosmol. Astropart. Phys. **2024**, 047 (2024).

[73] W. De Roeck and A. Kupiainen, Approach to ground state and time-independent photon bound for massless spin-boson models, in *Annales Henri Poincaré* (Springer, Berlin, 2013), pp. 253–311, Vol. 14.

[74] J. Faupin and I. M. Sigal, On Rayleigh scattering in non-relativistic quantum electrodynamics, Commun. Math. Phys. **328**, 1199 (2014).

[75] W. De Roeck, M. Griesemer, and A. Kupiainen, Asymptotic completeness for the massless spin-Boson model, Adv. Math. **268**, 62 (2015).

[76] D. Hasler and I. Herbst, Ground states in the spin Boson model, in *Annales Henri Poincaré* (Springer, Berlin, 2011), Vol. 12, pp. 621–677.

[77] D. Hasler, B. Hinrichs, and O. Siebert, On existence of ground states in the spin Boson model, Commun. Math. Phys. **388**, 419 (2021).

[78] H.-P. Breuer, B. Kappler, and F. Petruccione, Stochastic wave-function method for non-Markovian quantum master equations, Phys. Rev. A **59**, 1633 (1999).

[79] U. Weiss, *Quantum Dissipative Systems*, 4th ed. (World Scientific, Singapore, 2012).

[80] J. Dereziński, Van Hove Hamiltonians–exactly solvable models of the infrared and ultraviolet problem, in *Annales Henri Poincaré* (Springer, Berlin, 2003), Vol. 4, pp. 713–738.

[81] J. Dereziński and C. Gérard, Scattering theory of infrared divergent Pauli-Fierz Hamiltonians, in *Annales Henri Poincaré* (Springer, Berlin, 2004), Vol. 5, pp. 523–577.

[82] M. Merkli, The ideal quantum gas, in *Open Quantum Systems I: The Hamiltonian Approach* (Springer, Berlin, 2006), pp. 183–233.

[83] S. W. Hawking, Breakdown of predictability in gravitational collapse, Phys. Rev. D **14**, 2460 (1976).

[84] S. W. Hawking, M. J. Perry, and A. Strominger, Soft hair on black holes, Phys. Rev. Lett. **116**, 231301 (2016).

[85] D. Carney, L. Chaurette, D. Neuenfeld, and G. W. Semenoff, Infrared quantum information, Phys. Rev. Lett. **119**, 180502 (2017).

[86] A. J. Leggett, S. Chakravarty, A. T. Dorsey, M. P. A. Fisher, A. Garg, and W. Zwerger, Dynamics of the dissipative two-state system, Rev. Mod. Phys. **59**, 1 (1987).

[87] J. D. Cresser and J. Anders, Weak and ultrastrong coupling limits of the quantum mean force Gibbs state, Phys. Rev. Lett. **127**, 250601 (2021).

[88] M. Merkli, Quantum Markovian master equations: Resonance theory shows validity for all time scales, Ann. Phys. **412**, 167996 (2020).

[89] J. Seibt and T. Mančal, Ultrafast energy transfer with competing channels: Non-equilibrium Förster and modified Redfield theories, J. Chem. Phys. **146**, 174109 (2017).

[90] M. Yang and G. R. Fleming, Influence of phonons on exciton transfer dynamics: Comparison of the redfield, Förster, and modified Redfield equations, Chem. Phys. **282**, 163 (2002).

[91] M. B. Plenio and S. F. Huelga, Dephasing-assisted transport: Quantum networks and biomolecules, New J. Phys. **10**, 113019 (2008).

[92] M. Mohseni, P. Rebentrost, S. Lloyd, and A. Aspuru-Guzik, Environment-assisted quantum walks in photosynthetic energy transfer, J. Chem. Phys. **129**, 174106 (2008).

[93] S. Alterman, J. Berman, and F. W. Strauch, Optimal conditions for environment-assisted quantum transport on the fully connected network, Phys. Rev. E **109**, 014310 (2024).

[94] J. a. Ferreira, T. Jin, J. Mannhart, T. Giamarchi, and M. Filippone, Transport and nonreciprocity in monitored quantum devices: An exact study, Phys. Rev. Lett. **132**, 136301 (2024).

[95] H. Breuer, A. Ma, and F. Petruccione, Time-local master equations: Influence functional and cumulant expansion, in *Quantum Computing and Quantum Bits in Mesoscopic Systems*, edited by A. Leggett, B. Ruggiero, and P. Silvestrini (Springer, Boston, 2004).

[96] https://github.com/A-Beta-in-Iceland/TCL

[97] A. Purkayastha, G. Guarnieri, M. T. Mitchison, R. Filip, and J. Goold, Tunable phonon-induced steady-state coherence in a double-quantum-dot charge qubit, npj Quantum Inf. **6**, 27 (2020).

[98] P. Kumar, K. Athulya, and S. Ghosh, Equivalence between the second order steady state for spin-Boson model and its quantum mean force Gibbs state, Phys. Rev. B **111**, 115423 (2025).

[99] A. Trushechkin, Calculation of coherences in Förster and Modified Redfield theories of excitation energy transfer, J. Chem. Phys. **151**, 074101 (2019).